The Pennsylvania State University
The Graduate School

KINETICS OF ELECTRONS UNDER INFLUENCE OF EXTERNALLY APPLIED ELECTRIC FIELD IN WEAKLY IONIZED CARBON DIOXIDE PLASMA

A Thesis in
Electrical Engineering
by
Mohammad Zaid Pervez

Submitted in Partial Fulfillment
of the Requirements
for the Degree of

Master of Science

May 2023

The thesis of Mohammad Zaid Pervez was reviewed and approved by the following:

Victor P. Pasko
Professor of Electrical Engineering
Thesis Advisor

Julio Urbina
Associate Professor of Electrical Engineering

Reza Janalizadeh
Postdoctoral Fellow of Electrical Engineering
Special Signatory

Madhavan Swaminathan
Professor of Electrical Engineering
Department Head of Electrical Engineering

Abstract

The kinetics of electrons in weakly ionized plasma under the influence of an externally applied electric field plays an important role in the study of various physical phenomena, and has many scientific and industrial applications. In this thesis we focus primarily on weakly ionized CO_2 plasma and study the kinetics of electrons in this gas under an external electric field. A survey of experimental data for plasma fluid coefficients from prior studies is also presented. The Boltzmann equation for electrons is solved numerically using the BOLSIG+ solver, and the electron rate and transport coefficients thus obtained are found to be in good agreement with experimental data. Next, we consider weakly ionized magnetized plasma and present a theory to efficiently calculate plasma fluid coefficients in presence of electric and magnetic fields. Due to many practical applications, the CO_2 gas is chosen as a test bed to demonstrate practical application of the proposed theory. The method is justified with a rigorous mathematical formulation and provides results of satisfactory accuracy for range of input parameters corresponding to most applications of gas discharge plasma. This new approach allows for efficient modeling of electron kinetics in magnetized plasma and, in particular, has significant potential in the study and modeling of streamer discharges.

Table of Contents

List of Figures

List of Tables

Acknowledgments

First and foremost I would like to thank my advisor, Dr. Victor P. Pasko, for granting me this opportunity, and for his endless support, patience, and encouragement. None of this work would have been possible without his guidance. I look up to him as a role-model and hope to learn as much as I can from his experience and wisdom.

I am equally grateful to Dr. Reza Janalizadeh, who is my labmate at Penn State, and also served as a member of my thesis committee. He played the roles of both mentor and friend, and his support has been essential to every small step that led me here. It was an honor to work with both Dr. Pasko and Reza, and I am sure it will continue to be so in the years to come.

I would also like to thank Dr. Julio Urbina, for serving on my thesis committee, and for his time and consideration in reading my work and providing his invaluable suggestions and insights. In addition, I am also thankful to him and all the other professors whose classes I have attended, and who made my master's journey more enriching.

I am thankful to the wonderful staff of the Electrical Engineering department, whose guidance and help I have required each of these four semesters to fulfil all my degree requirements, and for all the help I needed these last few weeks with finishing paperwork and setting up my defense. I would especially like to thank Mrs. SherryDawn Jackson, Mrs. Mariah Drapcho, Mrs. Katherine Koenig, Mrs. Lisa Timko, Mrs. Autumn Montegna-Maginnis, and Ms. Halie Gummo, for all their help.

I made some good friends along the way. My gratitude to Tarek, Sakib, Patrick, Terelle, and Anerudh, for the long hours spent over homeworks, which of course we mostly spent chatting.

Lastly, but most importantly, I owe inexpressible gratitude to my family, my mother Kauser Khwaja, my father Mohd. Javed Pervez, and my dear brother Faiz Pervez, who were there every step of the way, and to whom I am forever indebted.

This research was supported by the Atmospheric and Geospace Sciences (AGS) division of the National Science Foundation (NSF) grants AGS-1744099, and AGS-2010088 to The Pennsylvania State University. Any opinions, findings, and conclusions or recommendations expressed in this publication are those of the author and do not necessarily reflect the views of NSF.

Dedicated to
Amma, Abba, and Faiz

Chapter 1
Introduction

The study of the behavior of electrons in a weakly ionized gas under the influence of an external electric field is important for various industrial applications such as dielectric barrier discharges and their associated applications, e.g., construction of devices such as plasma display panels, and the study of physical phenomena such as streamers and large scale atmospheric discharges. The most well known example of such discharges is lightning. A group of lightning induced optical phenomena is known as transient luminous events (TLEs). These are a variety of large scale optical events occurring in the stratosphere, mesosphere, and lower thermosphere over a wide range of altitudes from about 15 to 110 km, in close conjunction with thunderstorm activity at tropospheric altitudes [*Pasko et al.*, 2012, and references therein]. Although eyewitness reports of TLEs above thunderstorms have been recorded for more than a century, the first image of one referred to as sprite was serendipitously captured only in 1989, during a test of a low-light television camera [*Franz et al.*, 1990]. Since then, several different types of TLEs have been documented and classified. These include relatively slow-moving fountains of blue light, known as 'blue jets', which emanate from the top of thunderclouds up to an altitude of 40 km; upward moving 'gigantic jets', which establish a direct path of electrical contact between thundercloud tops and the lower ionosphere; 'sprites' that develop at the base of the ionosphere and move rapidly downwards at speeds up to 10,000 km/s; 'halos', which are brief descending glows with a lateral extent of $\sim$ 40-70 km, that sometimes (but not always) are observed to accompany or precede more structured sprites [*Pasko*, 2006; *Pasko et al.*, 2012, and references therein]; and 'elves', which are doughnut shaped optical flashes induced by the electromagnetic pulses radiated by lightning discharges and can spread over 300 km laterally [e.g., *Fukunishi et al.*, 1996; *Inan et al.*, 1997]. Figure 1.1 shows a schematic of these TLEs.

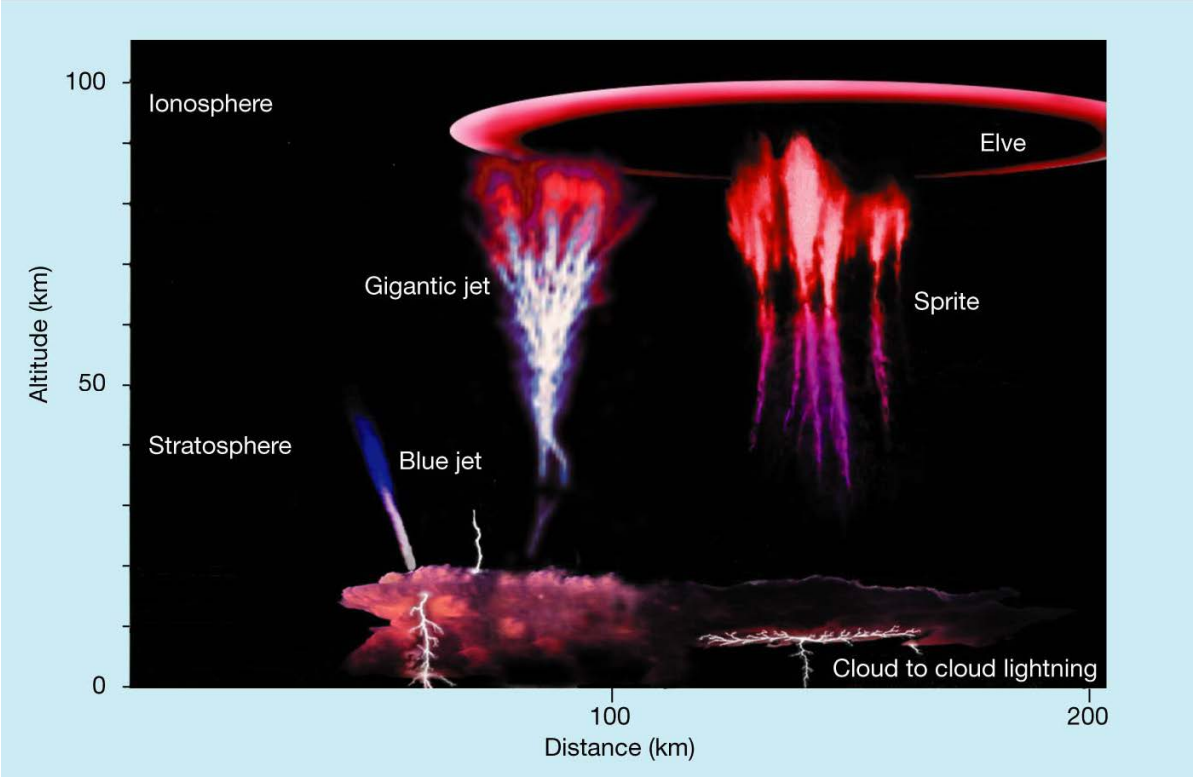

Figure 1.1. Lightning induced middle atmospheric transient luminous events including sprites, blue jets, elves, and gigantic jets [*Pasko*, 2003].

1.1 Motivation for current study

The carbon dioxide weakly ionized plasma is of significant interest, and a thorough understanding of the characteristics of carbon dioxide gas discharges is essential for numerous applications [e.g., *Pietanza et al.*, 2021, and references therein]. In particular, the development of streamer discharges in the presence of a strong magnetic field is of significant interest in the energy generation cycle of magnetohydrodynamic generators and in possible utilization of CO_2 in alternative renewable energy sources [*Starikovskiy et al.*, 2021]. It is also important for the possible utilization of CO_2 as an alternative to SF_6 as an insulator in high-voltage transmission and distribution networks due to its lower environmental impact [*Hernandez-Avila et al.*, 2002; *Seeger et al.*, 2017]. This understanding can also help study atmospheric discharges on planets with CO_2 dominant atmospheres, like Venus and Mars. Here we focus on weakly ionized gas only. The gas is assumed to be weakly ionized in a sense that electrons collide only with ambient neutral atoms or molecules and do not interact with other charged species. Although this thesis is mainly focused on CO_2 gas, we also discuss and present results for air, as it is of

primary importance for the study of atmospheric discharges on Earth. We also study the behavior of these discharges under the influence of an external magnetic field.

Since the first photographic discovery of TLEs in the Earth's atmosphere by *Franz et al.* [1990], numerous modeling and observational studies of them have been reported. These modeling studies require accurate simulation of the weakly ionized plasma encountered in lightning related discharges and also in the lower ionosphere. At the altitude of $\sim 85-100$ km in Earth's atmosphere TLEs known as elves are usually encountered. At these altitudes the geomagnetic field plays an important role, and its influence has to be included in any modeling study of the partially magnetized plasma. The importance of a magnetic field's influence can be inferred from the Hall parameter $\beta_{\mathrm{H}}(\varepsilon) = \omega_{\mathrm{ce}}/\nu_{\mathrm{m}}(\varepsilon)$ and the angle between the electric field and the magnetic field, hereafter denoted by $\angle\vec{E},\vec{B}$. The quantity denoted by ω_{ce} is the electron cyclotron frequency, defined as $q_{\mathrm{e}}B/m_{\mathrm{e}}$, and $\nu_{\mathrm{m}}(\varepsilon)$ is the effective momentum transfer collision frequency for an electron with energy ε. Here, q_{e} is the fundamental charge of an electron and m_{e} is the mass of an electron. A higher value of β_{H} indicates a stronger magnetic field influence. Also, the effect of the magnetic field of a particular strength is highest for $\angle\vec{E},\vec{B} = 90^{\circ}$ and absent for $\angle\vec{E},\vec{B} = 0^{\circ}$ [*Starikovskiy et al.*, 2021, equation (5)].

The studies of electromagnetic pulses associated with in-cloud processes has picked up pace over the past decade. These include energetic in-cloud pulses (EIPs), narrow bipolar events (NBEs) or compact intra-cloud discharges (CIDs). EIPs and NBEs are two distinct classes of intra-cloud (IC) discharges with very high peak current (> 200 kA) [*Lyu et al.*, 2015]. NBEs are IC discharges characterized by bipolar sferic waveforms of short durations ($10-30\,\mu$s) usually accompanied by very high frequency (VHF) radiation bursts [*Smith et al.*, 1999; *Soler et al.*, 2020]. Observations of positive NBEs suggest that they are corona discharges formed by streamers caused by IC discharges [*Soler et al.*, 2020]. EIPs, on the other hand, are a class of pulses of significantly longer time durantion. Furthermore, these pulses are not isolated, but instead, are typically associated with smaller discrete pulses that occur within a few millisecond time window [*Lyu et al.*, 2015]. A description of the salient features of these processes can be found in Table 1.1 [*Tilles et al.*, 2020, Table 1].

A 3-D finite difference time domain model is presented by *Marshall et al.* [2010] which simulates electromagnetic pulses and associated elves. This model accounts for the ambient geomagnetic field and concludes that the doughnut-shaped structure of elves exhibits asymmetry due to the presence of this magnetic field. *Marshall* [2012] improves this model by accounting for the Earth's curvature. It has been demonstrated that elves

Table 1.1. Salient features of some in-cloud processes [*Tilles et al.*, 2020]

Process	Description	Sferic and VHF
EIP (energetic in-cloud pulse)	High peak-current (>150 kA) relatively wide (∼50 μs) sferic, time-aligned with a subset of high-fluence TGFs; occurs after initial upward negative leader develops for several milliseconds and kilometers.	Sferic evolves independently of VHF activity.
NBE (narrow bipolar event)	Relatively narrow (∼10 μs) bipolar sferic; occurs in isolation or is a flash-initiating event; associated with lightning initiation; the most powerful natural terrestrial emitter of VHF.	VHF onset simultaneous with sferic.
FPB (fast positive breakdown)	Fast-propagating (10^7–10^8 m/s) positive breakdown; consists of a system of streamers; produces most NBEs. FPB is somehow involved in producing the EIP discharge.	VHF onset simultaneous with sferic.
FPB (fast negative breakdown)	Fast-propagating (10^7–10^8 m/s) negative breakdown; consists of a system of streamers; produces a small subset of NBEs. FNB is somehow involved in producing the EIP discharge.	VHF onset simultaneous with sferic.
IBP (initial breakdown pulse)	Relatively narrow (∼10 μs) bipolar sferic, sometimes superimposed by narrower (∼1 μs) subpulses; IBPs occur in trains starting about 1 ms after flash initiation and trains can continue for several milliseconds; associated with initial leader development.	VHF onset simultaneous with sferic.

may accompany terrestrial gamma ray flashes (TGFs) which are associated with EIPs [*Liu et al.*, 2017]. TGFs are brief bursts of energetic (up to tens of MeV) photons originating inside thunderstorms, lasting tens to hundreds of microseconds, and are generated as the result of bremsstrahlung radiation by relativistic runaway electrons [*Lehtinen et al.*, 1996; *Tilles et al.*, 2020]. The study of *Liu et al.* [2017] neglects the geomagnetic field, arguing that at $0.3E_{\mathrm{k}}$ electric field, where E_{k} is the conventional breakdown field, and 0.5 G magnetic field, $\beta_{\mathrm{H}} = 0.15$ at 85 km altitude and $\beta_{\mathrm{H}} \simeq 1$ at 90 km altitude. Satellite observations of TGFs with accompanying elves have also been recorded [*Bjørge-Engeland et al.*, 2022]. *Marshall et al.* [2015] demonstrates that elve doublets, which are elves occurring in pairs separated in time by 80-160 μs are the ionospheric signature of CIDs. However, as the authors note, the exclusion of the magnetic field fails to account for the asymmetry in elves [*Marshall et al.*, 2010]. Similarly, *Pérez-Invernón et al.* [2018] present a model for the study of elves and associated chemical changes in the mesosphere, but also ignore the geomagnetic field in model formulation, citing small values of $\angle\vec{E},\vec{B}$ ($< 45°$) at tropical latitudes.

The modeling of gas discharge phenomena requires electron transport and rate coefficients of electron impact processes, which depend on the electron velocity distribution function (EVDF). These coefficients are normally calculated by solving the Boltzmann equation for electrons, using the electron impact cross section data of all the species in the gas mixture. Although analytical solutions to the Boltzmann equation can be obtained in certain cases, most problems may only be solved numerically. A common approach is to use the classical two-term expansion [*Holstein*, 1946; *Hagelaar and Pitchford*, 2005; *Raizer*, 1991, p. 82-90], which solves for the electron energy distribution function (EEDF), which characterizes the energy dependence of the electron ensemble. The inclusion of a magnetic field $\vec{B}$ makes this problem more complicated. When $\vec{B} \neq 0$, it is possible to obtain an effective electric field E_{eff} which results in fluid coefficients similar to those obtained in exact form in presence of the original electric field $\vec{E}$ and magnetic field $\vec{B}$. We present a theory based on solution of Boltzmann kinetic equation for non-magnetized weakly ionized plasma to efficiently obtain electron rate and transport coefficients in a magnetized plasma for an arbitrary magnitude and direction of applied electric field $\vec{E}$ and magnetic field $\vec{B}$. The proposed method does not require the solution of the Boltzmann equation in magnetized plasma, where fluid coefficients generally vary as a function of reduced electric field E/N, reduced electron cyclotron frequency ω_{ce}/N, and angle $\angle\vec{E},\vec{B}$, where N is density of neutrals. The idea is to essentially reduce a problem with input parameters $(E/N, \omega_{\mathrm{ce}}/N, \angle\vec{E},\vec{B})$ to an equivalent problem with single input

parameter E_{eff}/N. This E_{eff} can then be used to calculate electron rate and transport coefficients for plasma fluid models. The validation of these solutions and comparison with recent work on CO_2 plasma [*Starikovskiy et al.*, 2021] represents one of the goals of this MS thesis. The new approach may be used in modeling of magnetized plasma encountered in the context of TLEs, e.g., sprite streamers in the atmosphere of Earth and Jupiter, in modeling the propagation of lightning's electromagnetic pulse in Earth's ionosphere, and in various laboratory and industrial applications of nonthermal plasmas [*Janalizadeh et al.*, 2023].

1.2 Kinetic theory of electrons in weakly ionized gas under influence of external electric field

In this section we present the basic theory that describes the behavior of electrons in a weakly ionized neutral gas under the influence of an external electric field. As already mentioned in Section 1.1, the gas is assumed to be weakly ionized in a sense that electrons collide only with neutral atoms or molecules and they do not interact with other charged species. In the rest of this thesis, the term 'plasma' implies weakly ionized plasma, unless specified otherwise. Our consideration allows us to account for complex effects of ionization and excitation of variety of degrees of freedom of the neutral gas upon electron impact as well as to calculate resultant electron distribution function (i.e., solve the Boltzmann equation). Here, we start with the definition of the electron velocity distribution function.

1.2.1 Electron velocity distribution function $f(\vec{r}, \vec{v}, t)$

Consider a single electron, which can be described by a position vector $\vec{r}$ in position space

$$\vec{r} = x\hat{i}_x + y\hat{i}_y + z\hat{i}_z \tag{1.1}$$

and a velocity vector $\vec{v}$ in velocity space

$$\vec{v} = v_x\hat{i}_x + v_y\hat{i}_y + v_z\hat{i}_z. \tag{1.2}$$

The combination of these two vectors $(\vec{r}, \vec{v})$ or the six coordinates (x, y, z, v_x, v_y, v_z) define the position of the electron in the phase space. We then define the electron velocity distribution function $f(\vec{r}, \vec{v}, t)$ such that $f(\vec{r}, \vec{v}, t)\, d\vec{r}\, d\vec{v}$ is the number of electrons at a

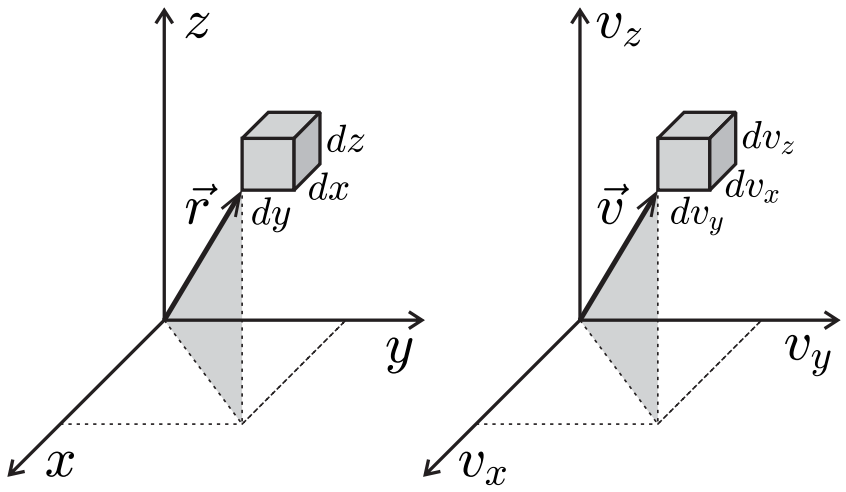

Figure 1.2. Left: The volume element $d\vec{r}$ at spatial position $\vec{r}$. Right: The equivalent volume element in velocity space $d\vec{v}$.

moment t in time in an element of volume $d\vec{r} = dx\,dy\,dz$ around a point $\vec{r}$, with velocity components from v_x to $v_x + dv_x$, v_y to $v_y + dv_y$, and v_z to $v_z + dv_z$, so that $d\vec{v} \equiv dv_x\,dv_y\,dv_z$. Figure 1.2 shows a representation of the volume element $d\vec{r}$ at spatial position $\vec{r}$, and the equivalent volume element in velocity space $d\vec{v}$. The integral of f over all velocity components equals electron density $n_\mathrm{e}(\vec{r}, t)$ [*Raizer*, 1991, p. 76]:

$$\int_{\vec{v}} f(\vec{r}, \vec{v}, t)\, d\vec{v} = \int_{v_x=-\infty}^{\infty} \int_{v_y=-\infty}^{\infty} \int_{v_z=-\infty}^{\infty} f(\vec{r}, \vec{v}, t)\, dv_x\, dv_y\, dv_z = n_\mathrm{e}(\vec{r}, t). \tag{1.3}$$

A particularly important model distribution function is the Maxwellian distribution [*Chen*, 2016, p. 212]:

$$f_\mathrm{M}(\vec{r}, \vec{v}, t) = n_\mathrm{e}(\vec{r}, t) \left(\frac{m_\mathrm{e}}{2\pi q_\mathrm{e} T_\mathrm{e}} \right)^{3/2} \exp\left(-v^2 / v_\mathrm{th}^2 \right) \tag{1.4}$$

in which

$$v = \left(v_x^2 + v_y^2 + v_z^2 \right)^{1/2}, \qquad v_\mathrm{th} = (2 q_\mathrm{e} T_\mathrm{e} / m_\mathrm{e})^{1/2}, \tag{1.5}$$

where T_e is temperature of electrons in eV (see [*Chen*, 2016, p. 4]), and v_th is the thermal velocity of electrons.

Since in the scenarios that we consider, we have an externally applied electric field $\vec{E}$, it is expedient to express velocity in terms of spherical coordinates, such that the vector $\vec{E}$ coincides with the polar axis. The vector $\vec{v}$ is characterized by its magnitude v, the angle ϑ it makes with the polar axis parallel to $\vec{E}$, and the azimuthal angle φ (see Figure

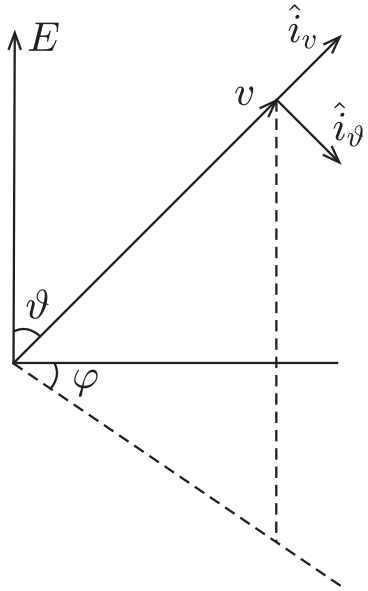

Figure 1.3. Velocity vector in spherical coordinates with $\vec{E}$ as the polar axis.

1.3). Subsequently, $d\vec{v} = v^2 dv d\Omega$, where $d\Omega = \sin\vartheta d\vartheta d\varphi$ is an element of solid angle around the direction of $\vec{v}$. It is easy to pass from the function $f(\vec{v})$ to a distribution function in energies, $P_0(\varepsilon)$, where ε is the energy of electrons in eV [*Raizer*, 1991, p. 76]:

$$P_0(\varepsilon)d\varepsilon = \frac{1}{n_\mathrm{e}} v^2 dv \int f(\vec{v}) d\Omega. \tag{1.6}$$

The function $P_0(\varepsilon)$ is normalized as

$$\int_0^\infty P_0(\varepsilon)\, d\varepsilon = 1 \tag{1.7}$$

and is hence called the electron probability distribution function. Its relation to $f(\vec{v})$ follows from the equality $\varepsilon = m_\mathrm{e} v^2 / 2q_\mathrm{e}$. From equations (1.4) and (1.6), for a Maxwellian distribution, the function $P_0(\varepsilon)$ is given by

$$P_{0_\mathrm{M}}(\varepsilon) = 2\left(\frac{\varepsilon}{\pi}\right)^{\frac{1}{2}} \frac{1}{T_\mathrm{e}^{\frac{3}{2}}} \exp\left(-\varepsilon/T_\mathrm{e}\right). \tag{1.8}$$

With the distribution function known, any quantity characterizing the electron gas can in principle be calculated, including all electron transport and rate coefficients. For instance, the frequency of ionization of neutrals with density N is given by

$$\nu_\mathrm{i} = N \int v \sigma_\mathrm{i}(\varepsilon) P_0(\varepsilon)\, d\varepsilon, \tag{1.9}$$

where σ_i is the electron impact ionization cross section of the neutral atoms or molecules. The total electric current density carried by electrons is [*Raizer*, 1991, p. 77]

$$\vec{j}_t = -q_\mathrm{e} \int \vec{v} f(\vec{v})\, d\vec{v}. \tag{1.10}$$

1.2.2 The Boltzmann equation for electrons

The distribution function for electrons $f(\vec{r}, \vec{v}, t)$ is governed by the Boltzmann equation:

$$\frac{\partial f}{\partial t} + (\vec{v} \cdot \nabla) f + \frac{1}{m_\mathrm{e}} (\vec{F} \cdot \nabla_v) f = C(f) \tag{1.11}$$

where $\vec{F}$ is the force acting on the electrons, $C(f)$ is the collision term which accounts for the dependence of f on particle collisions (see [*Loureiro and Amorim*, 2016, p. 101-104, 110-115] and [*Raizer*, 1991, p. 80-82, 88-90]), ∇ is the gradient operator in position space (x, y, z), and ∇_v is the gradient operator in velocity spce (v_x, v_y, v_z). In spherical coordinates we have

$$\nabla_v \equiv \hat{i}_v \frac{\partial}{\partial v} + \hat{i}_\vartheta \frac{1}{\vartheta} \frac{\partial}{\partial \vartheta} + \hat{i}_\varphi \frac{1}{v \sin \vartheta} \frac{\partial}{\partial \varphi} \tag{1.12}$$

A detailed derivation of equation (1.11) can be found in standard textbooks, e.g., [*Raizer*, 1991, p. 77-80], and [*Bittencourt*, 2004, p. 129-134]. Note that although the discussion here is for electrons, equation (1.11) is true for any species α in the gas if we simply replace f with f_α, and m_e with m_α.

If $\vec{F}$ is the Lorentz force, equation (1.11) becomes

$$\frac{\partial f}{\partial t} + (\vec{v} \cdot \nabla) f - \frac{q_\mathrm{e}}{m_\mathrm{e}} \left[(\vec{E} \times \vec{B}) \cdot \nabla_v \right] f = C(f) \tag{1.13}$$

For now we will consider $\vec{B} = 0$, such that

$$\frac{\partial f}{\partial t} + (\vec{v} \cdot \nabla) f - \frac{q_\mathrm{e}}{m_\mathrm{e}} (\vec{E} \cdot \nabla_v) f = C(f) \tag{1.14}$$

which is the Boltzmann equation for electrons under influence of an external electric field $\vec{E}$. If we consider a spatially uniform field, and also assume homogenous space, the electron distribution function f is then symmetric in velocity space around the electric field direction. In position space f may vary only along the field direction, which we place along the z axis [*Hagelaar and Pitchford*, 2005]. We can rewrite equation (1.14) in

spherical coordinates in velocity space as,

$$\frac{\partial f}{\partial t} + v\cos\vartheta\frac{df}{dz} - \frac{q_e E}{m_e}\left[\cos\vartheta\frac{\partial f}{\partial v} + \frac{\sin^2\vartheta}{v}\cdot\frac{\partial f}{\partial\cos\vartheta}\right] = C(f). \tag{1.15}$$

The electron distribution f in equation (1.15) depends on four coordinates: t, v, z and ϑ, and is independent of the angle φ because $\vec{E}$ defines an axis of symmetry.

We see from equation (1.15) that the distribution function f has dependence on the angle ϑ, i.e., the angle between $\vec{v}$ and $\vec{E}$. If the field were zero, f would be isotropic. The anisotropy in f is introduced by the fact that the field accelerates an excess of electrons in the direction opposite to $\vec{E}$ and shortage of those moving in the opposite direction. Assuming the field to be moderately strong, and the anisotropy caused by it to be small, we can represent f as a series expansion such that one term represents the isotropic part, and a second term represents the anisotropic part. This is done by making use of Legendre polynomials: $P_0 = 1, P_1 = \cos\vartheta$. We limit the series to the first two terms,

$$f(t,v,z,\vartheta) = f_0(t,v,z) + \vec{f_1}(t,v,z)\cdot\hat{i}_v = f_0(t,v,z) + f_1(t,v,z)\cos\vartheta. \tag{1.16}$$

The isotropic part f_0 determines the energy spectrum, since from equation (1.6), we have

$$P_0(\varepsilon)\,d\varepsilon = \frac{4\pi}{n_e}v^2 f_0(v)\,dv. \tag{1.17}$$

The anisotropic part $f_1\cos\vartheta$ determines the electric current. This current points along the field and its magnitude, from equations (1.10) and (1.16), is given by

$$j_t = -q_e\int\int v(\cos^2\vartheta)f_1 2\pi v^2\,dv\sin\vartheta\,d\vartheta = -\frac{4\pi}{3}q_e\int v^3 f_1\,dv. \tag{1.18}$$

Equations for f_0 and f_1 can be derived by making use of the orthogonality property of the Legendre polynomials. We first simply integrate equation (1.15) over the solid angle $d\Omega$ (since the zeroth polynomial $P_0 = 1$), and then we multiply equation (1.15) by $P_1 = \cos\vartheta$ and integrate again [e.g. *Raizer*, 1991, p. 82-87]. Following this procedure, we arrive at the following equation for f_0:

$$\frac{\partial f_0}{\partial t} = \frac{1}{3}\left(\frac{q_e}{m_e}\right)^2\frac{1}{v^2}\frac{\partial}{\partial v}\left[\frac{v^2}{\nu_m}E^2\frac{\partial f_0}{\partial v}\right] + C(f_0) \tag{1.19}$$

If, in addition, we consider the presence of an external magnetic field $\vec{B}$, we have the

following equation for f_{0_B}, [*Golant et al.*, 1980, p. 140]:

$$\frac{\partial f_{0_B}}{\partial t} = \frac{1}{3}\left(\frac{q_e}{m_e}\right)^2 \frac{1}{v^2}\frac{\partial}{\partial v}\left[\frac{v^2}{\nu_m}\left(\frac{E_\perp^2}{1+\beta_H^2} + E_\parallel^2\right)\frac{\partial f_{0_B}}{\partial v}\right] + C(f_{0_B}), \tag{1.20}$$

where the subscript 'B' in f_{0_B} denotes the presence of $\vec{B}$, $E_\parallel$ and $E_\perp$ are the components of $\vec{E}$ parallel and perpendicular to $\vec{B}$, respectively, and β_H is the Hall parameter as defined earlier.

1.2.3 Electron energy distribution function $F_0(\varepsilon)$

We earlier defined the electron probability distribution function $P_0(\varepsilon)$ in Section 1.2.1, which has units [eV^{-1}]. However, all results in this thesis were obtained using the Boltzmann equation solver BOLSIG+ [*Hagelaar and Pitchford*, 2005], which outputs the electron energy distribution function (EEDF) $F_0(\varepsilon)$ with units [eV$^{-3/2}$]. *Hagelaar and Pitchford* [2005] define $F_0(\varepsilon)$ in the following manner. Since $v = \gamma\varepsilon^{1/2}$, where $\gamma = (2q_e/m_e)^{1/2}$, we can represent $f_{0,1}(t, v, z)$ as $f_{0,1}(t, \varepsilon, z)$. The energy dependence of f can be separated from its dependence on time and space as

$$f_{0,1}(t, \varepsilon, z) = \frac{1}{2\pi\gamma^3}\, F_{0,1}(\varepsilon)\, n_e(t, z). \tag{1.21}$$

The energy distribution $F_{0,1}(\varepsilon)$ is constant in time and space. Substituting f_0 from equation (1.21) in equation (1.17), and using $v = \gamma\varepsilon^{1/2}$

$$P_0(\varepsilon) = \frac{4\pi}{n_e}\gamma^2\varepsilon\frac{1}{2\pi\gamma^3}F_0(\varepsilon)n_e\frac{dv}{d\varepsilon}. \tag{1.22}$$

Since,

$$v = \gamma\varepsilon^{\frac{1}{2}} \quad \Rightarrow \quad \frac{dv}{d\varepsilon} = \frac{\gamma}{2}\varepsilon^{-\frac{1}{2}} \tag{1.23}$$

$$\Rightarrow P_0(\varepsilon) = \frac{2\varepsilon}{\gamma}F_0(\varepsilon)\frac{\gamma}{2}\varepsilon^{-\frac{1}{2}} \tag{1.24}$$

$$\Rightarrow P_0(\varepsilon) = \varepsilon^{\frac{1}{2}}F_0(\varepsilon) \tag{1.25}$$

$$\Rightarrow F_0(\varepsilon) = \varepsilon^{-\frac{1}{2}}P_0(\varepsilon). \tag{1.26}$$

We finally note that $F_0(\varepsilon)$ is normalized as

$$\int_0^\infty P_0(\varepsilon)\, d\varepsilon = \int_0^\infty \varepsilon^{1/2}F_0(\varepsilon)\, d\varepsilon = 1. \tag{1.27}$$

1.2.4 Numerical solutions for air

Analytical solutions to equation (1.19) cannot be obtained without substantial assumptions and simplifications. For molecular gases, obtaining an analytical solution would be nearly impossible, since we would need to take into account the rotational and vibrational excitations of the molecules. Therefore, it is more common to solve equation (1.19) numerically. This requires cross section data of all the collisional processes involved. The greatest challenge in this regard is often the shortage of accurate cross section data.

We show numerical solutions of $F_0(\varepsilon)$ for air, which we consider to be a mixture of 78.11% molecular nitrogen N_2, 20.91% molecular oxygen O_2, and 0.98% argon Ar. These results were obtained using BOLSIG+. The cross section data were obtained from the consistent set of data that accompanies BOLSIG+. Figure 1.4 shows the EEDF $F_0(\varepsilon)$ on a semilogarithmic scale as a function of electron energy for air, for various values of the reduced field E/N. Also E/N has units of Townsend (Td), where $1\,\mathrm{Td} = 10^{-17}\,\mathrm{V\,cm^2}$.

From equations (1.8) and (1.26) we see that for a Maxwellian distribution, $F_0(\varepsilon)$ is

$$F_{0_\mathrm{M}}(\varepsilon) = \frac{2}{\pi^{\frac{1}{2}}\, T_\mathrm{e}^{\frac{3}{2}}} \exp\left(-\varepsilon/T_\mathrm{e}\right), \tag{1.28}$$

whose semilogarithmic plot is just a straight line, as seen in Figure 1.5, where a Maxwellian

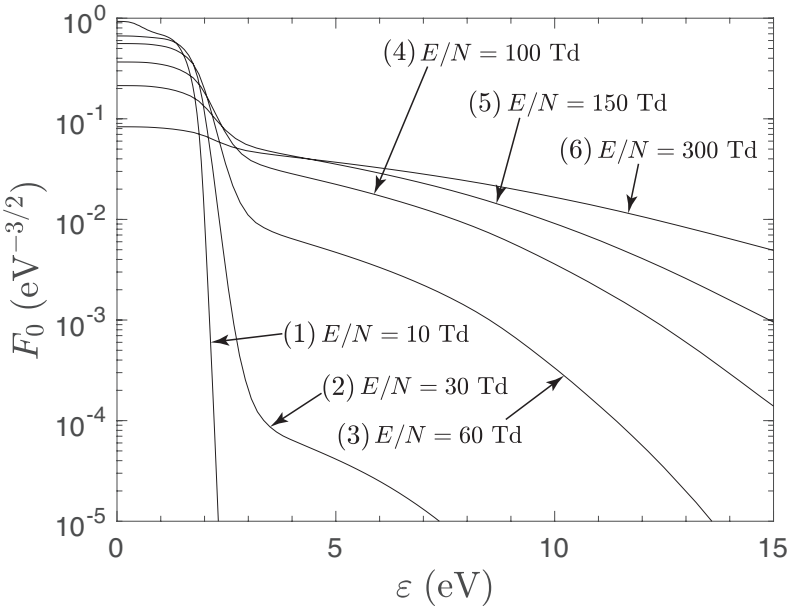

Figure 1.4. EEDF $F_0(\varepsilon)$ for air at various values of the reduced field E/N, where ε is energy of electrons in eV. The number in the parentheses refers to the corresponding Maxwellian distribution in Figure 1.5.

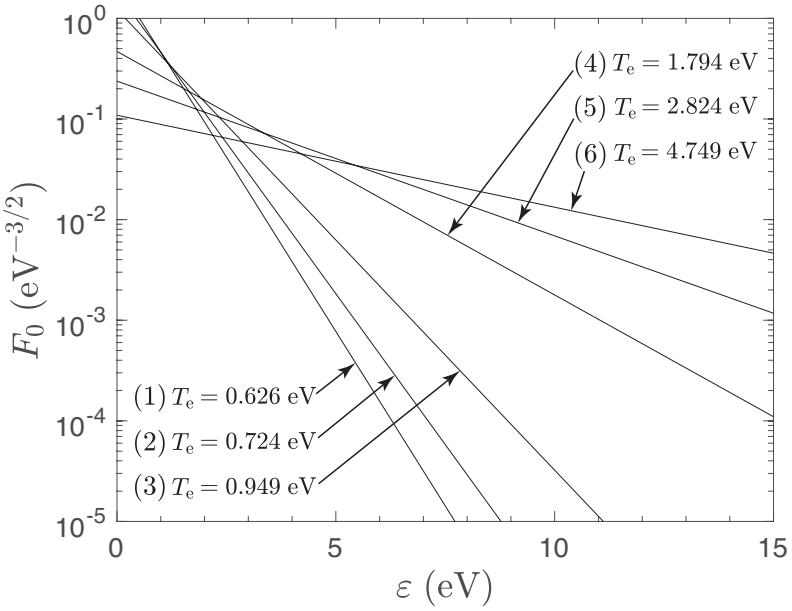

Figure 1.5. Maxwellian EEDF $F_0(\varepsilon)$ in air at various values of the reduced field E/N represented here by the corresponding electron temperature T_e. The number in the parentheses refers to the corresponding actual distribution in Figure 1.4.

distribution for air is assumed. This figure was plotted for values of electron temperature T_e in equation (1.28) which correspond respectively to the values of E/N in Figure 1.5. We can calculate these values of T_e, since for a Maxwellian distribution T_e is related to the mean energy of electrons ε_m via

$$\varepsilon_m = \frac{3}{2} T_e. \tag{1.29}$$

The mean energy ε_m is an output parameter of BOLSIG+. We note that for distributions significantly deviating from Maxwellian, expression (1.29) is an approximation. Figure 1.6 plots the exact $F_0(\varepsilon)$ outputted by BOLSIG+, and the Maxwellian $F_0(\varepsilon)$ for selected values of the reduced field. We see that for high values of the field the Maxwellian is a reasonable approximation to the exact EEDF, but at lower values it fails to approximate the exact EEDF.

We also present results for some electron transport and rate coefficients in air. Figures 1.7, 1.8, and 1.9 show electron mean energy ε_m, reduced electron mobility $\mu_e N/N_0$, and reduced electron impact ionization frequency $\nu_i N_0/N$, respectively, as a function of the reduced field EN_0/N. Note that $N_0 = 2.686 \times 10^{25}$ m^{-3} is the Loschmidt's number, which is the number of gas molecules in one cubic meter at 0 °C and one atmosphere pressure. We compare results from BOLSIG+ with those from a MATLAB

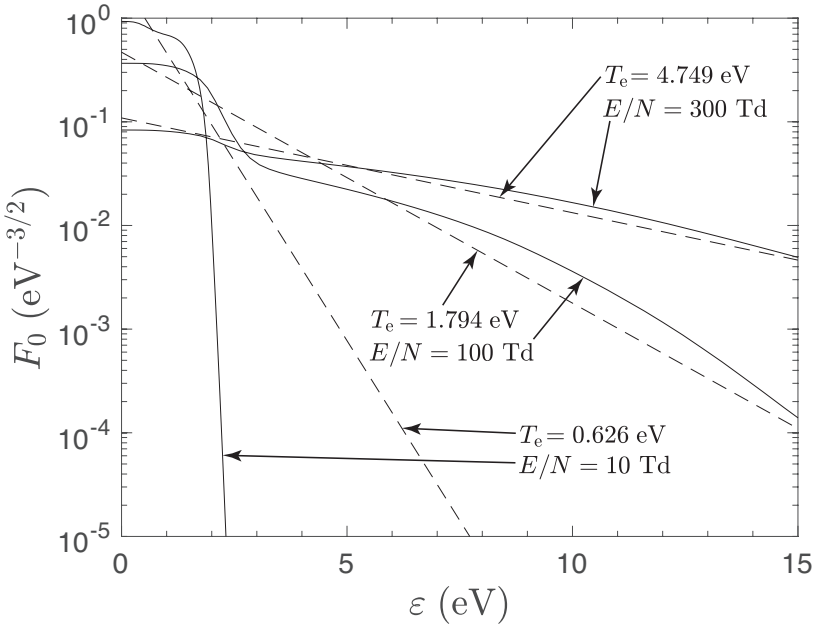

Figure 1.6. Exact distribution function $F_0(\varepsilon)$ calculated by BOLSIG+, and Maxwellian distribution with same electron mean energy for air at selected values of reduced field E/N.

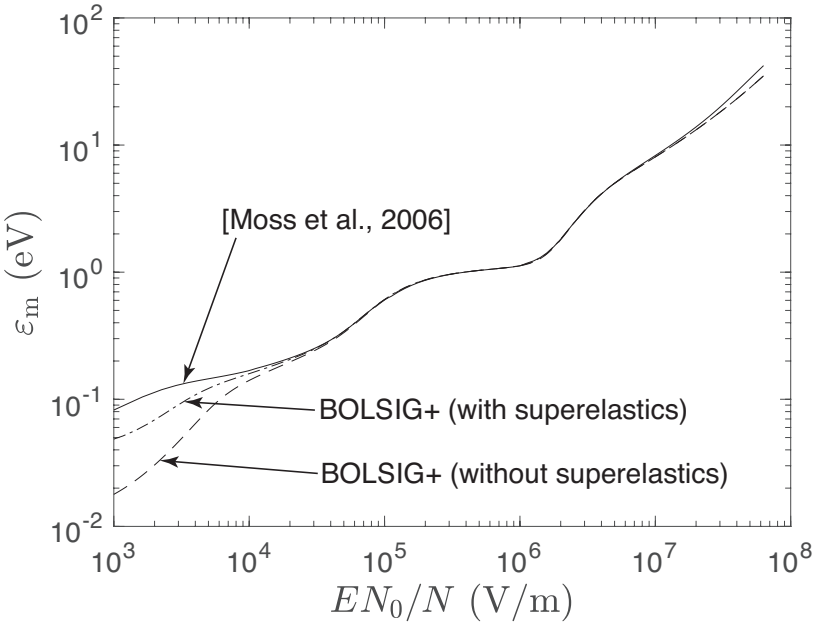

Figure 1.7. Electron mean energy ε_m in air as a function of reduced applied electric field EN_0/N.

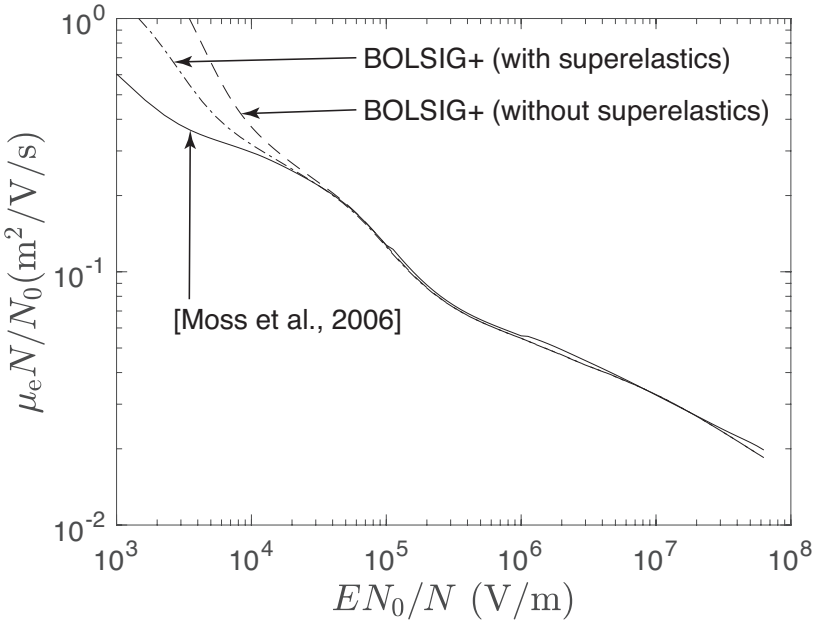

Figure 1.8. Reduced electron mobility $\mu_e N/N_0$ in air as a function of reduced applied electric field EN_0/N.

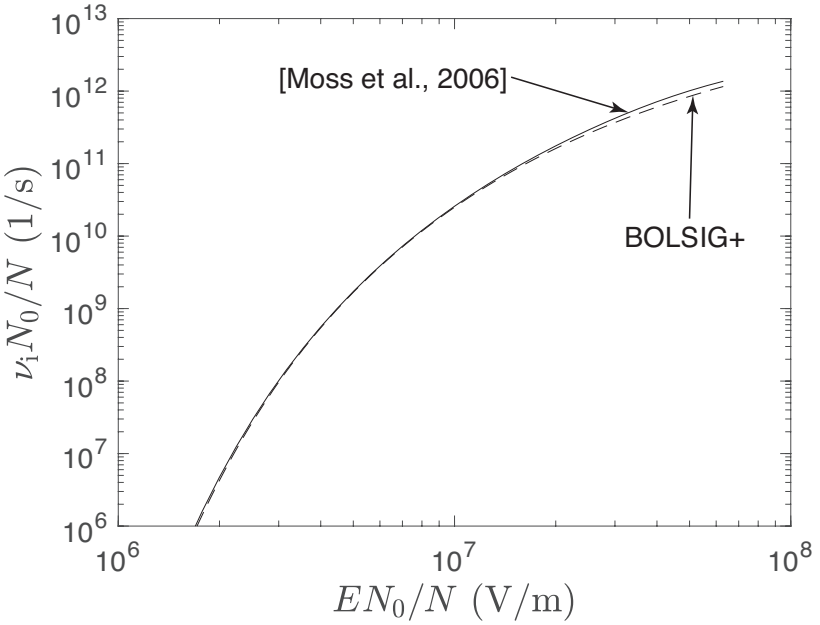

Figure 1.9. Reduced ionization frequency $\nu_i N_0/N$ in air as a function of reduced applied electric field EN_0/N.

function provided by *Moss et al.* [2006], referred to as `air1.m` (freely available at `http://pasko.ee.psu.edu/air`). This function is based on solutions from another Boltzmann equation solver, ELENDIF [*Morgan and Penetrante*, 1990]. Figures 1.7 and 1.8 show three plots each, one corresponding to results from `air1.m`, and the other two from BOLSIG+. We consider two cases for BOLSIG+, first with superelastic collisions excluded, and second with superelastic collisions included. When superelastic collisions were included, we set the associated BOLSIG+ input parameters to default values, i.e., excitation temperature was set to 300 K and transition energy to 0 eV. The results between BOLSIG+ and `air1.m` [*Moss et al.*, 2006] agree satisfactorily for both mean energy and mobility, except at very low applied reduced electric field ($EN_0/N < 2 \times 10^4$ V/m, or equivalently, $E/N < 1$ Td). At these low values of the reduced electric field, the results by BOLSIG+ with superelastics included have better agreement with `air1.m` compared to results by BOLSIG+ without superelastics. Figure 1.9 for the ionization frequency shows good agreement between BOLSIG+ and `air1.m` results. Here we ignore superelastic collisions since superelastics show up at low fields, and the lower limit of the reduced electric field for considerable ionization is much higher. At these higher values of reduced electric field electrons receive their energy from the field and the contribution of superelastic collisions is negligible, such that superelastic collisions do not affect the ionization rate.

1.3 Thesis components

This thesis is structured into five chapters. Below we provide a brief description of each chapter:

1. Chapter 1 introduces the scope and motivation of this work. It presents a description of certain areas of study which depend on the kinetics of electrons in a weakly ionized gas under the influence of an externally applied electric field, such as the study of TLEs. Some applications specific to CO_2, and a discussion of physical phenomena in the geophysical environment which include the study of plasma influenced by both the geomagnetic field and an external electric field are presented. This is followed by a section describing the kinetic theory of electrons, particularly the electron distribution function and the Boltzmann equation.

2. Chapter 2 presents a discussion of the kinetics of electrons in weakly ionized CO_2 plasma under the influence of an externally applied electric field. It contains a

survey of experimental data of electron swarm parameters for CO_2, numerical results obtained in the present study using BOLSIG+, and a comparison between the two sets of results.

3. Chapter 3 presents a theory to efficiently solve for electron transport and rate coefficients in weakly ionized magnetized plasma using a new method proposed in this thesis, that is hereafter referred to as the transcendental method. The chapter develops the transcendental method through a rigourous mathematical derivation. Results are presented for CO_2 to validate the accuracy of this method via comparison with the exact numerical solution of the Boltzmann equation obtained via BOLSIG+.

4. Chapter 4 extends results of the preceding chapter to weakly ionized magnetized plasma in air, and a 88% H_2 and 12% He mixture. These results are reproduced from [*Janalizadeh et al.*, 2023].

5. Chapter 5 summarizes the work completed in this thesis, and presents suggestions for future research based on obtained results.

1.4 Scientific contributions

The principal contributions presented in this thesis are as follows:

1. Compared experimental/numerical data on electron transport and rate coefficients such as mobility, diffusion, and ionization frequency in weakly ionized CO_2 plasma under the influence of external electric field with numerical solutions from kinetic theory. Performed survey of swarm experiments for CO_2 gas.

2. Developed efficient lookup representation and related MATLAB software based on solution of the Boltzmann equation for electrons in CO_2 which returns several major transport and rate coefficients of electrons in CO_2 for a broad range of input electric field in non-magnetized CO_2 plasma.

3. Developed a new approach to efficiently solve for plasma fluid coefficients in weakly ionized magnetized plasma with results consistent with exact solutions obtained from the Boltzmann equation via BOLSIG+. Also performed study of conditions required for convergence of the developed method to a solution, and described conditions for existence and uniqueness of a solution.

Chapter 2
Electron kinetics under an external electric field in CO_2 plasma

2.1 Introduction

A thorough understanding of the characteristics of CO_2 plasma is essential for numerous applications. We discussed some of these in Section 1.1. Additionally, advanced modeling and accurate experimental investigations have been recently developed to better understand the activation (dissociation) of CO_2 in non-equilibrium plasmas, with the aim to efficiently convert CO_2 in specific value-added chemicals. For this purpose, several types of non-equilibrium plasma discharges have been investigated to efficiently convert CO_2 into molecules with higher added value over a large range of pressures and frequencies [*Pietanza et al.*, 2021, and references therein]. To complement such studies we present here a discussion of transport and rate coefficients of electrons in weakly ionized CO_2 plasma. These transport and rate coefficients are obtained numerically by solving the Boltzmann equation governing the EVDF discussed previously in Section 1.2.2. We obtain these coefficients for a broad range of reduced electric field $E/N = 0$ to 4000 Td. As mentioned previously, the unit Townsend (Td) is defined as 1 Td $= 10^{-17}$ V cm^2. We also present a survey of experimental and numerical data on electron transport and rate coefficients in CO_2 and compare them with the results obtained in this study.

2.2 Survey of experimental data

The following section presents a review of the existing literature on experimental electron transport coefficients in CO_2 gas for electron swarms under the influence of a uniform

electric field. The measured quantities are presented as a function of the reduced electric field E/N, where N is the density of CO_2 molecules.

Experiments measuring electron swarm parameters in gases are generally carried out in drift tubes. Drift tubes have been serving as the principal sources of transport coefficient data for several decades. In these systems low density clouds or 'swarms' of electrons are created, which drift under the influence of an external electric field. Based on their operation principles drift tube experiments have three major types [*Vass et al.*, 2017]:

- Pulsed Townsend settings that consist of two plane-parallel electrodes. Electron swarms are usually initiated by fast UV light pulses that induce photoemission of electrons from the negatively biased electrode. Recordings are made of the time-dependent displacement current pulses.

- Time-of-flight settings that also employ pulsed electron sources and make use of the collection of particles that arrive at a detector, which can operate on the basis of different principles. In this case, the same transport coefficients can usually be determined as in pulsed Townsend settings.

- Steady-state Townsend settings that operate with continuous electron sources and provide information about the Townsend ionization coefficient via, e.g., the increase of electron current with increasing electrode separation.

Some of the earliest measurements of electron transport coefficients in CO_2 are provided in [*Bortner et al.*, 1957; *Bhalla and Craggs*, 1960; *Frommhold*, 1960]. In particular, *Bortner et al.* [1957] made measurements of the electron drift velocity in argon, nitrogen, methane, carbon dioxide, ethylene, cyclopropane, and a few mixtures of some of these gases. *Bhalla and Craggs* [1960] studied the growth of pre-breakdown currents in uniform field conditions in carbon dioxide at different pressures in the E/p range of 1200 to 26 V cm^{-1} Torr^{-1}, where p denotes the gas pressure. Experimental measurements of the Townsend ionization coefficient α and attachment coefficient η were made, and the mean cross sections for ionization and attachment were calculated. *Frommhold* [1960] measured electron drift velocities v_d primarily for nitrogen and hydrogen. However, some data for carbon dioxide are also presented. In addition, this paper gives details of some measurements of α, the electron diffusion coefficient D_e, and ionic drift velocities for certain gases.

Pack et al. [1962] measured v_d for various gases including carbon dioxide for E/p values between 2.5×10^{-4} and 30 V cm^{-1} Torr^{-1} at temperatures between 77 and 443 K.

Hasegawa et al. [1996] measured v_d and transverse diffusion coefficient of electrons D_T in carbon dioxide and nitrogen for E/N between 20 to 100 Td. Values of the momentum transfer cross section as a function of electron energy for electrons with energies between about 0.003 and 0.08 eV were obtained. *Schlumbohm* [1965] measured α and D_T from the analysis of oscillograms of electron avalanches for oxygen, methane, carbon dioxide, and some organic vapors at E/p values between some 100 and several 1000 V cm^{-1} Torr^{-1}. *Chatterton and Craggs* [1965] carried out experiments with a Bradbury electron filter apparatus to determine η in carbon dioxide, carbon monoxide, air and helium-oxygen mixtures. A Bradbury filter apparatus is a two electrode system in an RF field, and essentially measures the current collected at the anode. Different combination of two or three filters are placed between the electrodes. The filters are assumed to stop certain fractions of ions and electrons when they are inserted. These fractions alter when the RF field is switched on, which can be used to measure attachment and ionization [*Chatterton and Craggs*, 1961]. *Elford* [1966] provides measurements of v_d for E/N ranging from 0.3 to 21 Td. *Wagner et al.* [1967] and *Saelee et al.* [1977] used the time-of-flight method for the determination of D_e and v_d. *Roznerski and Leja* [1984] also used the time-of-flight method to measure v_d. *Lakshminarasimha et al.* [1974] measured the ratio of the transverse diffusion coefficient to electron mobility D_T/μ_e and α using current growth experiments. *Hernandez-Avila et al.* [2002] and *Chachereau et al.* [2016] used the Pulsed Townsend technique to measure v_d, α, D_T and the characteristic (or mean) energy of electrons D_T/μ_e. *Vass et al.* [2017] present the transport coefficients (v_d, D_T, and effective ionization frequency) in CO_2 measured under time-of-flight conditions over 15 Td $\leq E/N \leq$ 2660 Td in a scanning drift tube apparatus.

In addition, *Lowke and Parker* [1969], *Kucukarpaci and Lucas* [1979], and *Vojnović et al.* [2019] provide theoretical or computational solutions of the Boltzmann equation to obtain the transport coefficients. Specifically, *Lowke and Parker* [1969] present a theoretical solution, while *Kucukarpaci and Lucas* [1979], and *Vojnović et al.* [2019] performed Monte Carlo simulations to obtain the transport coefficients. *Vass et al.* [2017] also present results from various computational techniques in addition to the experimental results.

2.3 Cross sections for electron collisions with CO_2

The cross section data for CO_2 were obtained from the set of cross section data that accompanied BOLSIG+. This set includes cross section data for elastic collisions and

twelve inelastic collision processes for CO_2. It corresponds to the Morgan database of LXCat at www.lxcat.net, and was first published by [*Lowke et al.*, 1973]. We note that cross section data for rotational excitation of CO_2 is not included since its influence is very small in comparison to vibrational and electronic excitation of CO_2 [*Lowke et al.*, 1973; *Hake and Phelps*, 1967]. Table 2.1 lists all the collision processes for which cross section data is included in this study. We note that CO_2 molecules have three normal modes of vibration: symmetric stretching (v_1), bending (v_2), and antisymmetric stretching (v_3) [*Itikawa*, 2002]. The vibrational states are denoted by $v = (v_1\, v_2\, v_3)$, where v_1, v_2, and v_3 represent the vibrational quantum numbers of the symmetric-stretching, bending, and antisymmetric stretching modes, respectively.

Table 2.1. Molecular carbon dioxide (CO_2) collision processes

Collision Process	Reaction	Energy Loss (eV)	Threshold energy (eV)
Elastic	$e + CO_2 \rightarrow e + CO_2$	-	-
Vibrational excitation	$e + CO_2(v_1\, v_2\, v_3) \rightarrow e + CO_2(v_1'\, v_2'\, v_3')$		
	$(000) \rightarrow (010)$	0.083	0.083
	$(000) \rightarrow (020) + (100)$	0.167	0.167
	$(000) \rightarrow (001)$	0.291	0.291
	$(000) \rightarrow (0n0) + (n00)$	0.252	2.5
	$(000) \rightarrow (0n0) + (n00)$	0.339	1.5
	$(000) \rightarrow (0n0) + (n00)$	0.422	2.5
	$(000) \rightarrow (0n0) + (n00)$	0.505	2.5
	$(000) \rightarrow (0n0) + (n00)$	2.5	2.5
Dissociative attachment	$e + CO_2 \rightarrow CO + O^-$	3.85	3.85
Electronic excitation	$e + CO_2 \rightarrow e + CO_2^*$	7.0	7.0
	$e + CO_2 \rightarrow e + CO_2^*$	10.5	10.5
Ionization	$e + CO_2 \rightarrow CO_2^+ + 2e$	13.3	13.3

2.4 Numerical solution using BOLSIG+

We have used BOLSIG+ [*Hagelaar and Pitchford*, 2005] to solve for various transport and rate coefficients of CO_2 for E/N ranging from 0 to 4000 Td. These results were

compiled into a MATLAB function `bolsigco2.m` (see Appendix A), which uses linear interpolation to return a value for an arbitrary E/N within the given range.

2.4.1 Results

Figures 2.1, 2.2, and 2.3 show electron transport and rate coefficients obtained from `bolsigco2.m` compared to compiled experimental and numerical data. In particular, Figure 2.1 presents reduced electron mobility, $\mu_e N/N_0$ in comparison to data from [*Huxley and Crompton*, 1974; *Elford and Haddad*, 1980; *Roznerski and Leja*, 1984; *Vass et al.*, 2017]. The experimental data from [*Vass et al.*, 2017] goes up to $E/N = 2660$ Td, which is unusually high for such experimental studies. We note that their results agree well with the `bolsigco2.m` results for high E/N. For lower values of E/N the data from [*Huxley and Crompton*, 1974; *Elford and Haddad*, 1980] differ by $\sim 10\%$ from present results, but follow the same trend.

Figure 2.2 shows the reduced transverse diffusion coefficient $D_T N/N_0$. The experimental data for diffusion is more scattered compared to other transport coefficients. *Vass et al.* [2017] noted an uncertainty of 15% in the measurements for diffusion. Similarly,

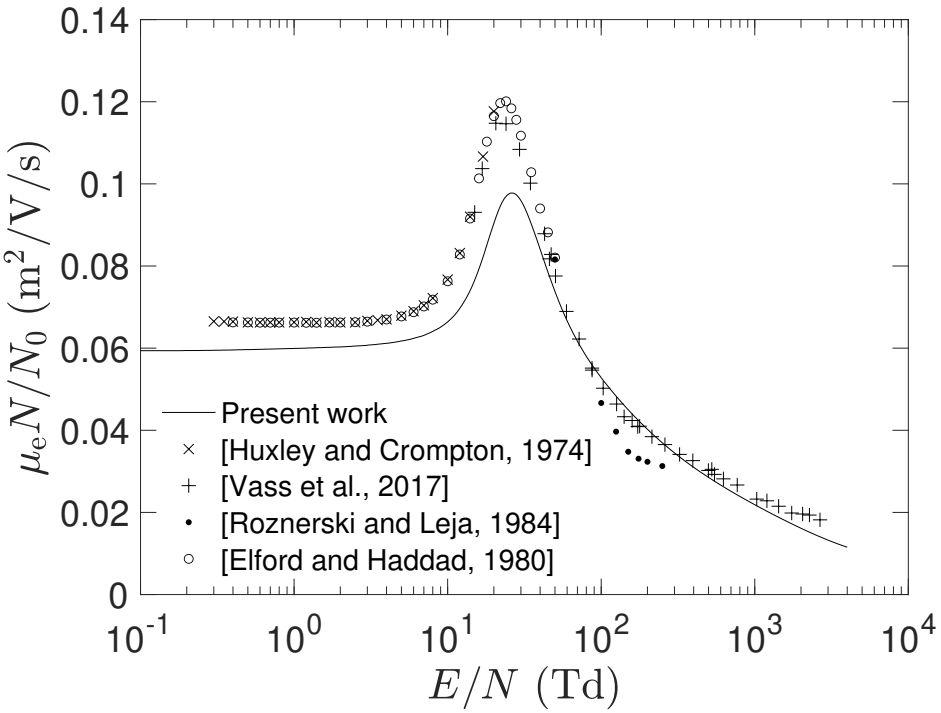

Figure 2.1. Reduced electron mobility $\mu_e N/N_0$ in weakly ionized CO_2 plasma as a function of reduced electric field E/N.

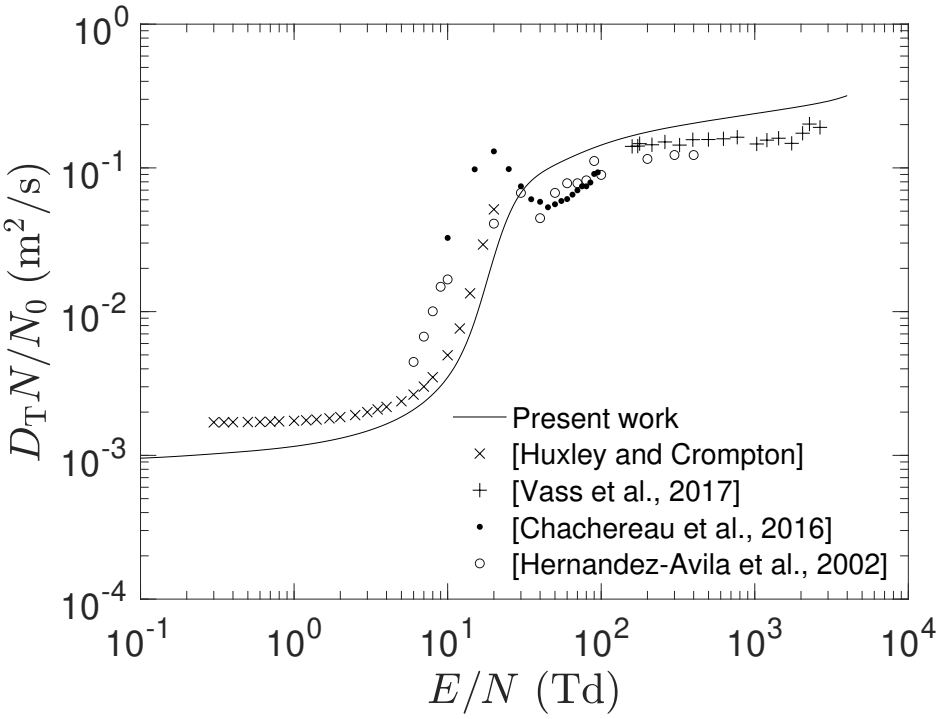

Figure 2.2. Reduced electron diffusion coefficient $D_{\mathrm{T}}N/N_0$ in weakly ionized CO_2 plasma as a function of reduced electric field E/N.

Hernandez-Avila et al. [2002] reports an uncertainty of 10%. The uncertainty for other transport coefficients such as v_{d} (or μ_{e}) and α is around 1-2%. We assume this also explains the non-monotonic behavior of $D_{\mathrm{T}}N$ seen in [*Hernandez-Avila et al.*, 2002; *Chachereau et al.*, 2016] for E/N between 10 and 100 Td.

Figure 2.3 shows the reduced effective ionization frequency $|\nu_{\mathrm{i}} - \nu_{\mathrm{a}}|N_0/N$ as a function of E/N, compared to experimental data from [*Hernandez-Avila et al.*, 2002; *Vass et al.*, 2017] and numerical data from [*Vojnović et al.*, 2019], which presents results obtained from a Monte Carlo simulation. We see that attachment is stronger than ionization for $E/N < 80$ Td, which is expected since electron-impact ionization has a high energy threshold (see Table 2.1) and at lower values of E/N fewer electrons have energy higher than this threshold. The value of the field where the ionization frequecy becomes equal to the attachment frequency is known as the breakdown electric field E_{k} [*Raizer*, 1991, p. 137], and we note that for CO_2, $E_{\mathrm{k}}/N \simeq 80$ Td. In conclusion, we note that the data from [*Hernandez-Avila et al.*, 2002; *Chachereau et al.*, 2016; *Vojnović et al.*, 2019] was digitized manually from the figures presented in these papers, which adds a small error to these data points. However, this should not be of much concern, since the general

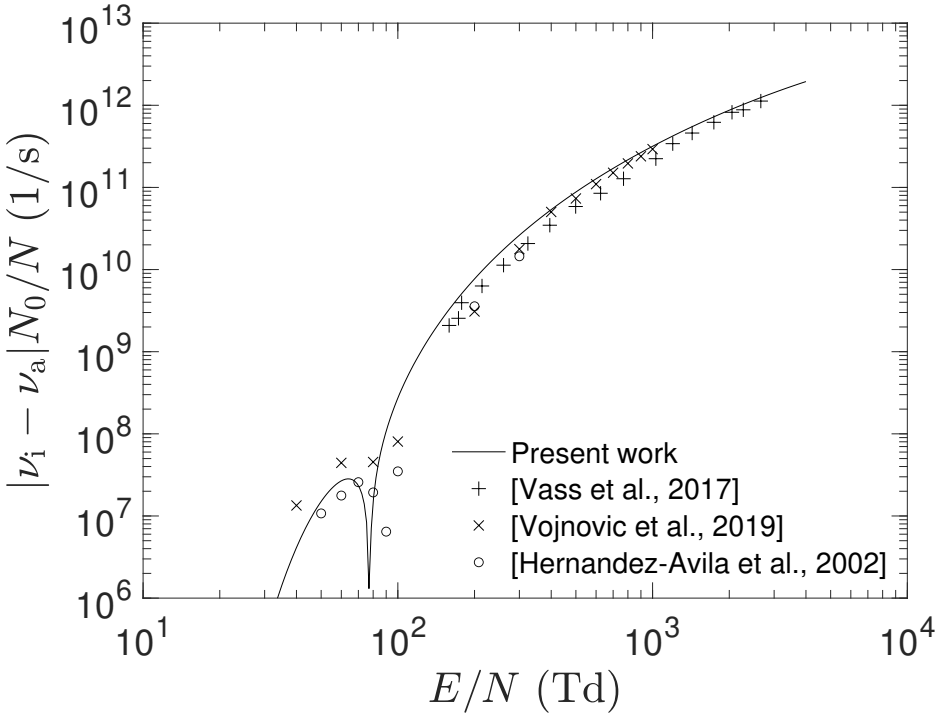

Figure 2.3. Reduced effective electron impact ionization frequency $|\nu_i - \nu_a|N_0/N$ in weakly ionized CO_2 plasma as a function of reduced electric field E/N.

trend still agrees well with our numerical results.

2.5 Conclusions

We obtain plasma fluid coefficients for weakly ionized CO_2 gas under the influence of an external electric field by numerically solving the Boltzmann equation for electrons in a broad range of reduced electric field using the publicly available solver BOLSIG+. The obtained coefficients agree well with experimental data from previous studies to within acceptable error, considering the uncertainties of experimental values. These results were compiled in a MATLAB function which can be used to efficiently compute these coefficients in plasma fluid models in future studies. In the next chapter we demonstrate practical use of these calculations, that do not include external magnetic field, for evaluation of transport and rate coefficients in magnetized plasma under influence of external magnetic field of arbitrary strength.

Chapter 3
Electron kinetics under an external electric field in magnetized CO_2 plasma

3.1 Introduction

The previous chapter discussed the kinetics of electrons under the influence of an external electric field in CO_2 plasma when there is no magnetic field ($\vec{B} = 0$). In this chapter we discuss electron kinetics under the influence of an external electric field when an external magnetic field is present (i.e., $\vec{B} \neq 0$). As discussed in Section 1.1, there are many instances where laboratory and modeling studies need to account for the effect of a magnetic field on plasmas. *Starikovskiy et al.* [2021] report the first plasma fluid model for magnetized streamer discharges. The authors study streamer propagation parallel to a magnetic field in pure CO_2. To the best of our knowledge, this is the only study which explores the influence of an external magnetic field on electron transport and rate coefficients in CO_2. In the context of the geophysical environment, the geomagnetic field plays an important role in the structure of elves. A three-dimensional finite difference time domain model that accounted for the effects of electron heating on electron mobility and for the asymmetry in the structure of elves due to the geomagnetic field was reported in [*Marshall*, 2009; *Marshall et al.*, 2010]. This asymmetry was not observed in studies which excluded the geomagnetic field [*Veronis et al.*, 1999; *Barrington-Leigh et al.*, 2001; *Kuo et al.*, 2007; *Liu et al.*, 2017; *Pérez-Invernón et al.*, 2018]. *Janalizadeh and Pasko* [2023] developed a numerical model for modeling of magnetized streamers in the presence of Jupiter's strong magnetic field. Similar to [*Starikovskiy et al.*, 2021], streamer

propagation was considered in a cylindrical coordinate system, where the magnetic field was parallel to the axis, and magnetized streamers were studied in the molecular hydrogen and atomic helium dominated atmosphere of Jupiter. *Janalizadeh and Pasko* [2023] demonstrate that in the presence of a magnetic field fluid coefficients of a weakly ionized plasma vary as a function of the reduced electric field E/N, reduced electron cyclotron frequency ω_{ce}/N, and the angle $\angle\vec{E},\vec{B}$ between the electric field $\vec{E}$ and the magnetic field $\vec{B}$ vectors. Here we present a new efficient method to calculate the electron transport and rate coefficients in magnetized plasma where the Boltzmann equation accounting for the Lorentz force with $\vec{B} \neq 0$ need not be solved. Instead an effective electric field, E_{eff}, can be evaluated such that the rate and transport coefficients are only a function of this new effective field. This essentially reduces the problem of magnetized plasma where $\vec{B} \neq 0$ to an equivalent problem in non-magnetized plasma where $\vec{B} = 0$.

We start this chapter with a discussion of the influence of a magnetic field on the electron energy distribution function in weakly ionized plasmas in Section 3.2. Due to $\vec{B} \neq 0$, electron fluid coefficients such as mean energy, mobility, and ionization frequency change in comparison to the non-magnetized case. We discuss results from [*Starikovskiy et al.*, 2021], and also introduce the concept of the Hall parameter, and how it describes the influence of a magnetic field on plasma characteristics. Section 3.3 presents an outline of the new transcendental method proposed, and how it can be implemented, with examples of solutions for CO_2 using this method, specifically comparing them with the results from [*Starikovskiy et al.*, 2021] where the authors obtained electron fluid coefficients in magnetized plasma by fitting analytical functions to lookup tables produced from electron rate and transport coefficients calculated by BOLSIG+. Section 3.4 presents a discussion on the question of convergence of the proposed transcendental method and the conditions which establish the existence and uniqueness of a solution. Section 3.5 sets the theoretical foundation required for the introduction of the effective electric field E_{eff} mentioned above and a more mathematically rigorous presentation of the method outlined in Section 3.3. Finally, Section 3.6 presents results for CO_2 and through comparison of some electron transport and rate coefficients with BOLSIG+ calculations corresponding to $\vec{B} \neq 0$, it is demonstrated that the proposed method and the magnetized plasma calculations of BOLSIG+ give consistent results.

The theory, results, and discussions in Sections 3.3-3.7 are originally presented in the paper [*Janalizadeh et al.*, 2023], submitted for publication to the Plasma Sources Science and Technology journal. In addition to the results we present here for CO_2, the paper presents corresponding results for air, and a mixture of 88% H_2 and 12% He (representing

the atmosphere of Jupiter and other giant gaseous planets of the solar system). For the sake of completeness, we show these additional results in the next chapter.

3.2 Magnetic field influence on electron plasma coefficients

The discussion in this section follows mostly from [*Starikovskiy et al.*, 2021, Section III]. The two-term expansion described in Section 1.2.2 to solve the Boltzmann equation for electron velocity/energy distribution function accounts for the presence of an external magnetic field by replacing the applied electric field by an effective electric field E_{eff}, given by [*Starikovskiy et al.*, 2021, equation (5)] (also see equation (1.20))

$$E_{\text{eff}}^2 = E_{\parallel}^2 + \frac{E_{\perp}^2}{1 + \beta_{\text{H}}^2(\varepsilon)}, \tag{3.1}$$

where $E_{\parallel}$ is the component of $\vec{E}$ parallel to $\vec{B}$, $E_{\perp}$ is the component of $\vec{E}$ perpendicular to $\vec{B}$, $\beta_{\text{H}}(\varepsilon) = \omega_{\text{ce}}/\nu_{\text{m}}(\varepsilon)$ is the Hall parameter, $\nu_{\text{m}}(\varepsilon) = Nv(\varepsilon)\sigma_{\text{m}}(\varepsilon)$ is the momentum transfer collision frequency for electrons with energy ε, $v(\varepsilon)$ is the magnitude of electron velocity, $\sigma_{\text{m}}(\varepsilon)$ is the electron momentum transfer cross section and N is the neutral gas density. The applicability of the two-term expansion to solving the Boltzmann equation for electron velocity/energy distribution function in presence of a strong magnetic field is discussed in [*Starikovskiy et al.*, 2021, Appendix A]. It is immediately clear that the magnetic field has no effect on electron behavior when $\angle\vec{E}, \vec{B} = 0°$, as in this case $E_{\perp} = 0$. However, if there exists a component of $\vec{E}$ that is perpendicular to $\vec{B}$ (i.e., $E_{\perp} \neq 0$), then according to equation (3.1) the effect of $E_{\perp}$ on the electron energy distribution function is reduced. This can be physically explained as follows. Electrons gain energy from the electric field in their movement between collisions, and lose energy during collisions with neutral particles. The magnetic field deflects electrons from their trajectories in the electric field and hence hinders their acceleration by the electric field. As a result we expect the electron energy distribution to reflect this physical behavior. This effect is strongest when $\angle\vec{E}, \vec{B} = 90°$ and $\beta_{\text{H}} \gg 1$. Here, the application of magnetic field inhibits electron heating by the electric field drastically and the effective electric field E_{eff} decreases substantially [*Starikovskiy et al.*, 2021].

Figure 3.1 shows the elastic electron impact momentum transfer cross section $\sigma_{\text{m}}(\varepsilon)$ for CO_2 and the corresponding $\beta_{\text{H}}(\varepsilon)$ as a function of electron energy for pressure $p = 50$

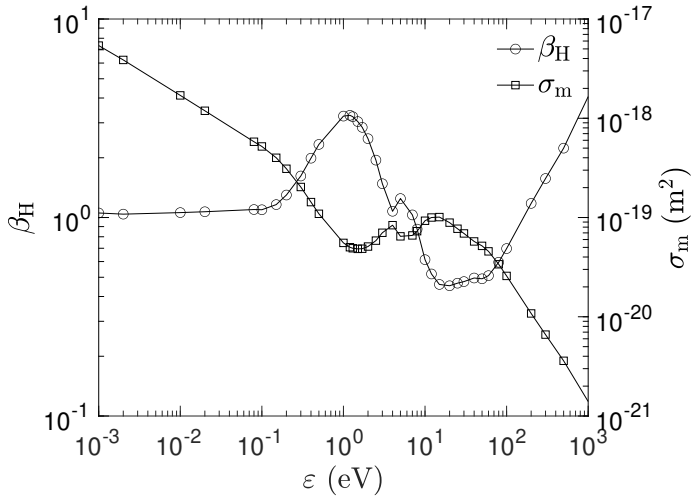

Figure 3.1. Electron impact momentum transfer cross section $\sigma_{\mathrm{m}}(\varepsilon)$ for CO_2 and the corresponding Hall parameter β_{H} as a function of electron energy at pressure $p = 50$ Torr, and magnetic field magnitude $B = 1$ T.

Torr, and $B = 1$ T. Since $\sigma_{\mathrm{m}}(\varepsilon)$ has a complex non-monotonic behavior as a function of ε, the same is reflected in the behavior of the Hall parameter. We see that the influence of the magnetic field is strongest for electrons with energy in the range $0.1 - 4$ eV, and weakest in the range $5 - 150$ eV. This figure has been created using momentum transfer cross section data from the Morrow database at `www.lxcat.net` and is an independent reproduction of [*Starikovskiy et al.*, 2021, Figure 2]. Figure 3.2 shows the EEDF for CO_2

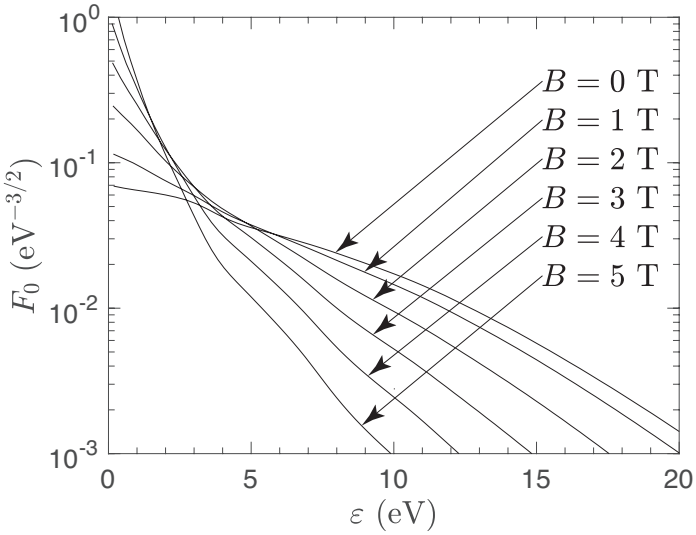

Figure 3.2. The EEDF $F_0(\varepsilon)$ in CO_2 at $E/N = 300$ Td, $p = 50$ Torr, room gas temperature, and various values of the magnetic field B when $\vec{E} \perp \vec{B}$.

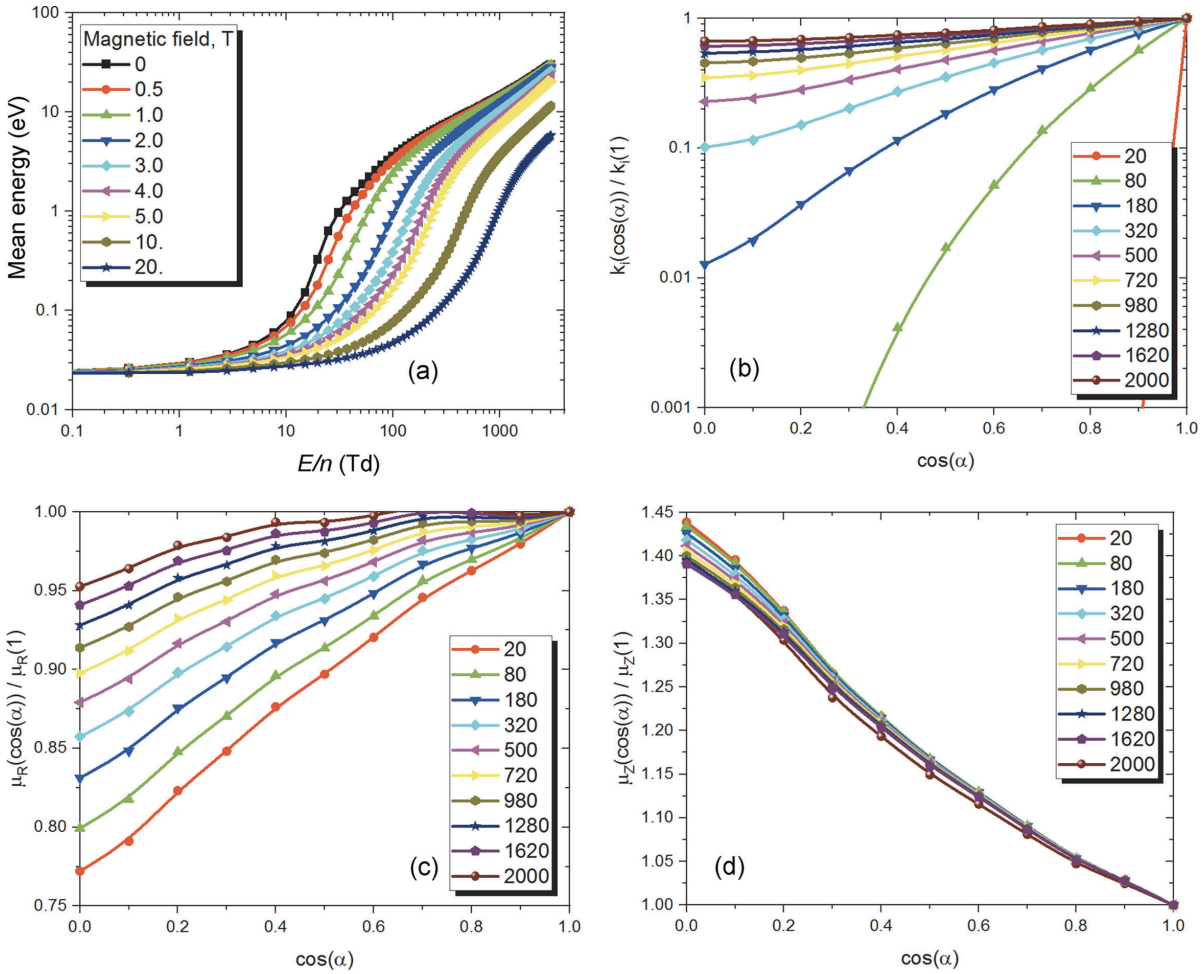

Figure 3.3. (a) Electron mean energy ε_m as a function of the reduced electric field E/N at various values of B, where $\angle\vec{E},\vec{B} = 90°$. (b) Electron-impact ionization rate coefficient $k_\mathrm{i} = \nu_\mathrm{i}/N$ normalized to $k_\mathrm{i}(\vec{E} \parallel \vec{B})$, (c) electron mobility perpendicular to the magnetic field $\mu_\perp$, normalized to $\mu_\perp(\vec{E} \parallel \vec{B})$, and (d) electron mobility parallel to the magnetic field $\mu_\parallel$, normalized to $\mu_\parallel(\vec{E} \parallel \vec{B})$, as a function of $\cos(\angle\vec{E},\vec{B})$ when $B = 3$ T, for various values of E/N [*Starikovskiy et al.*, 2021, Figure 4]. The difference in notation between the figure and this caption is explained in the text.

calculated at $E/N = 300$ Td, $p = 50$ Torr, room gas temperature, various values of the magnetic field B, and $\angle\vec{E},\vec{B} = 90°$. It is an independent reproduction of [*Starikovskiy et al.*, 2021, Figure 3]. The EEDF for high magnetic fields and $\varepsilon < 4$ eV shows a high rate of change, as compared to a more gradual rate of change for $\varepsilon > 4$ eV. The high energy tail of the EEDF falls off as the magnetic field is increased. The shape of the EEDF influences the electron transport and ionization rate coefficients.

Figure 3.3 shows the combined effects of the magnetic and electric fields on certain electron rate and transport coefficients. This figure has been taken directly from

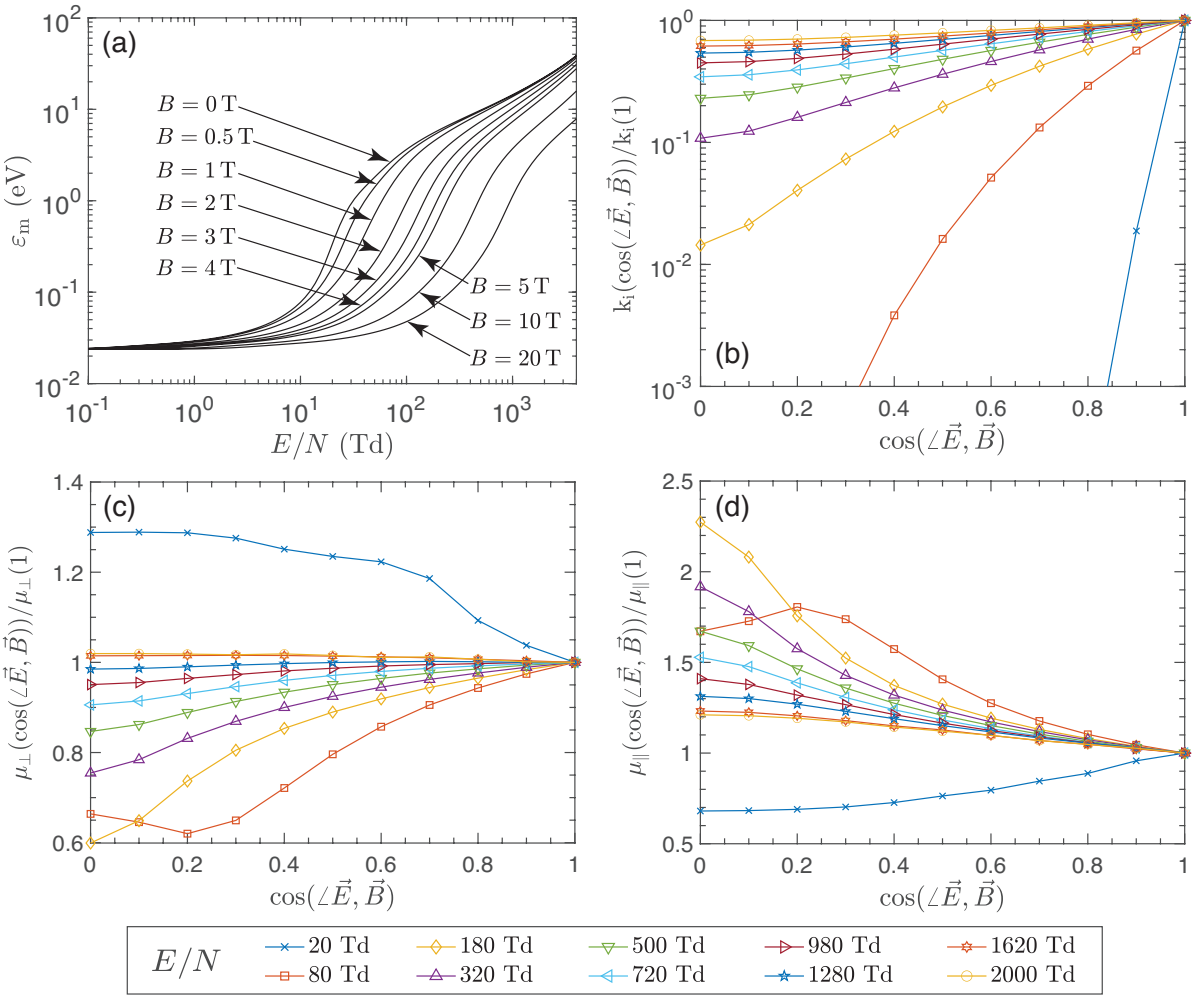

Figure 3.4. (a) Electron mean energy ε_m as a function of the reduced field E/N at various values of B, where $\angle\vec{E},\vec{B} = 90°$. (b) Electron-impact ionization rate coefficient $k_\mathrm{i} = \nu_\mathrm{i}/N$ normalized to $k_\mathrm{i}(\vec{E} \parallel \vec{B})$, (c) electron mobility perpendicular to the magnetic field $\mu_\perp$, normalized to $\mu_\perp(\vec{E} \parallel \vec{B})$, and (d) electron mobility parallel to the magnetic field $\mu_\parallel$, normalized to $\mu_\parallel(\vec{E} \parallel \vec{B})$, as a function of $\cos(\angle\vec{E},\vec{B})$ when $B = 3$ T, for various values of E/N .

[*Starikovskiy et al.*, 2021, Figure 4] to highlight certain differences between the results in this figure and the results we obtained in the process of replication, which are shown in Figure 3.4. We further note some difference in the notation between Figure 3.3 and the symbols we use in the current text. The angle α in Figure 3.3 corresponds to $\angle\vec{E},\vec{B}$, μ_R corresponds to mobility perpendicular to the magnetic field $\mu_\perp$, and μ_Z corresponds to mobility parallel to the magnetic field $\mu_\parallel$. Figure 3.3(a) demonstrates the effect of the magnetic field on electron mean energy ε_m for the case where $\angle\vec{E},\vec{B} = 90°$. We see that the mean energy rises with increasing E/N. However, this rise is retarded by the presence of the magnetic field. As described by *Starikovskiy et al.* [2021], for $B = 0$

T the mean energy reaches to 1 eV at $E/N \sim 31$ Td. The electric field required to reach $\varepsilon_m = 1$ eV rises to $E/N \sim 58$ Td for $B = 1$ T, $E/N \sim 147$ Td for $B = 3$ T, and $E/N \sim 960$ Td for $B = 20$ T. We note that the results in Figure 3.3(a) and 3.4(a) are identical. A reduction in the electron mean energy would naturally lead one to expect a decrease in the rate of ionization by electron impact, since fewer electrons would posses the energy to cause ionization on impact with a neutral, and this decrease would be most significant when the magnetic field is perpendicular to the electric field ($\angle\vec{E}, \vec{B} = 90°$). This is reflected in Figures 3.3(b) and 3.4(b), which show the ionization rate coefficient $k_i = \nu_i/N$ as a function of the cosine of $\angle\vec{E}, \vec{B}$, normalized by k_i at $\angle\vec{E}, \vec{B} = 0°$ for $B = 3$ T. The magnetic field has no effect on the ionization rate when $\angle\vec{E}, \vec{B} = 0°$. The rate of ionization for an ionization wave propagating across the magnetic field is lower by two orders of magnitude at $E/N = 180$ Td, and one order of magnitude lower at $E/N = 320$ Td. This effect becomes less prominent at higher electric fields, but is still quite significant, as k_i drops by a factor of ~ 0.5 even at an electric field as high as $E/N \sim 1000$ Td. Panel (b) of Figures 3.3 and 3.4 also agree quite well, except for the case of $E/N = 20$ Td, where the decrease in k_i is much sharper in Figure 3.3(b) compared to our results in Figure 3.4(b).

Panels (c) and (d) of Figures 3.3 and 3.4 show electron mobilities perpendicular ($\mu_\perp$) and parallel ($\mu_\parallel$) to the magnetic field, respectively, as a function of the cosine of $\angle\vec{E}, \vec{B}$, normalized to their values at $\cos(\angle\vec{E}, \vec{B}) = 1$. These results of [*Starikovskiy et al.*, 2021] are not in perfect agreement with our calculations (see Figure 3.4). Specifically, from Figure 3.4(c) we see that $\mu_\perp$ decreases in the presence of a magnetic field as E/N rises from 80 to 1280 Td. This decrease becomes greater as $\angle\vec{E}, \vec{B}$ increases, except for $E/N = 80$ Td where the lowest value for $\mu_\perp$ occurs when $\cos(\angle\vec{E}, \vec{B}) = 0.2$. Figure 3.3(c) does not reflect the same behavior at $E/N = 80$ Td. Also, Figure 3.4(c) shows that when $E/N = 20$ Td or when $E/N = 1620 - 2000$ Td, $\mu_\perp$ in the presence of magnetic field $B = 3$ T rises with increase of $\angle\vec{E}, \vec{B}$. The increase in $\mu_\perp$ is around 20% for the former case when $\angle\vec{E}, \vec{B} = 90°$, but is negligible for the latter case of high electric fields. This observation is not reflected in Figure 3.3(c) either.

From Figure 3.4(d), we see that the electron mobility parallel to the magnetic field, $\mu_\parallel$, shows an increase with the angle $\angle\vec{E}, \vec{B}$ when the magnetic field $B = 3$ T. The only exception to this rule is found to be when the electric field is very low ($E/N = 20$ Td) where the effect of the magnetic field is reverse of what is seen at higher electric fields. Also the greatest difference between $\mu_\parallel(\cos(\angle\vec{E}, \vec{B}))$ and $\mu_\parallel(\vec{E} \parallel \vec{B})$ for $E/N = 80$ Td is seen at $\cos(\angle\vec{E}, \vec{B}) = 0.2$, which was expected based on the results for $\mu_\perp$. We see

that the behavior discussed for $E/N = 80$ and 20 Td is not reflected in Figure 3.3. Also Figure 3.4(d) indicates a stronger dependence of $\mu_{\|}$ on the electric field compared to Figure 3.3(d).

3.3 The transcendental method to model magnetized plasma

We mentioned in Section 3.1 that in the presence of a magnetic field fluid coefficients of a weakly ionized plasma vary as a function of the reduced electric field E/N, reduced electron cyclotron frequency ω_{ce}/N, and the angle $\angle\vec{E},\vec{B}$ between the electric field $\vec{E}$ and the magnetic field $\vec{B}$ vectors [*Janalizadeh and Pasko*, 2023, and references therein]. Following *Starikovskiy et al.* [2021], one may dramatically reduce the execution time of a fluid model for magnetized plasma by fitting analytical functions to lookup tables produced from electron rate and transport coefficients calculated by BOLSIG+. In an alternative approach, however, it is possible to use electron rate and transport coefficients corresponding to an effective electric field E_{eff} in non-magnetized plasma (i.e., $\vec{B} = 0$) to deduce plasma fluid coefficients for the magnetized case (i.e., $\vec{B} \neq 0$). The electron transport and rate coefficients for various gas mixtures for non-magnetized case (i.e., $\vec{B} = 0$) are commonly represented as a function of reduced electric field E/N using various fits with analytical functions or lookup tables. These are usually formulated using a combination of solution of Boltzmann equation, swarm experiments, and Monte Carlo simulations, and are readily available to modelers. The idea behind the proposed transcendental method is that these $\vec{B} = 0$ representations can be directly used to obtain transport and rate coefficients for arbitrary magnitude and direction of applied magnetic field $\vec{B} \neq 0$. We note that ideas of self-consistently accounting for electron momentum transfer collision frequency varying as a function of applied electric field in evaluation of electron conductivity tensor in weakly ionized plasmas have appeared in previous publications [*Pasko et al.*, 1998; *Marshall*, 2009; *Marshall et al.*, 2010; *Kabirzadeh et al.*, 2015; *Salem et al.*, 2016; *Tonev and Velinov*, 2016]. However, these approaches have not been rigorously justified.

While a rigorous formulation and discussion of the validity of the proposed transcendental method follows in Sections 3.5 and 3.6, here we focus on the implementation of an approximation to the general transcendental method to illustrate and emphasize the accuracy and efficiency of the transcendental method in its simplest form. We begin by

introducing an effective Hall parameter β_{eff}, and replacing β_{H} in equation (3.1) with this new β_{eff}. We define $\beta_{\text{eff}} = (\omega_{\text{ce}}/N)/(\nu_{\text{m}}/N)$, where $\nu_{\text{m}} = q_{\text{e}}/m_{\text{e}}\mu_{\text{e}}(E_{\text{eff}})$, and $\mu_{\text{e}}(E_{\text{eff}})$ is only a function of the effective electric field E_{eff}. This μ_{e} is equivalent to the electron mobility parallel to the magnetic field $\mu_{\parallel}$, in the sense that when $\vec{B} = 0$, we have $\mu_{\text{e}} = \mu_{\parallel}$. The key idea here is that as opposed to $\beta_{\text{H}}(\varepsilon)$, which is a function of electron energy ε, this new β_{eff} is only a function of E_{eff}. The effect of the magnetic field is incorporated in ω_{ce}/N. We note that ω_{ce}/N depends only on the initial parameters of the problem (i.e., B and N), and for a particular external magnetic field is a constant in the problem formulation. Hence, we have a new transcendental equation for E_{eff}

$$E_{\text{eff}}^2 = E_{\parallel}^2 + \frac{E_{\perp}^2}{1 + \beta_{\text{eff}}^2(E_{\text{eff}})}. \tag{3.2}$$

The only unknown in this equation now is E_{eff}. Hence, we can solve it numerically for E_{eff}, given that we have a way to quantify β_{eff}, or equivalently $\mu_{\parallel}$ (since $\beta_{\text{eff}} = \omega_{\text{ce}}/(q_{\text{e}}/m_{\text{e}}\mu_{\parallel}) = B\mu_{\parallel}$) for some E_{eff}.

There are a number of sources available that may be used to calculate electron mobility and rate coefficients in various gas mixtures. For instance, *Aleksandrov et al.* [1995] provide simple analytical functions to calculate ionization cofficients, attachment coefficients, and various excitation coefficients for N_2 and O_2 in air. Similarly, in addition to electron mobility in air, *Morrow and Lowke* [1997] provide analytic functions for electron impact collision rate constants, which were used in previous modeling of streamers in air [e.g., *Bourdon et al.*, 2007; *Jánský and Pasko*, 2020]. Additionally, *Moss et al.* [2006] provide a MATLAB function `air1.m` compiled from the results of ELENDIF [*Morgan and Penetrante*, 1990], which returns electron mobility and mean energy in addition to rate coefficients for various electron impact processes in air. This function is freely available at `http://pasko.ee.psu.edu/air`. There are similar MATLAB functions based on BOLSIG+ [*Hagelaar and Pitchford*, 2005] for air [*Janalizadeh and Pasko*, 2020], Jupiter's atmosphere [*Janalizadeh and Pasko*, 2023], and CO_2 (`bolsigco2.m`, see Appendix A).

Equation (3.2) is a transcendental equation for E_{eff} and may be solved for E_{eff} using electron mobility given by the functions mentioned above to quantify β_{eff}. Once the value of E_{eff} which satisfies equation (3.2) is obtained, the kinetics of electrons under the influence of $(E/N, \omega_{\text{ce}}/N, \angle\vec{E}, \vec{B})$ is converted to an equivalent problem with $(E_{\text{eff}}/N, \vec{B} = 0)$. The electron rate and transport coefficients may then be calculated using the functions above, which were developed for non-magnetized plasma. In particular, the perpendicular and Hall mobilities may be obtained via $\mu_{\perp} = \mu_{\parallel}/(1 + \beta_{\text{eff}}^2)$ and

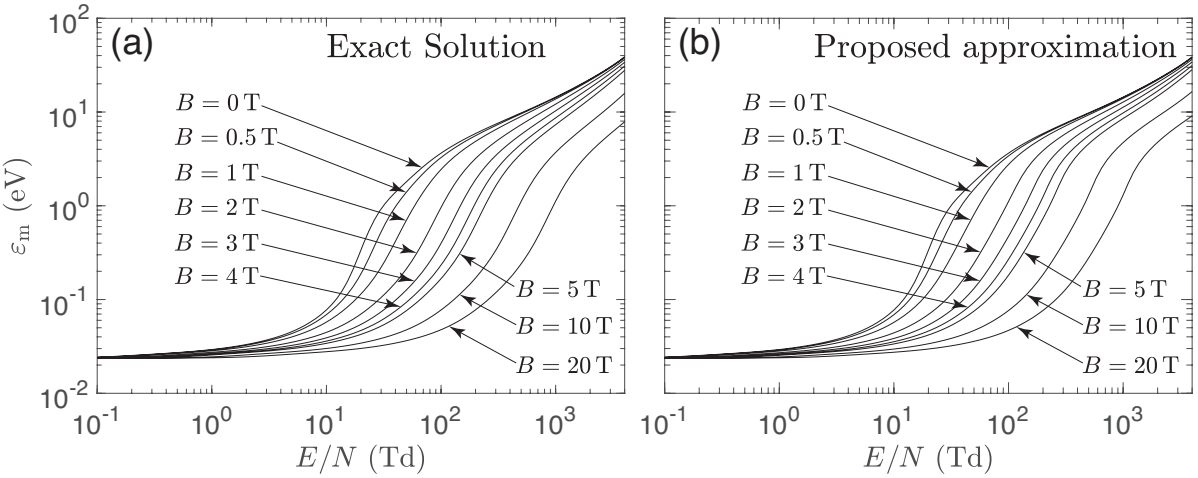

Figure 3.5. Electron mean energy ε_m as a function of the applied reduced electric field E/N calculated using (a) BOLSIG+, and (b) the proposed transcendental method for various values of the magnetic field B in pure CO_2 when $\vec{E} \perp \vec{B}$. Panel (a) is an independent reproduction of [*Starikovskiy et al.*, 2021, Figure 4(a)], and is the same as Figure 3.4(a).

$\mu_\mathrm{H} = \mu_\times = \mu_\parallel \beta_\mathrm{eff}/(1+\beta_\mathrm{eff}^2)$, respectively.

Figure 3.5(a) depicts electron mean energy ε_m in magnetized CO_2 plasma obtained directly using BOLSIG+ with accurate inclusion of external magnetic field, while Figure 3.5(b) depicts same results calculated using the proposed transcendental method (i.e., equation (3.2)). It may be inferred that the proposed transcendental method provides results in satisfactory agreement with BOLSIG+'s exact calculations. We note that Figure 3.5(a) is the same as Figure 3.4(a), which is an independent reproduction of Figure 3.3(a) [*Starikovskiy et al.*, 2021, Figure 4(a)], where the authors also use BOLSIG+ to calculate electron mean energy. Here we have replaced panels (b)-(d) of Figure 3.4 since the respective ionization frequency ν_i, electron mobility parallel to the magnetic field vector $\mu_\parallel$, and electron mobility perpendicular to the magnetic field vector $\mu_\perp$ are presented as dimensionless quantities there. Instead, in Figure 3.6 we compare results of BOLSIG+ and the transcendental method for ε_m, ν_i, $\mu_\parallel$, and $\mu_\perp$, as a function of $\angle\vec{E},\vec{B}$. Here the applied electric field $E = 1.5E_k$, where $E_k/N \simeq 80$ Td ($1\,\mathrm{Td} = 10^{-17}\,\mathrm{V\,cm^2}$), is the reduced breakdown electric field [*Raizer*, 1991, p. 137] in pure CO_2 calculated via BOLSIG+ (also see Figure 2.3). The values of reduced electron cyclotron frequency used for the calculations are $(\omega_\mathrm{ce}/N)_1 = 10^{-14}$, $(\omega_\mathrm{ce}/N)_2 = 10^{-13}$, and $(\omega_\mathrm{ce}/N)_3 = 10^{-12}$ rad $\mathrm{m^3\ s^{-1}}$. As seen later in Section 3.6, this interval of ω_ce/N covers the entire range between non-magnetized ($\beta_\mathrm{eff} \ll 1$) and highly ($\beta_\mathrm{eff} \gg 1$) magnetized electrons, and consequently it is demonstrated in Figure 3.6 that the results from the two methods are in satisfactory agreement in the entire range of magnetized CO_2 plasma. We also note

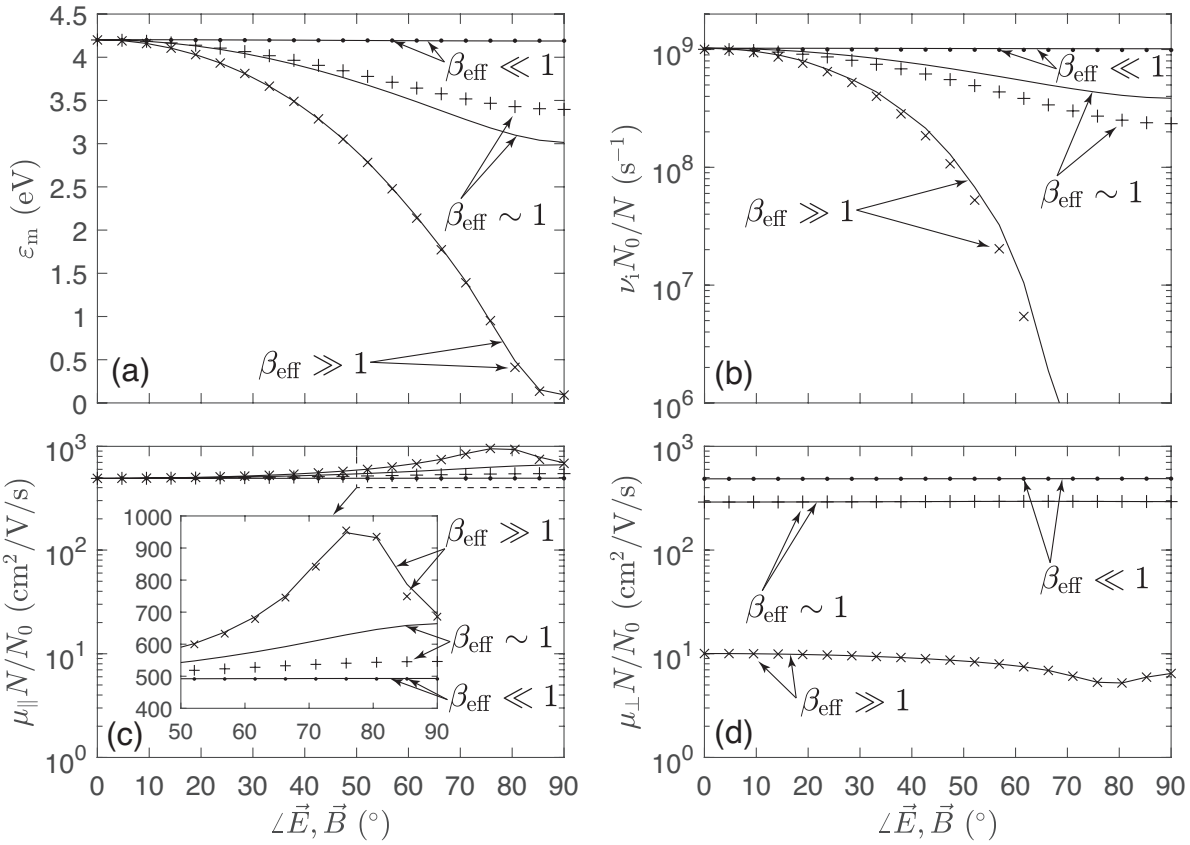

Figure 3.6. (a) Electron mean energy ε_m, (b) reduced electron-impact ionization frequency $\nu_i N_0/N$, (c) reduced electron mobility parallel to magnetic field $\mu_\parallel N/N_0$, and (d) reduced electron mobility perpendicular to magnetic field $\mu_\perp N/N_0$ as a function of the angle between the electric field $E = 1.5E_k$ ($E_k = 80$ Td) and the magnetic field calculated for $(\omega_{ce}/N)_1 = 10^{-14}$ rad m^3 s^{-1} (•), $(\omega_{ce}/N)_2 = 10^{-13}$ rad m^3 s^{-1} (+), and $(\omega_{ce}/N)_3 = 10^{-12}$ rad m^3 s^{-1} (×) in pure CO_2 gas. Solid lines denote the exact solutions and markers denote the proposed transcendental method solutions. The Loschmidt number $N_0 = 2.686 \times 10^{25}$ m^{-3} and similar to [*Starikovskiy et al.*, 2021] simulations are performed at $p = 50$ Torr (with atmospheric pressure $p_0 = 760$ Torr). See Figures 3.7 and 3.9 for numerical values of $\beta_{\rm eff}$ corresponding to $(\omega_{ce}/N)_{1-3}$ used here.

that the inset in panel (c) shows the same behavior for $\mu_\parallel$ when $\beta_{\rm eff} \gg 1$ as the case for $E/N = 80$ Td in Figure 3.4(d).

In conclusion of this section, we reiterate the outline used above for studies that require calculation of electron rate and transport coefficients in a magnetized plasma. As demonstrated above, this approach reduces the problem of magnetized plasma (i.e., $\vec{B} \neq 0$) in presence of an applied electric field $\vec{E}$ to an equivalent problem of non-magnetized plasma (i.e., $\vec{B} = 0$) in the presence of an effective electric field $E_{\rm eff}$ by the following steps.

1. Calculate E_{eff} for a given $(E/N, \omega_{\text{ce}}/N, \angle\vec{E}, \vec{B})$ satisfying the transcendental equation (3.2), and corresponding $\beta_{\text{eff}}(E_{\text{eff}})$.

2. Calculate electron transport and rate coefficients as if $\vec{B} = 0$ using this newly obtained E_{eff} as electron mean energy $\varepsilon_{\text{m}}(E_{\text{eff}})$, electron impact ionization frequency $\nu_{\text{i}}(E_{\text{eff}})$, electron momentum transfer collision frequency $\nu_{\text{m}}(E_{\text{eff}})$, electron mobility parallel to the magnetic field $\mu_{\parallel} = q_{\text{e}}/(m_{\text{e}}\nu_{\text{m}}(E_{\text{eff}}))$, and electron mobility perpendicular to the magnetic field $\mu_{\perp} = \mu_{\parallel}/(1 + \beta^2_{\text{eff}}(E_{\text{eff}}))$.

The solution of equation (3.2) can be simplified if β_{eff} can be assumed to be constant or weakly dependent on reduced electric field E_{eff}/N. However, we note that for typical electric fields used in applications, β_{eff} parameter in equation (3.2) can exhibit significant variations as a function of E_{eff}/N. For example, for CO_2 gas it changes by a factor of 5, and for air by a factor of 10. As β_{eff} enters in quadratic form in (3.2), these variations are important and one needs to find solution E_{eff} of non-linear equaiton (3.2) to accurately solve the problem. The solutions can be simplified when $\beta_{\text{eff}} \ll 1$ due to high collision frequency $\nu_{\text{m}}(E_{\text{eff}}) \gtrsim \omega_{\text{ce}}$ in strong applied electric fields [e.g., *Liu et al.*, 2017] or when orientation of electric field with respect to the external magnetic field has preferentially $E_{\parallel}$ component [e.g., *Pérez-Invernón et al.*, 2018]. In both cases effects of magnetic field on system behavior can be ignored. We note that the solution flow described here follows from the case labeled as $w = w_3$ for $\beta^2_{\text{H}} \gg 1$, where w is a weight function that will be defined in the following sections.

3.4 Convergence of the transcendental method

We earlier demonstrated that the problem of solving for the electron rate and transport coefficients under the influence of an external electric field $\vec{E}$ and magnetic field $\vec{B}$ can be converted to an equivalent problem with no magnetic field (i.e., $\vec{B} = 0$) by calculating an effective electric field E_{eff} that is a solution of the transcendental equation (3.2) where $\beta_{\text{eff}} = \omega_{\text{ce}}/\nu_{\text{m}}(E_{\text{eff}})$ is an effective Hall parameter. As noted earlier, here $\nu_{\text{m}} \propto 1/\mu_{\parallel}(E_{\text{eff}})$ is only a function of E_{eff}. Additionally, we also note that $E^2 = E^2_{\parallel} + E^2_{\perp}$. In the rest of this section, we will drop the subscript 'eff' from β_{eff} for convenience and simply refer to it as β.

We consider the question of convergence when numerically solving for E_{eff}. We can equivalently solve for E_{eff}/N, since in our consideration, the gas density N is a constant.

If we define $x \equiv E_{\text{eff}}/N$ and

$$\phi(x) \equiv \frac{1}{N}\left[E_{\parallel}^2 + \frac{E_{\perp}^2}{1+\beta^2(x)}\right]^{1/2}, \tag{3.3}$$

then x is a fixed point of the function $\phi(x)$, i.e.,

$$x = \phi(x). \tag{3.4}$$

Since $\beta(x) \in C[0, E/N]$, where $C[a, b]$ is the space of all continuous functions in the interval $[a, b]$ and $a, b \in \mathbb{R}$ (see Figure 3.7), we conclude $\phi(x) \in C[0, E/N]$. It is clear from equation (3.3) that $\phi(x) \in [0, E/N]$, since $E_{\text{eff}}/N \leq E/N$ always. The previous two statements imply that ϕ has a fixed point in $[0, E/N]$ [*Burden and Faires*, 2005, p. 54, Theorem 2.2a]. This answers the question of existence of a solution to equation (3.2). If, in addition, $\phi'(x) = d\phi/dx$ exists in $(0, E/N)$ and a positive constant $k < 1$ exists with

$$|\phi'(x)| \leq k, \quad \text{for all } x \in (0, E/N), \tag{3.5}$$

then the fixed point in $[0, E/N]$ is unique [*Burden and Faires*, 2005, p. 54, Theorem 2.2b]. The simple fixed-point iteration method can be used to solve equation (3.4) for x. The method starts with an initial approximation x_0 and then improves on this approximation using

$$x_{n+1} = \phi(x_n), \quad \text{where } n = 0, 1, 2, \ldots \tag{3.6}$$

until the convergence criterion is achieved. If condition (3.5) is satisfied, then it also ensures that for any initial value x_0, the sequence $\{x_n\}$ defined by equation (3.6) converges to the unique fixed point x [*Burden and Faires*, 2005, p. 58-59, Theorem 2.3]. Although checking condition (3.5) analytically might not be possible since $\beta(x)$ has a highly non-linear dependence on the electron energy distribution function for any x, below we use numerical results to show that convergence is indeed achieved, provided a judicious choice of the initial value x_0.

Consider the problem of calculating E_{eff}/N in pure CO_2 gas. We assume the worst-case scenario in terms of the performance of the transcendental method where $\angle\vec{E}, \vec{B} = 90°$, i.e., $E_{\parallel} = 0$ and $E_{\perp} = E$, since this is when the effect of the magnetic field is strongest and results in the highest reduction of E_{eff} compared to E. Thus,

$$\phi(x) = \frac{E/N}{[1+\beta^2(x)]^{1/2}}. \tag{3.7}$$

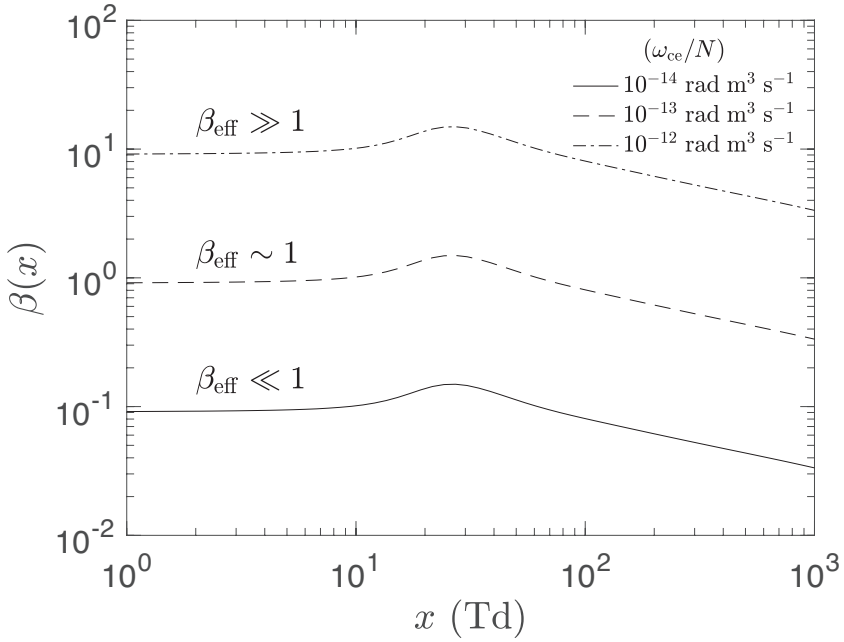

Figure 3.7. $\beta(x)$ for weakly ($\beta \ll 1$), partially ($\beta \sim 1$), and highly ($\beta \gg 1$) magnetized CO_2 plasma.

We consider solutions for three values of the magnetic field (or equivalently, the reduced electron cyclotron frequency ω_{ce}/N), where $(\omega_{ce}/N)_1 = 10^{-14}$ rad m^3 s^{-1} corresponds to weakly magnetized electrons ($\beta \ll 1$), $(\omega_{ce}/N)_2 = 10^{-13}$ rad m^3 s^{-1} corresponds to partially magnetized electrons ($\beta \sim 1$), and $(\omega_{ce}/N)_3 = 10^{-12}$ rad m^3 s^{-1} corresponds to highly magnetized electrons ($\beta \gg 1$). Figure 3.7 shows $\beta(x)$ as a function of x in Townsends for all three chosen values of ω_{ce}/N in CO_2. In addition we consider three representative values of the applied reduced electric field for each case, i.e., $E/N = 10$, 100, and 1000 Td.

Figure 3.8 shows $\phi(x)$ and $|d\phi/dx|$ as functions of x for all three values of E/N and for each value of ω_{ce}/N considered. A dashed line representing $y = x$ is also shown. Graphically, we can determine the root as the intersection of $\phi(x)$ with $y = x$. We note that for the weakly magnetized case, i.e., $(\omega_{ce}/N)_1$, condition (3.5) is satisfied for all three values of E/N (Figure 3.8(b)), which ensures both the uniqueness of the solution, and convergence of the fixed-point iteration method to the unique fixed-point. For the partially magnetized case, i.e., $(\omega_{ce}/N)_2$, condition (3.5) is still satisfied for $E/N = 10$ Td, but it is not satisfied for $E/N = 100$ and 1000 Td (Figure 3.8(d)) in the entire range of $[0, E]$. However, we note that for $E = 100$ Td, condition (3.5) is satisfied for $x \in [\simeq 20 \text{ Td}, E/N]$. So we conclude that a unique root does exist in the range $[\simeq 20 \text{ Td}, E/N]$. We further confirm graphically from Figure 3.8(c) that this

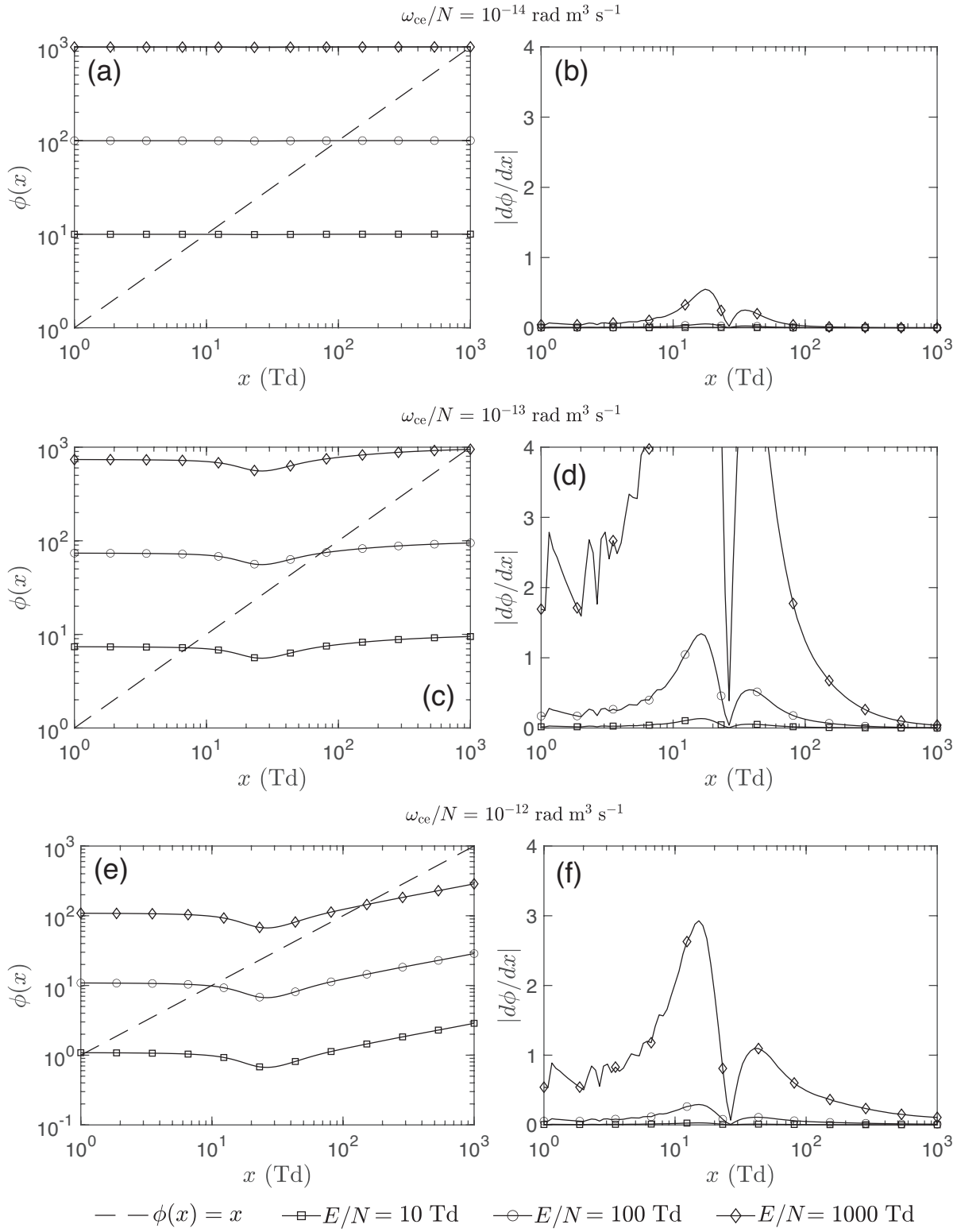

Figure 3.8. $\phi(x)$ and $|d\phi/dx|$ for weakly, partially, and highly magnetized CO_2 plasma. The dashed line represents the $y = x$ line, and the intersection of $\phi(x)$ with this line is the root of the equation $x = \phi(x)$.

root indeed exists, and is unique not only in $[\simeq 20$ Td$, E/N]$, but in the entire range $[0, E/N]$. We note that due to the log scale chosen for plotting, Figure 3.8(c) only shows $x \in [1, 1000]$ Td. It is easy to check that the root is indeed unique in $[0, E/N]$. Similarly, for $E/N = 1000$ Td, condition (3.5) is satisfied for $x \in [\sim 120$ Td$, E/N]$ and a unique root exists in this range. For the highly magnetized case, i.e., $(\omega_{ce}/N)_3$, condition (3.5) is satisfied for $E/N = 10$ and 100 Td, and hence a unique root exists. For $E/N = 1000$ Td, condition (3.5) is satisfied for $x \in [\simeq 60$ Td$, E/N]$, and we conclude, following a similar discussion as for the partially magnetized case, that a unique root exists.

We hence conclude that a unique solution to equation (3.4), and consequently to equation (3.2), exists for the wide range of values of magnetic field and applied electric field presented. We further note that $|d\phi/dx|$ becomes smaller as x becomes larger, such that x_0 should be chosen to lie towards the upper bound of the $[0, E/N]$ interval to ensure that condition (3.5) is satisfied (see Figures 3.8, 4.6, and 4.7). Furthermore, it is recommended that x_0 be chosen such that it is greater than the solution x. Although this x is not known initially, we know that $x \leq E/N$, and hence, a simple choice that always satisfies this condition is $x_0 = E/N$, and we note that this choice always led to convergence in tests conducted. Corresponding results for air, and the (88% H_2, 12% He) mixture resembling the atmospheres of the giant gaseous planets of the solar system are presented later on in Chapter 4 (Figures 4.6 and 4.7, respectively), where an analysis similar to that presented here for CO_2 leads to the same conclusion, i.e., the fixed-point iteration method converges to a unique solution for both air and the (88% H_2, 12% He) mixture in all cases. These conditions for convergence can be similarly checked for an arbitrary gas mixture of interest.

3.5 Model formulation

Assuming steady state and homogeneous space, in the presence of a constant electric and magnetic field, the isotropic part of the electron velocity distribution function (EVDF) f_{0_B} in the Lorentzian approximation [e.g., *Holstein*, 1946] $f_B(\vec{v}) = f_{0_B}(v) + \vec{f}_{1_B}(v) \cdot \vec{i}_v$ (see equation (1.16)), where $\vec{i}_v$ is the radial unit vector in velocity space, is the solution to the differential equation [e.g., *Golant et al.*, 1980, p. 140]:

$$\frac{1}{3}\left(\frac{q_e}{m_e}\right)^2 \frac{1}{v^2}\frac{\partial}{\partial v}\left[\frac{v^2}{\nu_m}\left(\frac{E_\perp^2}{1+\beta_H^2} + E_\parallel^2\right)\frac{\partial f_{0_B}}{\partial v}\right] + C(f_{0_B}) = 0 \tag{3.8}$$

where the subscript B emphasizes that the EVDF is calculated for magnetic field $\vec{B} \neq 0$. The anisotropic part $\vec{f}_{1_B}$ is given in [e.g., *Janalizadeh and Pasko*, 2023, Appendix B] for $\vec{B} \parallel \hat{z}$, where $\hat{z}$ is unit vector in direction of z axis. In the above equation and in a conventional cylindrical coordinate system we have $E_\perp^2 = E_\rho^2 + E_\varphi^2, E_\parallel = E_z$, $E^2 = E_\perp^2 + E_\parallel^2$, and $\beta_{\rm H}(\varepsilon) = \omega_{\rm ce}\nu_{\rm m}^{-1}(\varepsilon)$. Also, as already mentioned, $\angle\vec{E},\vec{B}$ is the angle between $\vec{E}$ and $\vec{B}$ such that $\tan(\angle\vec{E},\vec{B}) = E_\perp/E_\parallel$, and $C(f_{0_B})$ denotes the collision term [e.g., *Loureiro and Amorim*, 2016, pp. 101-104, 110-115]. The solution of equation (3.8) as a function of v varies with any combination of $(E/N, \omega_{\rm ce}/N, \angle\vec{E},\vec{B})$, i.e., $f_{0_B} = f_{0_B}(v; E/N, \omega_{\rm ce}/N, \angle\vec{E},\vec{B})$. In the remainder of this chapter, symbols after a semicolon represent independent external parameters on which an introduced quantity depends.

As a result of the Lorentzian, i.e., two-term expansion of the EVDF, electron impact collision rates are determined exclusively by f_{0_B} ($\int_{v=0}^{\infty} f_{0_B}(v)4\pi v^2 dv = n_{\rm e}$, where $n_{\rm e}$ denotes electron density). On the other hand, electron transport coefficients are dependent on $\vec{f}_{1_{\rm B}}$. As can be seen from sources cited above ([e.g., *Janalizadeh and Pasko*, 2023, Appendix A1]), for a given set of $(E/N, \omega_{\rm ce}/N, \angle\vec{E},\vec{B})$, the latter is solely dependent on the derivative of the isotropic term with respect to v. Thus, in an alternative approach that does not require solving equation (3.8) for magnetized electrons, here we substitute f_{0_B} with f_0 in search of the isotropic part of an EVDF in the absence of a magnetic field, i.e., $\vec{B} = 0$ that minimizes the residual

$$R(v) = R[f_0(v)] = \frac{1}{3}\left(\frac{q_{\rm e}}{m_{\rm e}}\right)^2 \frac{1}{v^2}\frac{\partial}{\partial v}\left[\frac{v^2}{\nu_{\rm m}}\left(\frac{E_\perp^2}{1+\beta_{\rm H}^2} + E_\parallel^2\right)\frac{\partial f_0}{\partial v}\right] + C(f_0) \tag{3.9}$$

over the $v \in [0, \infty]$ interval. Before presenting the minimization process, we note that as demonstrated in equation (3.8), the residual is zero for f_{0_B}. As such, $R(v)$ may be interpreted as a measure quantifying the difference between f_{0_B} and $f_0 = f_0(v; E_{\rm eff}/N)$ at given electron velocity v. We note that $f_0(v)$ is the solution to [e.g., *Raizer*, 1991, p. 87]

$$\frac{1}{3}\left(\frac{q_{\rm e}}{m_{\rm e}}\right)^2 \frac{1}{v^2}\frac{\partial}{\partial v}\left[\frac{v^2}{\nu_{\rm m}}E_{\rm eff}^2\frac{\partial f_0}{\partial v}\right] + C(f_0) = 0 \tag{3.10}$$

where we have let $\beta_{\rm H} = 0$ in equation (3.8) to obtain the above equation for a given $E_{\rm eff}$. Subsequently, we can replace the collision term $C(f_0)$ in equation (3.9) using the

definition in equation (3.10) to obtain

$$R(v) = \frac{1}{3}\left(\frac{q_e}{m_e}\right)^2 \frac{1}{v^2}\frac{\partial}{\partial v}\left[\frac{v^2}{\nu_m}\left(\frac{E_\perp^2}{1+\beta_H^2} + E_\parallel^2 - E_{eff}^2\right)\frac{\partial f_0}{\partial v}\right] \tag{3.11}$$

The minimization of defined residual over $v \in [0, \infty]$ may be quantified by introducing a weight function $w(v)$ and subsequently defining an error function

$$\mathcal{E}(E_{eff}/N; E/N, \omega_{ce}/N, \angle\vec{E}, \vec{B}) = \int_{v=0}^{\infty} R^2(v) w(v) dv \tag{3.12}$$

Here we wish to find the value of E_{eff} that minimizes the error $\mathcal{E}$. By definition in that case we should have $\partial\mathcal{E}/\partial E_{eff} = 0$. We emphasize that this minimization generally should be performed for every set of three independent external parameters used in formulation of lookup tables [e.g., *Starikovskiy et al.*, 2021], namely, E/N, ω_{ce}/N, and $\angle\vec{E}, \vec{B}$. Nevertheless, as demonstrated in Appendix B, this analysis results in the general transcendental expression

$$E_{eff}^2 = E_\parallel^2 + \frac{E_\perp^2}{1+\beta_{eff}^2} \tag{3.13}$$

where $1+\beta_{eff}^2$ is the factor by which the square of the perpendicular component of the applied electric field is reduced due to the presence of a magnetic field. The quantity β_{eff} varies only as a function of E_{eff}/N for a given ω_{ce}/N and is given by $\beta_{eff} = \sqrt{I_1/I_2 - 1}$, where

$$I_1 = \int_{v=0}^{\infty} \left[\frac{1}{v^2}\frac{\partial}{\partial v}\left(\frac{v^2}{\nu_m}\frac{\partial f_0}{\partial v}\right)\right]^2 w(v) dv \tag{3.14}$$

and

$$I_2 = \int_{v=0}^{\infty} \left\{\frac{1}{v^2}\frac{\partial}{\partial v}\left[\left(\frac{1}{1+\beta_H^2}\right)\left(\frac{v^2}{\nu_m}\frac{\partial f_0}{\partial v}\right)\right]\right\} \cdot \left\{\frac{1}{v^2}\frac{\partial}{\partial v}\left(\frac{v^2}{\nu_m}\frac{\partial f_0}{\partial v}\right)\right\} w(v) dv \tag{3.15}$$

The dependence of β_{eff} (through I_2) on ω_{ce}/N is only through β_H since as already mentioned, f_0 corresponds to a non-magnetized EVDF such that one does not need to solve equation (3.8) for magnetized plasma.

Generally E_{eff} will be located in the $[E\cos(\angle\vec{E}, \vec{B}), E]$ interval where the upper (lower) limit of this search interval corresponds to nonmagnetized, $\beta_{eff} \ll 1$, (fully magnetized, $\beta_{eff} \gg 1$) electrons, respectively. Therefore, once β_{eff} is quantified, one can employ a

root-finding algorithm to solve equation (3.13) and obtain E_{eff}/N for a given set of input parameters $(E/N, \omega_{\text{ce}}/N, \angle\vec{E}, \vec{B})$. The question of existence and uniqueness of a solution to equation (3.13) was addressed previously in Section 3.4. Specifically, it was demonstrated that a solution always exists and conditions for uniqueness of a solution and convergence of a fixed-point iteration method to find E_{eff} are obtained such that for any given set of input parameters $(E/N, \omega_{\text{ce}}/N, \angle\vec{E}, \vec{B})$ one can verify these conditions. We note that the interested reader may accelerate the root-finding process by creating a two-dimensional array of β_{eff} values varying as a function of the $(E_{\text{eff}}/N, \omega_{\text{ce}}/N)$ pair to be subsequently used in solving the transcendental equation (3.13).

To numerically quantify β_{eff} we introduce three weight functions denoted by $w_1(v)$, $w_2(v)$, $w_3(v)$ to demonstrate the performance of the presented transcendental method. The corresponding weight function in energy space is defined via $W(\varepsilon)d\varepsilon = w(v)dv$ where as mentioned above ε denotes electron energy in units of eV. The weight functions we use in this work are

1. $w_1(v) = 1$, i.e., constant weight function in velocity space. Thus, $W(\varepsilon) = \frac{\gamma}{2}\varepsilon^{-\frac{1}{2}}$
2. $w_2(v) = \frac{1}{n_{\text{e}}} f_0(v) 4\pi v^2$ such that $w_2(v)dv = \frac{1}{n_{\text{e}}} \frac{n_{\text{e}}}{2\pi\gamma^3} F_0(\varepsilon)\, 4\pi\gamma^2\varepsilon\, \frac{\gamma}{2}\varepsilon^{-\frac{1}{2}} d\varepsilon = P_0(\varepsilon)d\varepsilon$
3. $w_3(v) = v^6 \left[\frac{\partial}{\partial v}\left(\frac{v^2}{\nu_{\text{m}}}\frac{\partial f_0}{\partial v}\right)\right]^{-1}$ such that

$$
\begin{aligned}
w_3(v)dv &= \frac{\left(\gamma^2\varepsilon\right)^3}{2\gamma^{-1}\varepsilon^{\frac{1}{2}}\frac{\partial}{\partial\varepsilon}\left\{\frac{\gamma^2\varepsilon}{\nu_{\text{m}}} 2\gamma^{-1}\varepsilon^{\frac{1}{2}}\frac{\partial}{\partial\varepsilon}\left[\frac{n_{\text{e}}}{2\pi\gamma^3}F_0(\varepsilon)\right]\right\}} \frac{\gamma}{2}\varepsilon^{-\frac{1}{2}}d\varepsilon \\
&= \frac{\pi\gamma^{10}}{4n_{\text{e}}} \frac{\varepsilon^2 d\varepsilon}{\frac{\partial}{\partial\varepsilon}\left[\frac{\varepsilon^{\frac{3}{2}}}{\nu_{\text{m}}}\frac{\partial F_0(\varepsilon)}{\partial\varepsilon}\right]}
\end{aligned}
\tag{3.16}
$$

where $\gamma = (2q_{\text{e}}/m_{\text{e}})^{\frac{1}{2}}$, and $P_0(\varepsilon)$ were defined in Section 1.2.3. Note that since $\beta_{\text{eff}} \propto I_1/I_2$, the absolute value of electron density or the constant γ present in the weight function do not affect any results of this analysis as the weight function is included in both I_1 and I_2.

We emphasize that the formulation presented in the present work is valid irrespective of the peculiarities of each weight function. As such, in choosing w_1 and w_2 we have prioritized simplicity of the weight function itself. However, this is not the case for w_3. Specifically, w_3 has been chosen such that β_{eff} will become proportional to electron transport and rate coefficients directly outputted by BOLSIG+ (see Appendix C). In other words, calculating β_{eff} when $w = w_1$ or $w = w_2$ requires the EEDF calculated by BOLSIG+ for evaluation of the integrals I_1 and I_2. However, when $w = w_3$ these integrals

reduce to specific electron rate and transport coefficients that are already calculated by BOLSIG+ in non-magnetized case (i.e., $\vec{B} = 0$).

Specifically, the transcendental method in the special case of $w = w_3$ reduces to

$$E_{\text{eff}}^2 = E_{\parallel}^2 + \frac{E_{\perp}^2}{\left(\frac{\mu_{\parallel}}{\mu_{\perp}^0}\right)} \tag{3.17}$$

where in general the mobilities parallel and perpendicular to the magnetic field are respectively defined as [*Hagelaar and Pitchford*, 2005, manual]

$$\mu_{\parallel} N = -\frac{\gamma}{3} \int_{\varepsilon=0}^{\infty} \frac{\varepsilon}{\sigma_{\text{m}}} \frac{\partial}{\partial \varepsilon} F_0(\varepsilon)\, d\varepsilon \tag{3.18}$$

and

$$\mu_{\perp} N = -\frac{\gamma}{3} \int_{\varepsilon=0}^{\infty} \frac{1}{1+\beta_{\text{H}}^2} \frac{\varepsilon}{\sigma_{\text{m}}} \frac{\partial}{\partial \varepsilon} F_0(\varepsilon)\, d\varepsilon \tag{3.19}$$

We note that whereas $\mu_{\perp}^0$ is in the same format of perpendicular mobility defined in [*Hagelaar and Pitchford*, 2005, manual], as opposed to $\mu_{\perp}$ it is not a direct output of BOLSIG+ since calculation of $\mu_{\perp}$ by BOLSIG+ happens when $\vec{B} \neq 0$ while $\mu_{\perp}^0$ is dependent on BOLSIG+ only through BOLSIG+'s EEDF calculated for $\vec{B} = 0$. As such, we calculate $\mu_{\perp}^0$ manually (in MATLAB) using the EEDF output of BOLSIG+ corresponding to defined range of E_{eff}/N values. A given reduced gyrofrequency ω_{ce}/N quantifies $\beta_{\text{H}} = \omega_{\text{ce}}/\nu_{\text{m}}(\varepsilon)$ in definition of $\mu_{\perp}^0$ through $\nu_{\text{m}}(\varepsilon) = N\sigma_{\text{m}}(\varepsilon)v = N\sigma_{\text{m}}(\varepsilon)\gamma\varepsilon^{\frac{1}{2}}$. In calculation of $\mu_{\perp}^0$ and more generally β_{eff}, we quantified the momentum transfer cross section $\sigma_{\text{m}}(\varepsilon)$ of each mixture using the LXCat set of cross sections, which accompanied BOLSIG+. Since for CO_2, $\sigma_{\text{m}}(\varepsilon)$ was not readily available in the accompanying data, we calculated $\sigma_{\text{m}}(\varepsilon)$ by summing the cross section for all inelastic processes in addition to the elastic momentum transfer cross section.

3.6 Results and discussion

3.6.1 Calculation of effective Hall parameter β_{eff} in CO_2

As inferred from Section 3.5, whereas the determination of E_{eff} through the transcendental equation is dependent on the applied electric and magnetic fields in addition to the angle between the two, the calculation of β_{eff} for a given E_{eff}/N may proceed in a standalone

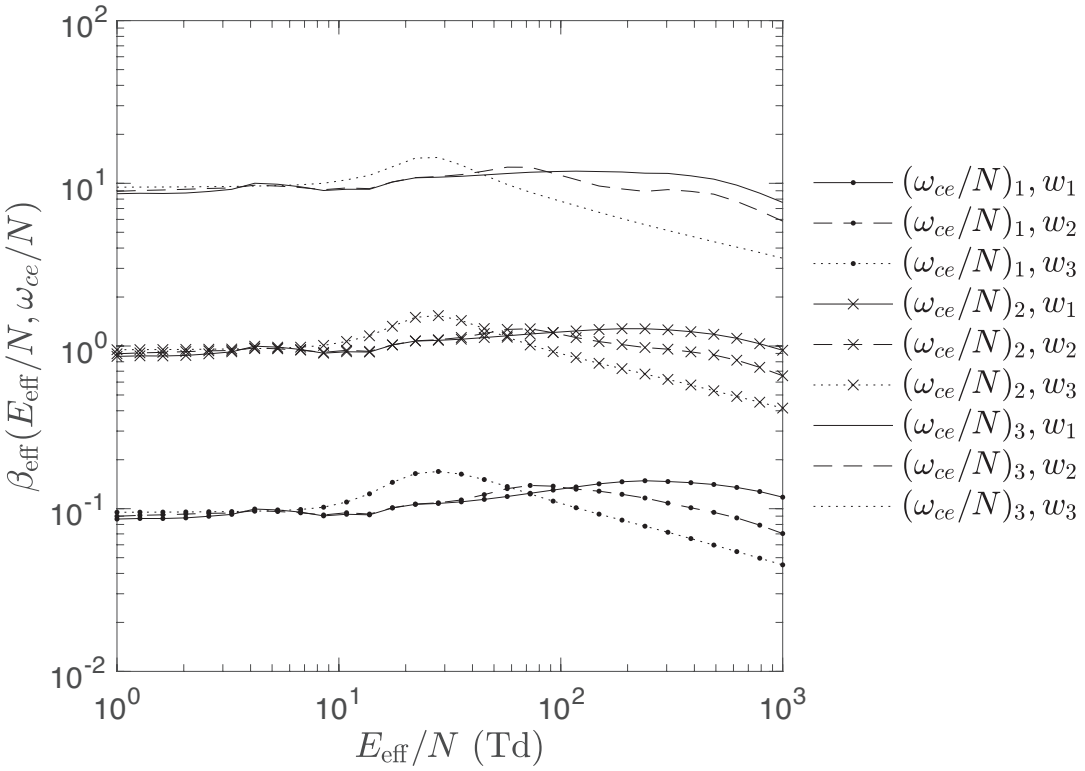

Figure 3.9. Values of $\beta_{\rm eff} = \beta_{\rm eff}\,(E_{\rm eff}/N; \omega_{\rm ce}/N)$ in pure CO_2 as a function of given reduced effective field $E_{\rm eff}/N$ for values of $(\omega_{\rm ce}/N)_1 = 10^{-14}$ rad m^3 s^{-1}, $(\omega_{\rm ce}/N)_2 = 10^{-13}$ rad m^3 s^{-1}, and $(\omega_{\rm ce}/N)_3 = 10^{-12}$ rad m^3 s^{-1}.

fashion. To quantify $\beta_{\rm eff}$ for various weight functions, here we use BOLSIG+ to calculate the EEDF (with $\vec{B} = 0$) in gas mixtures considered for a wide range of $E_{\rm eff}/N$ values. As already mentioned, the magnetic field enters our calculations of $\beta_{\rm eff}$ only through the Hall parameter included in the definition of I_2.

In Figure 3.9 we illustrate calculated values of $\beta_{\rm eff}$ for CO_2. The values of reduced gyrofrequency chosen for the calculations are $10^{-14}, 10^{-13}$, and 10^{-12} rad m^3 s^{-1}, and are respectively denoted by $(\omega_{\rm ce}/N)_1\,, (\omega_{\rm ce}/N)_2$, and $(\omega_{\rm ce}/N)_3$. As seen in Figure 3.9, this interval of $\omega_{\rm ce}/N$ covers the entire range between non-magnetized ($\beta_{\rm eff} \ll 1$) and highly magnetized ($\beta_{\rm eff} \gg 1$) electrons. We note that in [*Starikovskiy et al.*, 2021] magnetized streamers were studied in the $\omega_{\rm ce}/N = 0 - 20 \times 10^{-13}$ rad m^3 s^{-1} range. Furthermore, it is inferred from Figure 3.9 that the difference between $\beta_{\rm eff}$ values corresponding to various weight functions $w(v)$ is practically insignificant. We note that $\beta_{\rm eff}$ for w_3 resembles closely the $\beta_{\rm eff}$ in Figure 3.7, calculated by solving equation (3.2). Additionally, as already mentioned in Section 3.5 and demonstrated in Appendix C, $w = w_3$ results in the expression of $\beta_{\rm eff}$ in terms of electron rate and transport coefficients, which are already

calculated by BOLSIG+ in non-magnetized case (i.e., $\vec{B} = 0$). Therefore, for the sake of simplicity and brevity, in the remainder of this chapter we let $w = w_3$.

3.6.2 Comparison of BOLSIG+ exact coefficients with present work's results

As demonstrated in Appendix D, when $w = w_3$ the presented trascendental method for considerably magnetized electrons may be simplified even further. Specifically, if

$$\int_{\varepsilon=0}^{\infty} \varepsilon \frac{\partial}{\partial \varepsilon} \left(\sigma_{\mathrm{m}} \varepsilon^{\frac{1}{2}} \right) P_0 d\varepsilon \equiv \left\langle \varepsilon \frac{\partial}{\partial \varepsilon} \left(\sigma_{\mathrm{m}} \varepsilon^{\frac{1}{2}} \right) \right\rangle \tag{3.20}$$

is negligible, one can use $\beta_{\mathrm{eff}} = \beta_{\mathrm{eff}} = \omega_{\mathrm{ce}}/\nu_{\mathrm{m}} = (\omega_{\mathrm{ce}}/N)/k_{\mathrm{m}}(E_{\mathrm{eff}}/N)$, where $k_{\mathrm{m}} = \nu_{\mathrm{m}}/N$ is the momentum transfer rate constant as a function of E_{eff}/N exclusively. This is a standard rate coefficient calculated by BOLSIG+ itself such that the implementation of the transcendental method using the EEDFs calculated by BOLSIG+ may be avoided. The average $\left\langle \varepsilon \frac{\partial}{\partial \varepsilon} \left(\sigma_{\mathrm{m}} \varepsilon^{\frac{1}{2}} \right) \right\rangle$ is a measure of the variation of momentum transfer collision frequency as a function of electron energy. That is, $\sigma_{\mathrm{m}}(\varepsilon) \propto \varepsilon^{-\frac{1}{2}}$ for which the average is identically zero corresponds to a constant momentum transfer collision frequency since in that case $\nu_{\mathrm{m}}(\varepsilon) = N k_{\mathrm{m}}(\varepsilon) = N \sigma_{\mathrm{m}}(\varepsilon) v \propto \varepsilon^{-\frac{1}{2}} \left(\gamma \varepsilon^{\frac{1}{2}} \right) = \text{const}$ [e.g., *Starikovskiy et al.*, 2021]. Consequently, in this section we assume that this average is in fact negligible and compare results with the general transcendental method with $w = w_3$ and β_{eff}. We will also include the exact (no assumptions made) calculations of BOLSIG+, which have been compiled in lookup tables and subsequently interpolated for cases considered here.

Specifically, we consider two cases of $\angle \vec{E}, \vec{B}$, 45° and 90°, in addition to a large range of applied reduced fields E/N. We choose ω_{ce}/N (or equivalently $\omega_{\mathrm{ce}} N_0/N$, where $N_0 = 2.686 \times 10^{25}$ m^{-3}) such that $\beta_{\mathrm{eff}} \simeq 1$ for both $\angle \vec{E}, \vec{B}$ considered and in the majority of the E/N range. The purpose of this choice of $\omega_{\mathrm{ce}} N_0/N = 5.25 \times 10^{12}$ rad s^{-1} is to demonstrate the performance of the transcendental method in the partially magnetized regime where as opposed to $\beta_{\mathrm{eff}} \gg 1$ ($\beta_{\mathrm{eff}} \ll 1$), the effective electric field is not trivially $E_{\mathrm{eff}} = E_{\parallel}$ ($E_{\mathrm{eff}} = E$). This gives $\omega_{\mathrm{ce}}/N \simeq 2 \times 10^{-13}$ rad m^3 s^{-1}, which is close to the $(\omega_{\mathrm{ce}}/N)_2$ value in Figure 3.9 and corresponds to partially magnetized electrons. The quantities used for comparison are mean energy of electrons ε_{m}, electron impact ionization frequency ν_{i}, mobility parallel to the magnetic field $\mu_{\parallel}$, and mobility perpendicular to the magnetic field $\mu_{\perp}$. This choice of comparisons has been made to investigate the performance of the proposed transcendental method as it pertains to both of the f_0 and

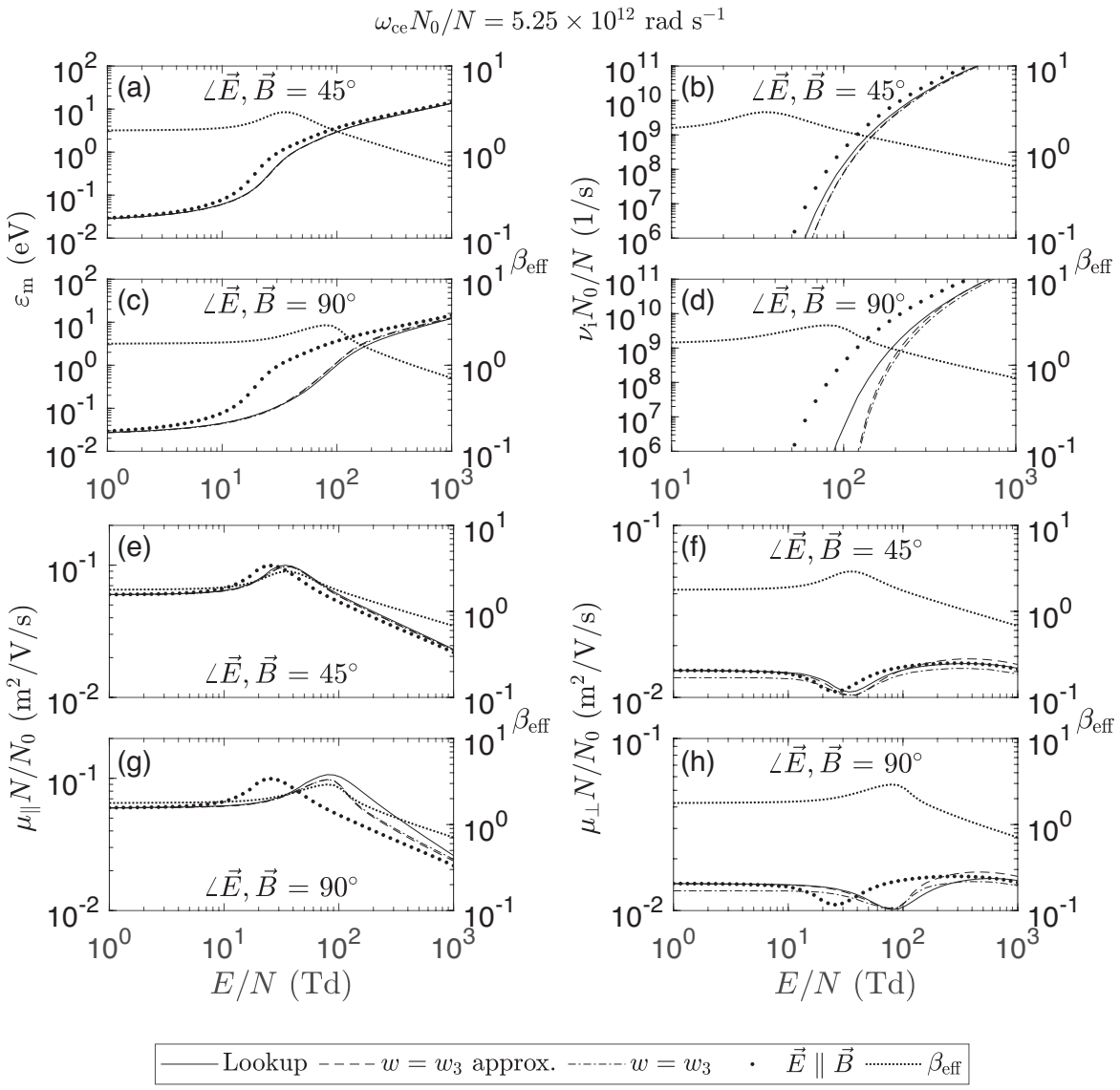

Figure 3.10. (a) Electron mean energy ε_m and (b) reduced electron impact ionization frequency $\nu_i N_0/N$ for $\angle\vec{E},\vec{B} = 45°$. (c) Electron mean energy ε_m and (d) reduced electron impact ionization frequency $\nu_i N_0/N$ for $\angle\vec{E},\vec{B} = 90°$. Reduced mobility of electrons (e) parallel, $\mu_\parallel N/N_0$ and (f) perpendicular, $\mu_\perp N/N_0$, to $\vec{B}$ for $\angle\vec{E},\vec{B} = 45°$. Reduced mobility of electrons (g) parallel, $\mu_\parallel N/N_0$, and (h) perpendicular, $\mu_\perp N/N_0$, to $\vec{B}$ for $\angle\vec{E},\vec{B} = 90°$. Results are for pure CO_2.

$\vec{f}_1$ terms in the two-term expansion of the EVDF. These results are shown in Figure 3.10. All panels include $\beta_{eff} = (\omega_{ce}/N)/k_m(E_{eff}/N)$ after finding the solution to equation (3.2) to illustrate the degree of magnetization of the electrons. It is inferred from this figure that the transcendental method for $w = w_3$ and the approximation to this method agree to a satisfactory degree for CO_2. In addition, both methods agree with exact calculations

of BOLSIG+ for the majority of the E/N range.

The observed deviation of ν_i results of BOLSIG+ from that of both transcendental methods at $\angle\vec{E},\vec{B} = 90°$ (i.e., $E_\parallel = 0$) is generally considerable. On the other hand, the agreement between ε_m calculated for the same scenario by all methods is satisfactory. This observation emphasizes the difference in the high energy tail of the exact EEDF calculated by BOLSIG+ for $\vec{B} \neq 0$ and the EEDFs (corresponding to $\vec{B} = 0$) used in the transcendental methods. Specifically, both ε_m and ν_i depend on the isotropic term of the EVDF. However, the latter involves, exclusively, the high energy electrons represented in the tail of the EEDF (vs ε) since electron impact ionization is a collision with an energy threshold. While the abundance of these ionizing electrons controls the ionization rate constant, their exponentially lower population compared to low energy electrons results in a negligible impact on ε_m values presented. We note that the same analysis is true for rate constants of other electron impact processes with an energy threshold. The disagreement is more pronounced for electron impact collisions with a higher energy threshold.

Values corresponding to $\vec{E} \parallel \vec{B}$ are also included in all panels. Specifically, the extremely low ionization levels when $\angle\vec{E},\vec{B} = 90°$ are demonstrated. While $\angle\vec{E},\vec{B} = 90°$ corresponds to the lowest agreement between ν_i results of BOLSIG+ and the transcendental methods, the exact results of BOLSIG+ are still orders of magnitude less than scenarios in which $\angle\vec{E},\vec{B} \to 0$. We note that this holds even for $\angle\vec{E},\vec{B}$ as high as 45° (see panels (b) and (d) in Figure 3.10). As such, one may conclude that in a realistic scenario where $\angle\vec{E},\vec{B}$ may vary in the entire range of $\angle\vec{E},\vec{B} = 0 - 90°$, even exact ν_i values corresponding to $\angle\vec{E},\vec{B} = 90°$ are so insignificant that the disagreement between BOLSIG+ and the transcendental methods has no practical significance in the framework of plasma fluid models in which these coefficients are typically employed [e.g., *Starikovskiy et al.*, 2021; *Janalizadeh and Pasko*, 2023].

Figure 3.11 shows 2-D plots presenting the percentage error of the proposed approximate transcendental method compared to exact solutions for electron mean energy ε_m, electron impact ionization frequency ν_i, electron mobility parallel to magnetic field $\mu_\parallel$, and electron mobility perpendicular to magnetic field $\mu_\perp$, as a function of the angle $\angle\vec{E},\vec{B}$ and reduced electron gyrofrequency ω_ce/N, for selected values of reduced applied electric field E/N. The values selected for the reduced field E/N are $0.5E_\mathrm{k}/N$, E_k/N, and $1.5E_\mathrm{k}/N$, where E_k/N is the reduced breakdown field for the gas, equal to ~ 80 Td for pure CO_2. The proposed method provides good results for all the electron rate and transport coefficients shown, except for the ionization frequency ν_i. We note that the

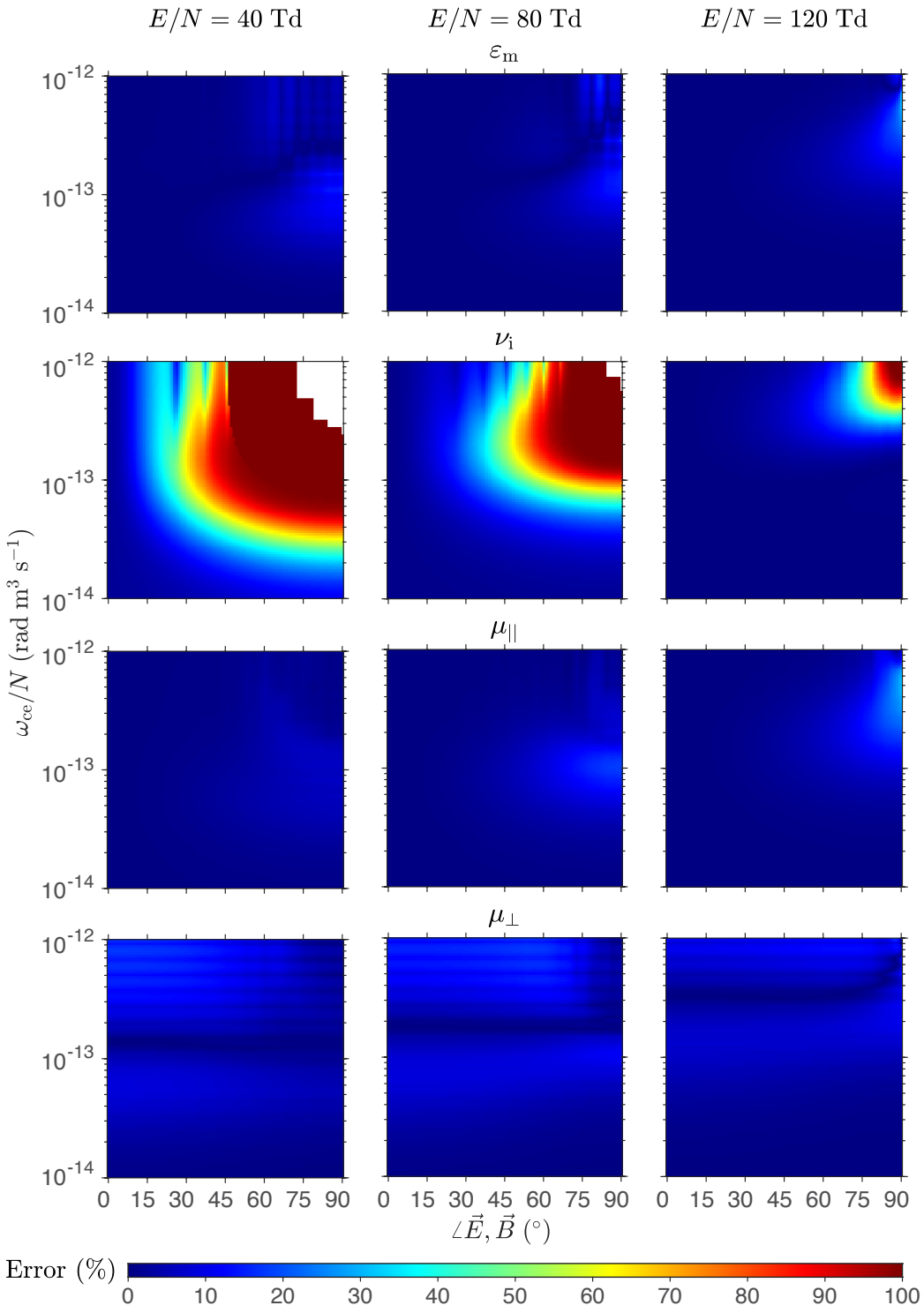

Figure 3.11. Percentage error of proposed transcendental method in approximate form for electron mean energy ε_{m}, electron impact ionization frequency ν_{i}, electron mobility parallel to magnetic field $\mu_{\parallel}$, and electron mobility perpendicular to magnetic field $\mu_{\perp}$, as a function of the angle $\angle\vec{E},\vec{B}$ and reduced electron gyrofrequency ω_{ce}/N, for selected values of applied reduced electric field E/N, in CO_2 plasma.

error is quite low for $\varepsilon_{\rm m}$, $\mu_{\parallel}$, and $\mu_{\perp}$ throughout the considered range of input parameters $(E/N, \omega_{\rm ce}/N, \angle\vec{E}, \vec{B})$, except for very small regions in the upper right quadrants, which is expected as one moves from the regime of non-magnetized ($\beta_{\rm eff} \ll 1$) to highly magnetized ($\beta_{\rm eff} \gg 1$) plasma, i.e, as $\omega_{\rm ce}/N$ approaches 10^{-12} rad m^3 s^{-1}, and $\angle\vec{E}, \vec{B}$ approaches 90°. Significantly larger errors are seen for the electron impact ionization frequency $\nu_{\rm i}$, and the error becomes considerable as we move towards the upper right quadrants. However, as already addressed above, in a realistic scenario where $\omega_{\rm ce}/N$ and $\angle\vec{E}, \vec{B}$ may vary in the entire range shown, $\nu_{\rm i}$ values corresponding to high $\omega_{\rm ce}/N$ and large $\angle\vec{E}, \vec{B}$ are so insignificant that the large error has no practical significance in the framework of plasma fluid models in which these coefficients are typically employed. The white spaces in these panels correspond to regimes where the plasma is highly magnetized such that $\nu_{\rm i}$ is identically zero.

In the end of this section we emphasize that the presented results targeted the regime of partially magnetized plasma. One expects better agreement between the transcendental method and BOLSIG+ exact calculations in either cases of essentially non-magnetized ($\beta_{\rm eff} \ll 1$) and fully magnetized $\beta_{\rm eff} \gg 1$ plasma since in those cases $E_{\rm eff} = E$ and $E_{\rm eff} = E_{\parallel}$, respectively (see Figure 3.6).

3.7 Conclusions

We introduced a new transcendental approach to the calculation of electron transport and rate coefficients in a magnetized plasma using the theory and results of non-magnetized plasma. The obtained effective electric field results in plasma fluid coefficients that are in satisfactory agreement with BOLSIG+'s exact calculations for pure carbon dioxide. Furthermore, the effective electric field is in the same format of the electric field a single electron experiences in the presence of a magnetic field. This provides an intuitive picture, which accompanies the rigorous mathematical derivations presented here. Subsequently, a special case of the formulation is further explored to reduce calculations and use electron rate and transport coefficients outputted by BOLSIG+. While as a result of the kinetic theory of weakly ionized and magnetized plasma, electron transport and rate coefficients are defined through a distribution function that varies with $(E/N, \omega_{\rm ce}/N, \angle\vec{E}, \vec{B})$, the new method proceeds in two steps: (1) calculation of $E_{\rm eff}$ for a given $(E/N, \omega_{\rm ce}/N, \angle\vec{E}, \vec{B})$ through a simple transcendental equation, and (2) calculation of electron transport and rate coefficients in absence of a magnetic field using $E_{\rm eff}/N$ (since when $\vec{B} = 0$ fluid coefficients become functions of $E_{\rm eff}/N$, exclusively).

Chapter 4
Results for magnetized plasma in air and (88% H_2, 12% He) mixture

4.1 Introduction

The new transcendental method proposed and developed in the previous chapter to efficiently solve for electron fluid coefficients in weakly ionized plasma was applied to three gas mixtures: (1) air, (2) a mixture of 88% H_2 and 12% He (representing the atmospheres of the giant gaseous planets of the solar system), and (3) pure CO_2 in [*Janalizadeh et al.*, 2023]. Unlike in Section 1.2.4, here we consider air to be a mixture of 80% N_2 and 20% O_2. The work of this thesis primarily focusses on CO_2, but we present the results for gas mixtures (1) and (2) in this chapter to complement the discussion on CO_2, and illustrate the applicability of the proposed method on a variety of gas mixtures.

4.2 Effective Hall parameter β_{eff} for air and (88% H_2, 12% He) mixture

We use the procedure outlined in Sections 3.5 and 3.6.1 to calculate β_{eff} for gas mixtures (1) and (2) for the three weight functions w_1, w_2, and w_3 introduced in Section 3.5, following the same procedure described in Chapter 3 for CO_2. The calculated values of β_{eff} for these two gas mixtures are shown in Figure 4.1. We note that the reduced breakdown electric fields [e.g., *Raizer*, 1991, p. 137] in mixtures (1), and (2) have been calculated via BOLSIG+ and are respectively ∼120, and 40 Td. In air we choose $E_{\text{eff}}/N = 10^0 - 10^3$

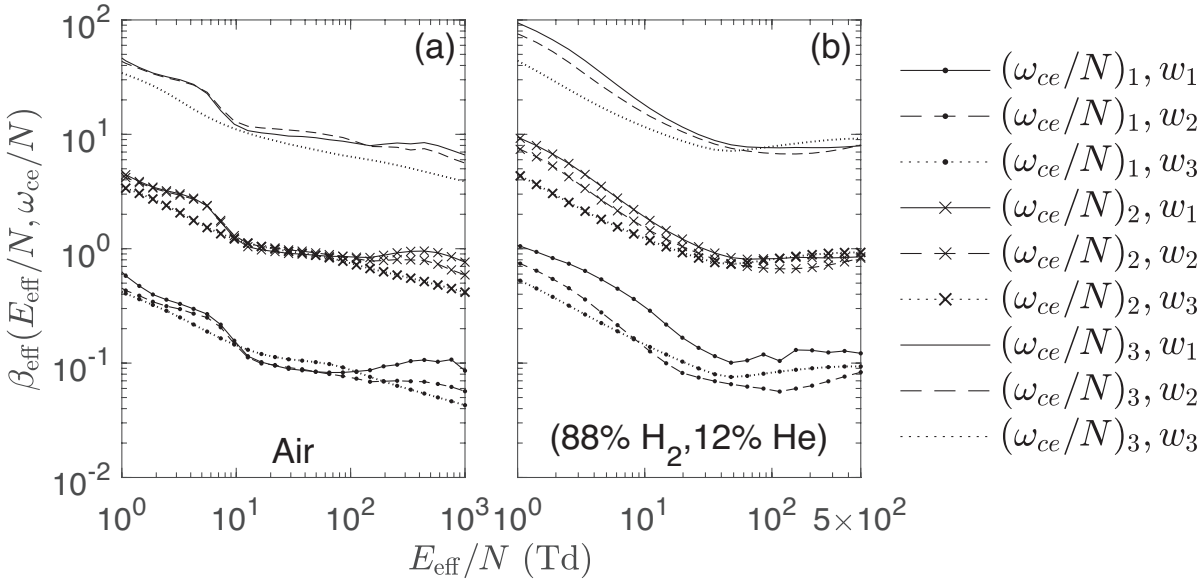

Figure 4.1. Values of $\beta_{\rm eff} = \beta_{\rm eff}\,(E_{\rm eff}/N; \omega_{\rm ce}/N)$ in (a) air, and (b) (88% H_2,12% He) as a function of given reduced effective field $E_{\rm eff}/N$ for values of $(\omega_{\rm ce}/N)_1 = 10^{-14}$ rad m^3 s^{-1}, $(\omega_{\rm ce}/N)_2 = 10^{-13}$ rad m^3 s^{-1}, and $(\omega_{\rm ce}/N)_3 = 10^{-12}$ rad m^3 s^{-1}.

Td. Due to the much lower breakdown threshold in mixture (2), results are shown for a maximum of $E_{\rm eff}/N = 500$ Td. The values of reduced gyrofrequency chosen for the calculations are as before $10^{-14}, 10^{-13}$, and 10^{-12} rad m^3 s^{-1}, and are respectively denoted by $(\omega_{\rm ce}/N)_1\,, (\omega_{\rm ce}/N)_2$, and $(\omega_{\rm ce}/N)_3$. We reiterate that this interval of $\omega_{\rm ce}/N$ covers the entire range between non-magnetized ($\beta_{\rm eff} \ll 1$) and highly magnetized ($\beta_{\rm eff} \gg 1$) electrons. We also note that *Janalizadeh and Pasko* [2023] modeled magnetized sprite streamers at 250 km altitude in the atmosphere of Jupiter, where $\omega_{\rm ce}/N \simeq 1.4 \times 10^{-13}$ rad m^3 s^{-1}, and the reduced gyrofrequency at ∼100 km altitude in the atmosphere of Earth (where elves are observed [e.g., *Fukunishi et al.*, 1996]) is $\omega_{\rm ce}/N \simeq 5.8 \times 10^{-13}$ rad m^3 s^{-1}.

Furthermore, similar to the discussion on CO_2, it is inferred from Figure 4.1 that the difference between $\beta_{\rm eff}$ values corresponding to various weight functions $w(v)$ is practically insignificant. Since $w = w_3$ results in the expression of $\beta_{\rm eff}$ in terms of electron rate and transport coefficients which are already calculated by BOLSIG+ in non-magnetized case, i.e., $\vec{B} = 0$ (see Section 3.5 and Appendix C), for further discussion in the following section, we let $w = w_3$.

4.3 Comparison with BOLSIG+ exact solutions

This section presents results for gas mixtures (1) and (2) following corresponding results for CO_2 presented in Section 3.6.2. Figures 4.2 and 4.3 present these results for gas mixtures (1) and (2), respectively. As in the case of CO_2, we consider two cases of $\angle\vec{E},\vec{B}$, 45° and 90°, in addition to a large range of applied reduced fields E/N. We choose $\omega_{ce}N_0/N = 5.00\times10^{12}$ rad s^{-1} for air, and $\omega_{ce}N_0/N = 6.00\times10^{12}$ rad s^{-1} for the 88% H_2 and 12% He mixture, such that $\beta_{\text{eff}} \simeq 1$ for both $\angle\vec{E},\vec{B}$ considered and in the majority of the E/N range. As mentioned before, the purpose of this choice of $\omega_{ce}N_0/N$ is to demonstrate the performance of the transcendental method in the partially magnetized regime. In what follows $\omega_{ce}/N \simeq 10^{-13}$ rad m^3 s^{-1} (for both gases), which is close to the $(\omega_{ce}/N)_2$ value in Figure 4.1 and corresponds to partially magnetized electrons. Similar to Figure 3.10, the quantities used for comparison are mean energy of electrons ε_m, electron impact ionization frequency ν_i, mobility parallel to the magnetic field $\mu_\parallel$, and mobility perpendicular to the magnetic field $\mu_\perp$. All panels include $\beta_{\text{eff}} = (\omega_{ce}/N)/k_m(E_{\text{eff}}/N)$ after finding the solution to equation (3.2) to illustrate the degree of magnetization of the electrons. It is inferred from this figure that the transcendental method for $w = w_3$ and the approximation to this method agree to a satisfactory degree for both the gases considered in this chapter. In addition, both methods agree with exact calculations of BOLSIG+ for the majority of the E/N range. Considering the satisfactory results for all three gas mixtures, this highlights the applicability of the proposed method to a variety of gas mixtures.

We note the deviation of the electron-impact ionization frequency ν_i at $\angle\vec{E},\vec{B} = 90°$ in panel (d) of Figures 4.2 and 4.3 calculated by the two transcendental methods from the exact results of BOLSIG+. This behavior is similar to that seen in the results for CO_2 in Figure 3.10(d). This deviation is explained similarly to the case of CO_2 in Section 3.6.2, where we noted that such deviation is expected for electron impact collision processes with a higher energy threshold, such as electron impact ionization. We again emphasize that in a realistic scenario where $\angle\vec{E},\vec{B}$ may vary in the entire range of $\angle\vec{E},\vec{B} = 0-90°$, even exact ν_i values corresponding to $\angle\vec{E},\vec{B} = 90°$ are so insignificant that the disagreement between BOLSIG+ and the transcendental methods has no practical significance in the framework of plasma fluid models in which these coefficients are typically employed [e.g., *Starikovskiy et al.*, 2021; *Janalizadeh and Pasko*, 2023]. A similar argument may be made for the parallel mobility panel in Figure 4.2, i.e., Figure 4.2(g) where one observes clear disagreement between BOLSIG+ exact results

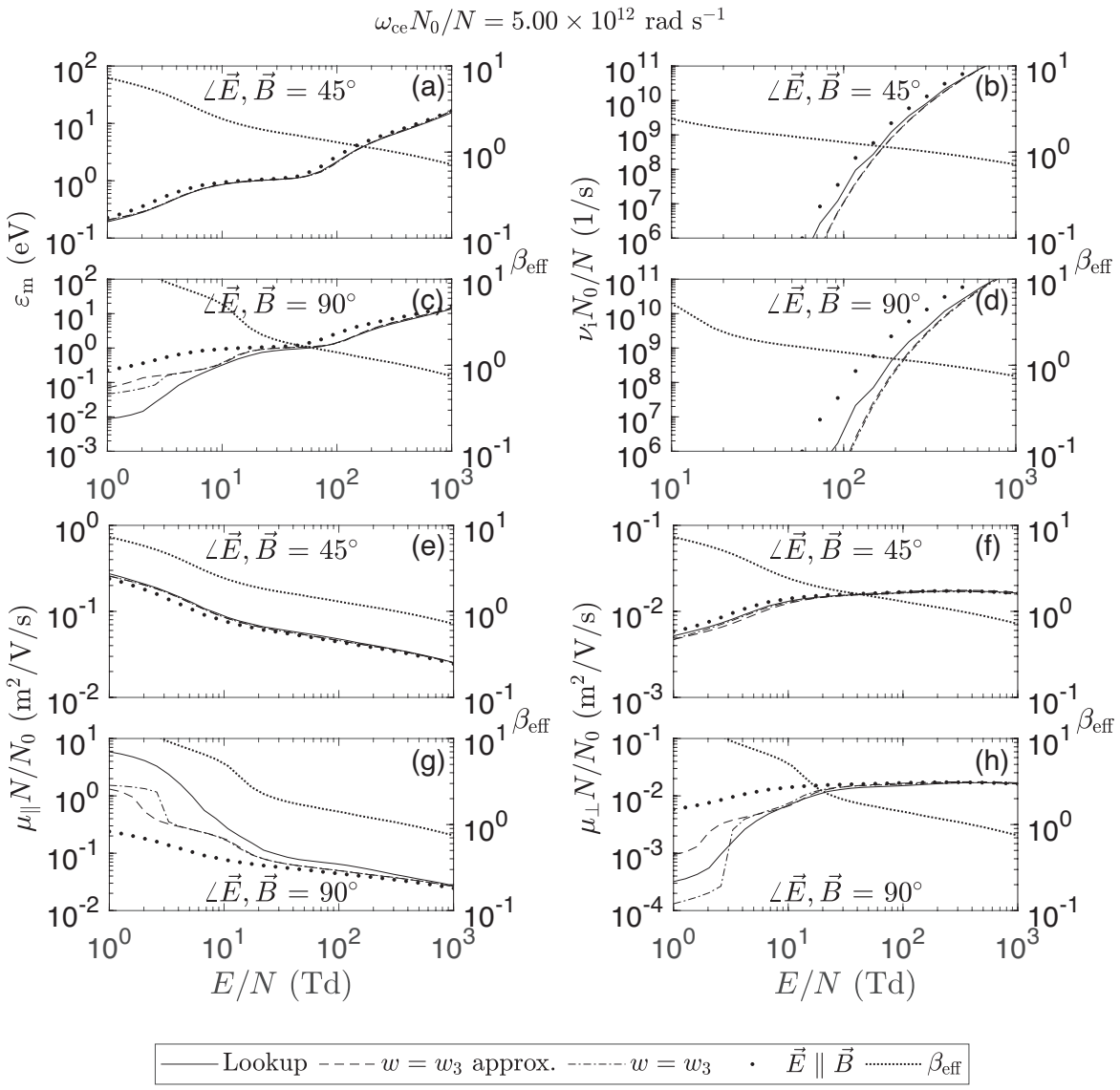

Figure 4.2. (a) Electron mean energy ε_m and (b) reduced electron impact ionization frequency $\nu_i N_0/N$ for $\angle\vec{E},\vec{B} = 45°$. (c) Electron mean energy ε_m and (d) reduced electron impact ionization frequency $\nu_i N_0/N$ for $\angle\vec{E},\vec{B} = 90°$. Reduced mobility of electrons (e) parallel, $\mu_\parallel N/N_0$ and (f) perpendicular, $\mu_\perp N/N_0$, to $\vec{B}$ for $\angle\vec{E},\vec{B} = 45°$. Reduced mobility of electrons (g) parallel, $\mu_\parallel N/N_0$, and (h) perpendicular, $\mu_\perp N/N_0$, to $\vec{B}$ for $\angle\vec{E},\vec{B} = 90°$. Results are for air.

and both transcendental methods in the low E/N region. Specifically, in this case $E_\parallel = 0$ such that drift of electrons parallel to $\vec{B}$ is absent.

Figures 4.4 and 4.5 present the 2-D error plots for air, and a mixture of 88% H_2 and 12% He, respectively. These correspond to Figure 3.11 for CO_2. The figures show the percentage error of the proposed approximate transcendental method compared

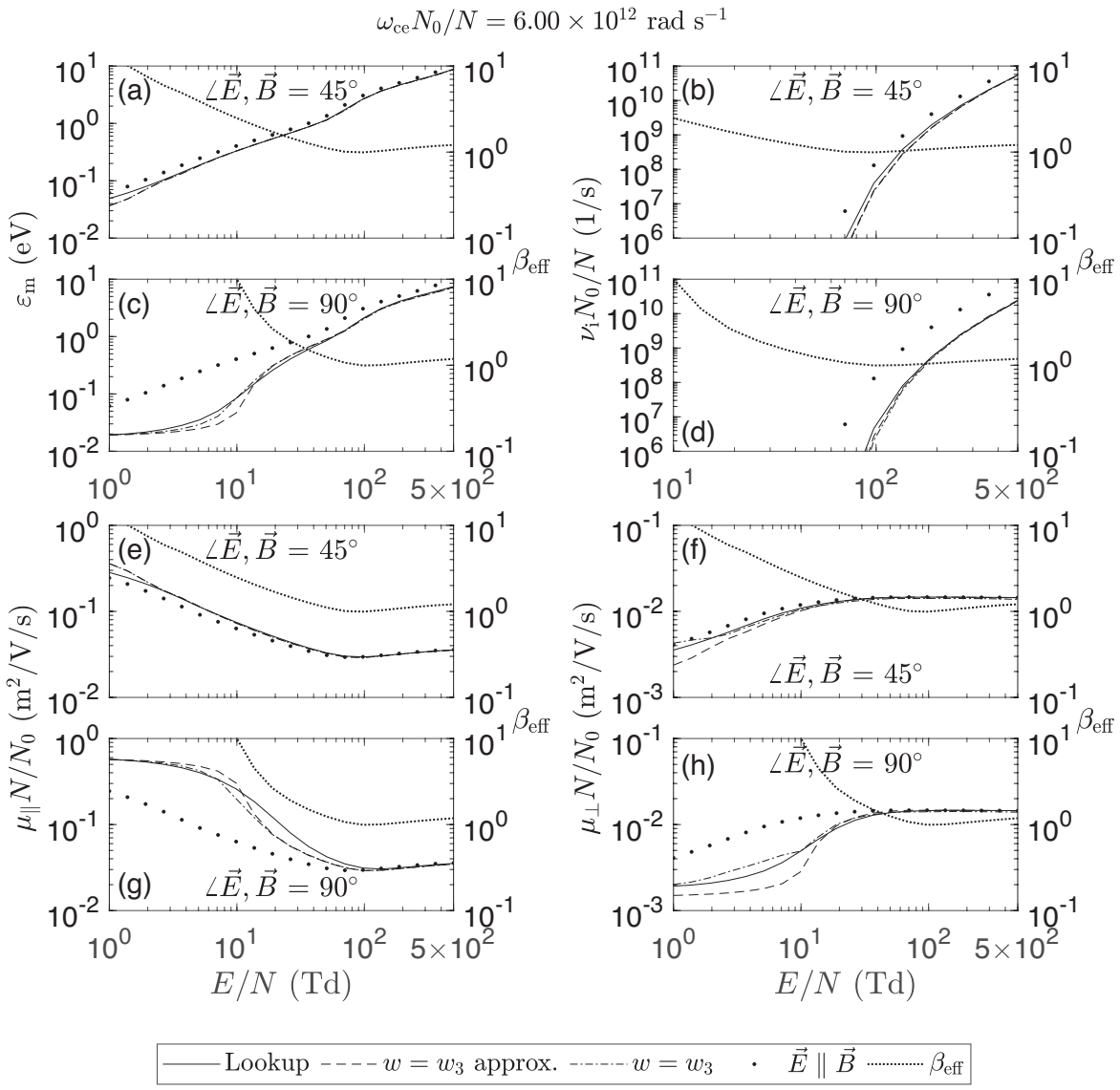

Figure 4.3. (a) Electron mean energy ε_m and (b) reduced electron impact ionization frequency $\nu_i N_0/N$ for $\angle\vec{E},\vec{B} = 45°$. (c) Electron mean energy ε_m and (d) reduced electron impact ionization frequency $\nu_i N_0/N$ for $\angle\vec{E},\vec{B} = 90°$. Reduced mobility of electrons (e) parallel, $\mu_\parallel N/N_0$ and (f) perpendicular, $\mu_\perp N/N_0$, to $\vec{B}$ for $\angle\vec{E},\vec{B} = 45°$. Reduced mobility of electrons (g) parallel, $\mu_\parallel N/N_0$, and (h) perpendicular, $\mu_\perp N/N_0$, to $\vec{B}$ for $\angle\vec{E},\vec{B} = 90°$. Results are for a mixture of 88% H_2 and 12% He.

to exact solution calculated by BOLSIG+ when $\vec{B} \neq 0$ for electron mean energy ε_m, electron impact ionization frequency ν_i, electron mobility parallel to magnetic field $\mu_\parallel$, and electron mobility perpendicular to magnetic field $\mu_\perp$, as a function of the angle $\angle\vec{E},\vec{B}$ and reduced electron gyrofrequency ω_{ce}/N, for selected values of reduced applied electric field E/N. As before, the values selected for the reduced field E/N for each gas

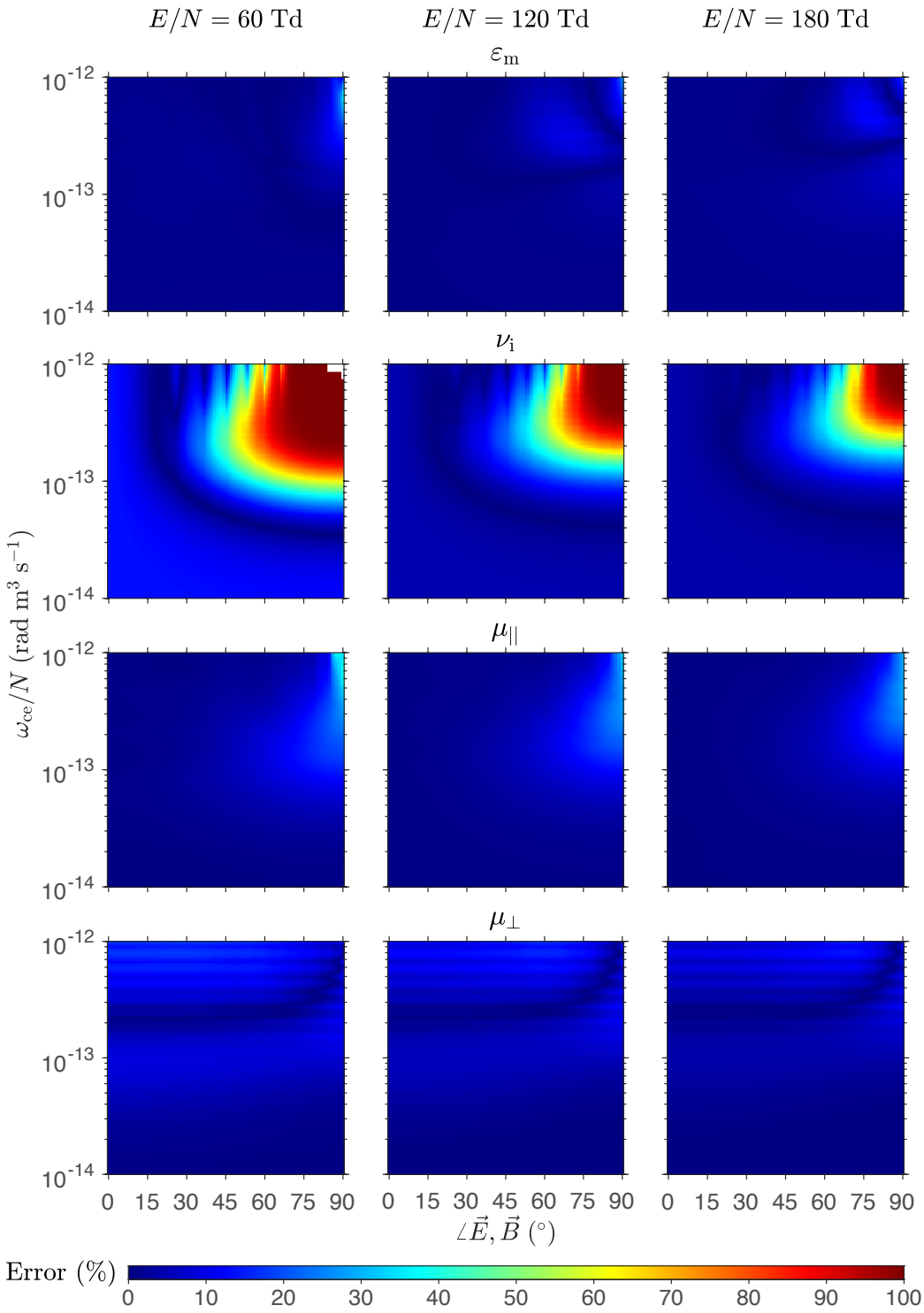

Figure 4.4. Percentage error of proposed transcendental method in approximate form for electron mean energy ε_{m}, electron impact ionization frequency ν_{i}, electron mobility parallel to magnetic field $\mu_{\parallel}$, and electron mobility perpendicular to magnetic field $\mu_{\perp}$, as a function of the angle $\angle\vec{E},\vec{B}$ and reduced electron gyrofrequency ω_{ce}/N, for selected values of applied reduced electric field E/N. Results are for air.

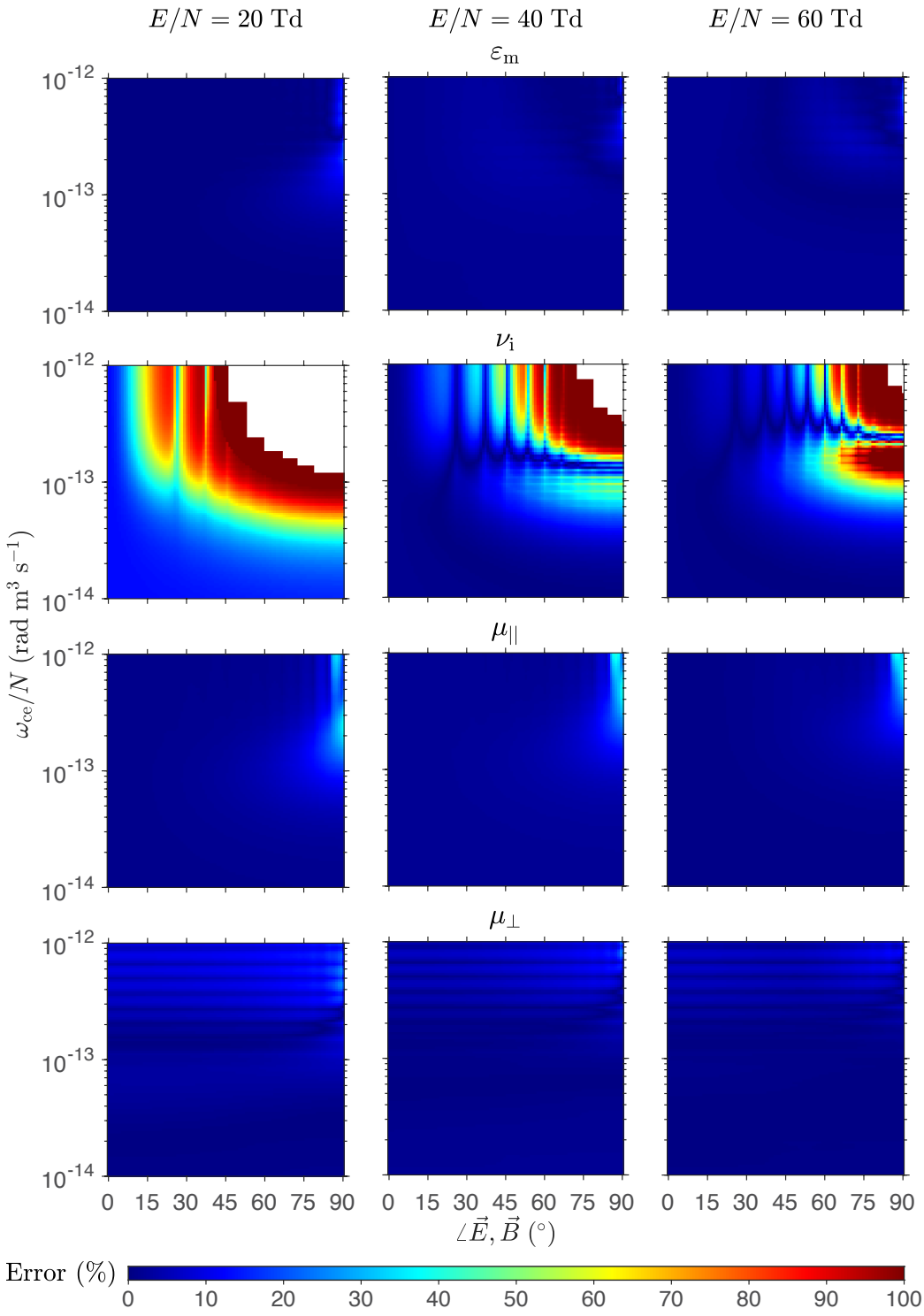

Figure 4.5. Percentage error of proposed transcendental method in approximate form for electron mean energy ε_{m}, electron impact ionization frequency ν_{i}, electron mobility parallel to magnetic field $\mu_{\parallel}$, and electron mobility perpendicular to magnetic field $\mu_{\perp}$, as a functions of the angle $\angle\vec{E}, \vec{B}$ and reduced electron gyrofrequency ω_{ce}/N, for selected values of applied reduced electric field E/N. Results are for a mixture of 88% H_2 and 12% He.

are $0.5E_k/N$, E_k/N, and $1.5E_k/N$, where E_k/N is the reduced breakdown field for the gas, equal to ~ 120, and 40 Td respectively for air, and a mixture of 88% H_2 and 12% He. A similar discussion as presented in context of Figure 3.11 in Section 3.6.2 applies to Figures 4.4 and 4.5 as well, and we do not repeat it here. We simply summarize by noting that the transcendental method presents excellent agreement with exact solutions for ε_m, $\mu_\parallel$, and $\mu_\perp$, except in the regime of highly magnetized ($\beta_{eff} \gg 1$) plasma, i.e, when ω_{ce}/N approaches 10^{-12} rad m^3 s^{-1}, and $\angle\vec{E}, \vec{B}$ approaches 90°. The large error for ν_i has already been addressed above. We finally note that for the panel corresponding to ν_i in the 88% H_2 and 12% He mixture at $E/N = 20$ Td, on account of the low electric field, ν_i is practically zero almost everywhere, and we used a much higher precision in our BOLSIG+ calculations than the default value to plot the ν_i panels shown.

4.4 Convergence of solutions for air and (88% H_2, 12% He) mixture

In Section 3.4 we discussed the sufficient conditions to ensure the existence and uniqueness of a solution to equation (3.2) to calculate E_{eff} using the proposed transcendental method. We further presented the criteria based on the derivative $\phi'(x)$ of the function $\phi(x)$ (see equation (3.5) and associated text) which ensures that the fixed point iteration method to solve equation (3.4) converges to the solution. As previously mentioned, checking condition (3.5) analytically might not be possible due to the highly non-linear dependence of $\beta(x)$ on the electron energy distribution function for given x. We, however, presented a methodology to check for convergence in the case of CO_2 using numerical results. This methodology can be applied to any arbitrary gas mixture to check condition (3.5) for convergence. In this section, we perform the same for gas mixtures (1), and (2).

Figures 4.6 and 4.7 present this analysis for gas mixtures (1), and (2), respectively. Specifically, they show $\phi(x)$ and $|d\phi/dx|$ as a function of x for all three values of E/N, i.e., $E/N = 10$, 100, and 1000 Td. Three values of ω_{ce}/N, i.e., $\omega_{ce}/N = 10^{-14}$, 10^{-13}, and 10^{-12} rad m^3 s^{-1} are considered for each reduced applied field. Following the same discussion as presented in context of Figure 3.8 in Section 3.4 for CO_2, we note that in the region where the solution exists, condition (3.5) is satisfied for both gas mixtures (1), and (2). We conclude that a unique solution to equation (3.4), and consequently equation (3.2) exists for the wide range of values of magnetic field and applied electric field considered here for both gas mixtures. We finally note that the

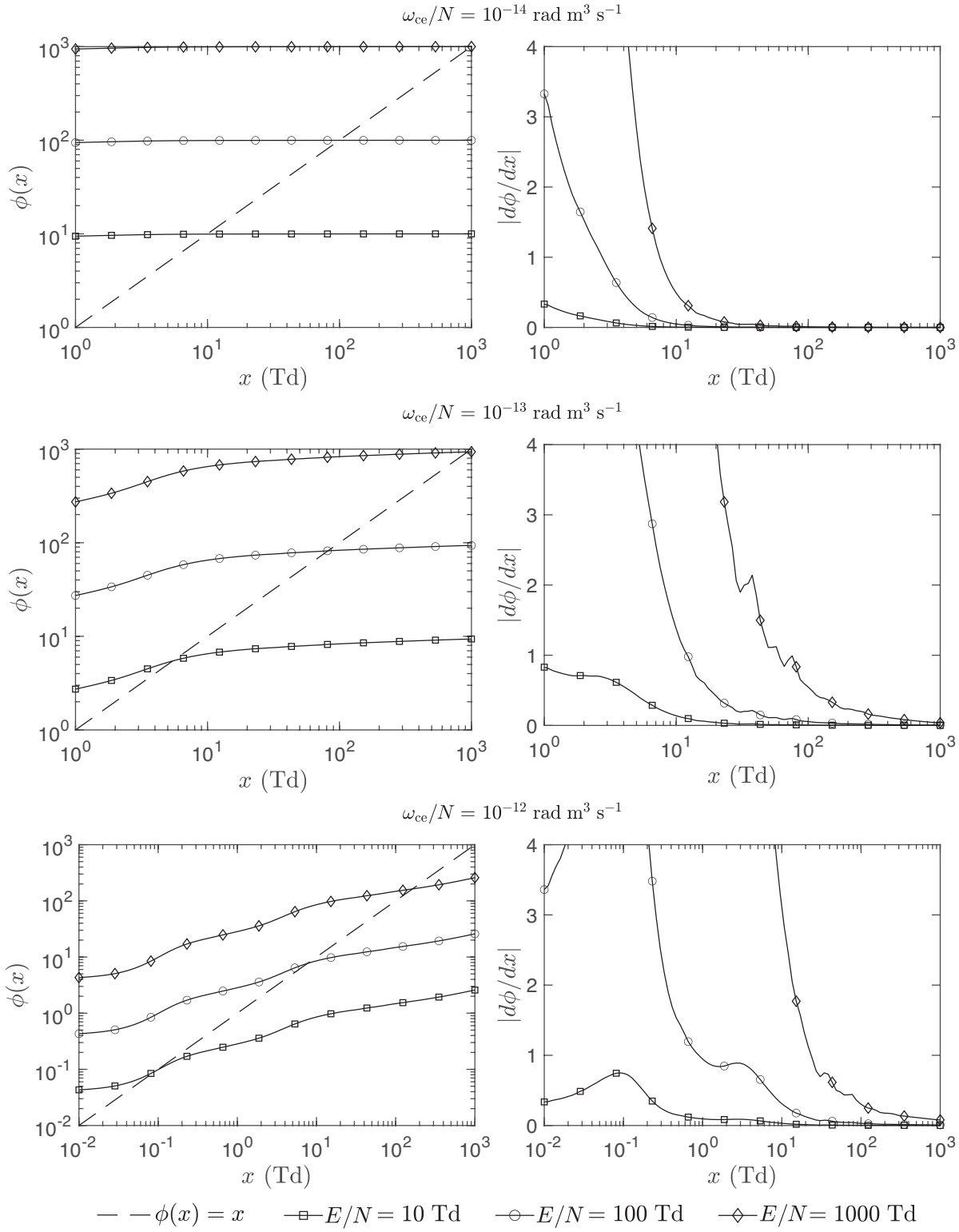

Figure 4.6. $\phi(x)$ and $|d\phi/dx|$ for weakly ($\omega_{ce}/N = 10^{-14}$ rad m^3 s^{-1}), partially ($\omega_{ce}/N = 10^{-13}$ rad m^3 s^{-1}), and highly ($\omega_{ce}/N = 10^{-12}$ rad m^3 s^{-1}) magnetized plasma in air. The dashed line represents the $y = x$ line, and the intersection of $\phi(x)$ with this line is the root of the equation $x = \phi(x)$.

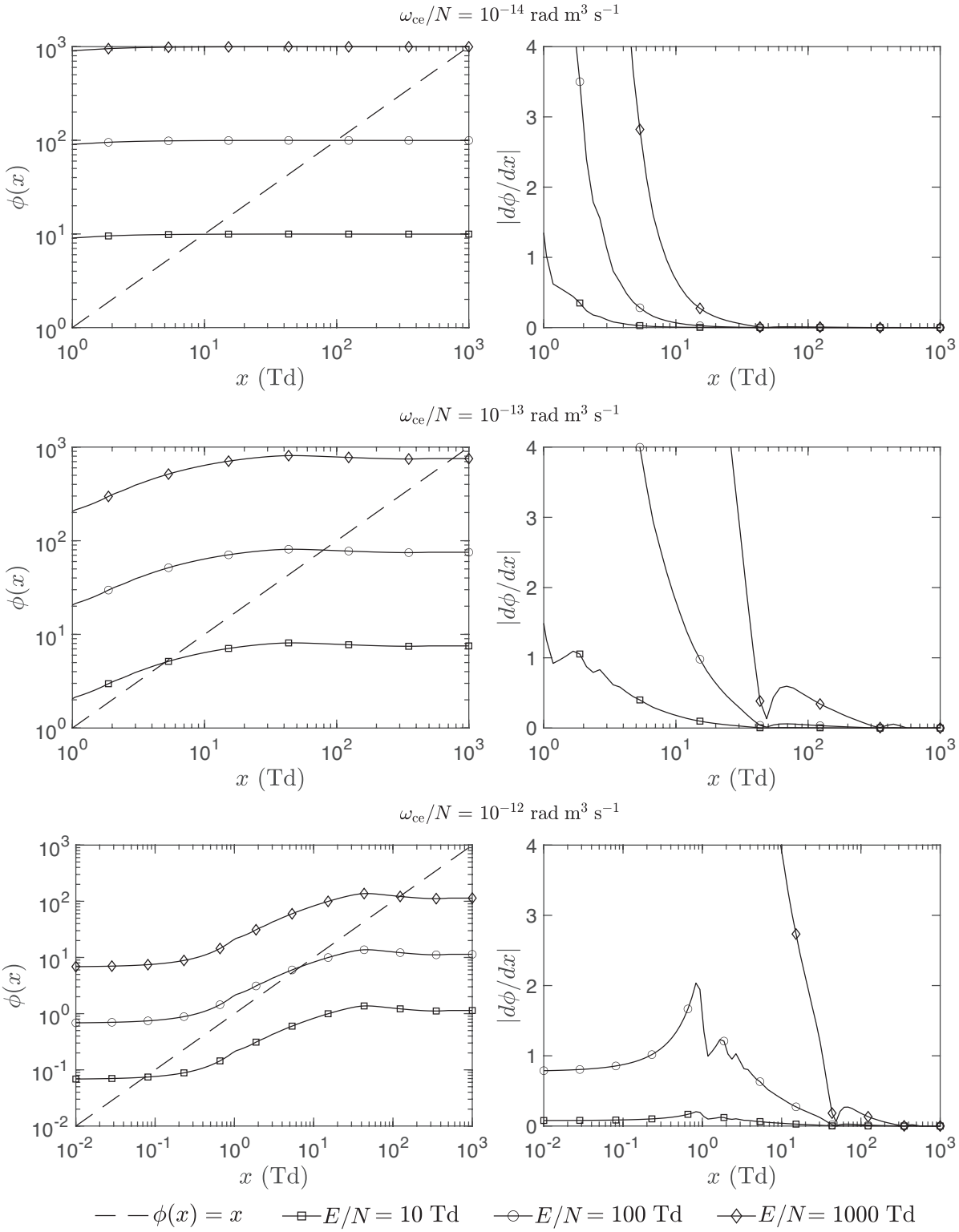

Figure 4.7. $\phi(x)$ and $|d\phi/dx|$ for weakly ($\omega_{ce}/N = 10^{-14}$ rad m^3 s^{-1}), partially ($\omega_{ce}/N = 10^{-13}$ rad m^3 s^{-1}), and highly ($\omega_{ce}/N = 10^{-12}$ rad m^3 s^{-1}) magnetized plasma in a mixture of 88% H_2 and 12% He. The dashed line represents the $y = x$ line, and the intersection of $\phi(x)$ with this line is the root of the equation $x = \phi(x)$.

simple choice of $x_0 = E/N$, where x_0 is the initial value used to start the fixed point iterations (see equation (3.6)), always led to convergence in tests conducted.

4.5 Conclusions

We conclude that the new transcendental method proposed and developed in Chapter 3, and subsequently applied to magnetized CO_2 plasma, can be satisfactorily applied to the calculation of electron transport and rate coefficients in a magnetized plasma for a variety of gas mixtures, as demonstrated in this chapter for air, and a mixture of 88% H_2 and 12% He. Furthermore, convergence of the fixed point iteration method to solve for E_{eff} is also satisfied for both these gas mixtures, and the methodology developed to perform these checks can be applied to an arbitrary gas mixture. Finally, we conclude that the developed theory and model can be used to obtain plasma fluid coefficients in magnetized plasma of an arbitrary gas, using existing tools for obtaining electron rate and transport coefficients in non-magnetized plasma corresponding to E_{eff}.

Chapter 5
Summary and suggestions for future research

In this chapter we provide a brief summary of the work presented in this thesis. Suggestions for possible future research are given based on the results and conclusions we arrived at in previous chapters.

5.1 Summary

There are many applications in the field of gas discharge physics that require a rigorous description of the kinetics of electrons in weakly ionized gases under the influence of an external electric field. We discussed some of these applications, both for research and industrial purposes. In this regard a brief presentation of the kinetic theory of electrons was provided, emphasizing primarily on the concept and significance of the electron velocity/energy distribution function and the Boltzmann equation that governs the distribution function.

The work was primarily focussed on weakly ionized CO_2 gas. As previously mentioned, analytical solutions of the Boltzmann equation are almost impossible to obtain, especially for molecular gases. Numerical solutions, however, are possible and regularly employed. This approach requires electron impact cross section data as a function of energy for all the collision processes involved. We presented and discussed the data used in this study. This data was used as input to BOLSIG+, a popular numerical solver of the Boltzmann equation for the electron energy distribution function $F_0(\varepsilon)$. Results from this approach were compiled and compared to laboratory based experimental data from prior studies. A survey of such experimental data was also presented. We provide a MATLAB function `bolsigco2.m` in which BOLSIG+ outputs are compiled to efficiently provide plasma

fluid coefficients for CO_2, which were found to be in good agreement with corresponding experimental data.

There also exist many applications in which the effect of a magnetic field on electron transport and rate coefficients need to be taken into account. We introduced a new approach to address this problem efficiently by evaluating an effective electric field E_{eff}, that can then be used similar to the case without a magnetic field to obtain plasma fluid coefficients. In other words, this alternative approach provides a new effective electric field, E_{eff}, with $\vec{B} = 0$, which results in satisfactory coefficients (within acceptable accuracy) when compared to ones obtained by solving the Boltzmann equation using the original applied electric field $\vec{E}$ and the magnetic field $\vec{B}$. As such, one can use the function mentioned in the previous paragraph to calculate electron transport and rate coefficients using E_{eff}. A rigorous mathematical derivation of the new method was provided, and the results of the new method were validated by comparison with exact calculations performed using BOLSIG+. In addition to CO_2, corresponding results were also presented for air, and a mixture of 88% H_2 and 12% He [*Janalizadeh et al.*, 2023].

5.2 Suggestions for future research

Various problems in weakly ionized magnetized plasma can make use of the new approach we presented. Specifically, it can be used in CO_2 applications such as the study of magnetized streamer discharges. In the geophysical environment, there are many phenomena associated with lightning related electromagnetic pulses, such as narrow bipolar events, and energetic in-cloud pulses, which originate from in-cloud lightning discharges. Combined with cloud to ground lightning discharges these sources represent the strongest natural emitters of electromagnetic radiation in HF to VLF bands in the Earth's atmosphere. The understanding of electron heating and related effects on electron momentum transfer collision frequency is important for understanding of upward transport of this radiation through magnetized ionospheric plasma. The asymmetry in the morphology of elves, which is also due to the geomagnetic field can also be modeled using this new approach.

Appendix A
The MATLAB function `bolsigco2.m`

The MATLAB function `bolsigco2.m` was developed using results from BOLSIG+ [*Hagelaar and Pitchford*, 2005]. It calculates excitation coefficients/frequencies of various excited states of CO_2 produced by electron impact as a function of the applied electric field E in weakly ionized nonthermal CO_2 plasma. It also calculates electron mean energy, and electron transport parameters such as electron mobility, and the diffusion coefficient for electrons. To create the function, BOLSIG+ (2019 version for Windows) was run for reduced electric fields E/N ranging from 10^{-6} Td to 4000 Td, where, as defined earlier, N is the density of CO_2, and Townsend (Td) is a unit of reduced field such that 1 Td = 10^{-17} V cm^2. The E/N grid contained 500 points spaced exponentially. The temperature was set to 300 K. Superelastic collisions were ignored. All the other input parameters were set to default values. The cross section data for CO_2 was taken from the LXCat cross section file accompanying BOLSIG+. This file contains cross section data for thirteen collision processes, which have already been discussed in Section 2.3 and listed in Table 2.1. The function uses linear interpolation to evaluate the rate or transport coefficient required as output.

The function can be called in MATLAB using either of the two syntaxes listed below.

1. `r = bolsigco2(e,i,n)` where, `r` is the output parameter, `e` is the applied electric field in units V/m, `n` is the neutral density in m^3, and `i` is an integer parameter specifying the process to be calculated. A list of all the output parameters for corresponding values of `i` is provided in Table A.1.

2. `r = bolsigco2(en,i)` where, `r` is the output parameter, `en` is the applied reduced electric field in units Td, and as before, `i` is an integer parameter specifying the process to be calculated. A list of all the output parameters for corresponding values of `i` is provided in Table A.2.

Table A.1. Output parameters for `bolsigco2.m` for syntax 1.

`i`	Output parameter	Units
1	Electron mean energy	eV
2	Electron mobility	$m^2/V/s$
3	Electron diffusion coefficient	m^2/s
4	Ionization frequency (13.3 eV)	1/s
5	Two-body attachment frequency (3.85 eV)	1/s
6	Elastic momentum transfer collision frequency	1/s
7	Vibrational excitation frequency (0.083 eV)	1/s
8	Vibrational excitation frequency (0.167 eV)	1/s
9	Vibrational excitation frequency (0.252 eV)	1/s
10	Vibrational excitation frequency (0.291 eV)	1/s
11	Vibrational excitation frequency (0.339 eV)	1/s
12	Vibrational excitation frequency (0.422 eV)	1/s
13	Vibrational excitation frequency (0.505 eV)	1/s
14	Vibrational excitation frequency (2.5 eV)	1/s
15	Electronic excitation frequency (7.0 eV)	1/s
16	Electronic excitation frequency (10.5 eV)	1/s

Table A.2. Output parameters for `bolsigco2.m` for syntax 2.

`i`	Output parameter	Units
1	Electron mean energy	eV
2	Electron mobility $\times N$	1/m/V/s
3	Electron diffusion coefficient $\times N$	1/m/s
4	Ionization rate coefficient (13.3 eV)	m^3/s
5	Two-body attachment rate coefficient (3.85 eV)	m^3/s
6	Elastic momentum transfer collision rate coefficient	m^3/s
7	Vibrational excitation rate coefficient (0.083 eV)	m^3/s
8	Vibrational excitation rate coefficient (0.167 eV)	m^3/s
9	Vibrational excitation rate coefficient (0.252 eV)	m^3/s
10	Vibrational excitation rate coefficient (0.291 eV)	m^3/s
11	Vibrational excitation rate coefficient (0.339 eV)	m^3/s
12	Vibrational excitation rate coefficient (0.422 eV)	m^3/s
13	Vibrational excitation rate coefficient (0.505 eV)	m^3/s
14	Vibrational excitation rate coefficient (2.5 eV)	m^3/s
15	Electronic excitation rate coefficient (7.0 eV)	m^3/s
16	Electronic excitation rate coefficient (10.5 eV)	m^3/s

Appendix B
Theory of the transcendental method

In this section we start with the definition of the error function introduced in equation (3.12):

$$\mathcal{E} = \int_{v=0}^{\infty} R^2(v) w(v) dv \tag{B.1}$$

Using the definition of the residual $R(v)$ given in equation (3.11) we have

$$\mathcal{E} = \int_{v=0}^{\infty} \frac{1}{9} \left(\frac{q_e}{m_e}\right)^4 \frac{1}{v^4} \left\{ \frac{\partial}{\partial v} \left[\left(\frac{E_\perp^2}{1+\beta_H^2} + E_\parallel^2 - E_{\text{eff}}^2 \right) \frac{v^2}{\nu_m} \frac{\partial f_0}{\partial v} \right] \right\}^2 w(v)\, dv \tag{B.2}$$

and therefore,

$$\begin{aligned} \frac{\partial \mathcal{E}}{\partial E_{\text{eff}}} = \int_{v=0}^{\infty} \frac{1}{9} \left(\frac{q_e}{m_e}\right)^4 \frac{1}{v^4} (2) \left\{ \frac{\partial}{\partial v} \left[\left(\frac{E_\perp^2}{1+\beta_H^2} + E_\parallel^2 - E_{\text{eff}}^2 \right) \frac{v^2}{\nu_m} \frac{\partial f_0}{\partial v} \right] \right\} \cdot \\ \frac{\partial}{\partial E_{\text{eff}}} \left\{ \frac{\partial}{\partial v} \left[\left(\frac{E_\perp^2}{1+\beta_H^2} + E_\parallel^2 - E_{\text{eff}}^2 \right) \frac{v^2}{\nu_m} \frac{\partial f_0}{\partial v} \right] \right\} w(v)\, dv \end{aligned} \tag{B.3}$$

Since

$$\begin{aligned} \frac{\partial}{\partial E_{\text{eff}}} \left\{ \frac{\partial}{\partial v} \left[\left(\frac{E_\perp^2}{1+\beta_H^2} + E_\parallel^2 - E_{\text{eff}}^2 \right) \frac{v^2}{\nu_m} \frac{\partial f_0}{\partial v} \right] \right\} = \\ \frac{\partial}{\partial v} \left\{ \frac{\partial}{\partial E_{\text{eff}}} \left[\left(\frac{E_\perp^2}{1+\beta_H^2} + E_\parallel^2 - E_{\text{eff}}^2 \right) \frac{v^2}{\nu_m} \frac{\partial f_0}{\partial v} \right] \right\} \end{aligned} \tag{B.4}$$

we have

$$\frac{\partial}{\partial v} \left\{ \frac{\partial}{\partial E_{\text{eff}}} \left[\left(\frac{E_\perp^2}{1+\beta_H^2} + E_\parallel^2 - E_{\text{eff}}^2 \right) \frac{v^2}{\nu_m} \frac{\partial f_0}{\partial v} \right] \right\} = -2E_{\text{eff}} \frac{\partial}{\partial v} \left[\frac{v^2}{\nu_m} \frac{\partial f_0}{\partial v} \right] \tag{B.5}$$

We note that based on the definition of electron velocity distribution function, f_0 here is only a function of v and therefore, $\frac{\partial f_0}{\partial E_{\text{eff}}} = 0$. Subsequently,

$$\frac{\partial \mathcal{E}}{\partial E_{\text{eff}}} = -\frac{4}{9}\left(\frac{q_{\text{e}}}{m_{\text{e}}}\right)^4 E_{\text{eff}} \int_{v=0}^{\infty} \frac{1}{v^4} \left\{ \frac{\partial}{\partial v}\left[\left(\frac{E_\perp^2}{1+\beta_{\text{H}}^2} + E_\parallel^2 - E_{\text{eff}}^2\right)\frac{v^2}{\nu_{\text{m}}}\frac{\partial f_0}{\partial v}\right]\right\} \cdot \frac{\partial}{\partial v}\left[\frac{v^2}{\nu_{\text{m}}}\frac{\partial f_0}{\partial v}\right] w(v)\, dv \tag{B.6}$$

Since the trivial solution $E_{\text{eff}} = 0$ is unacceptable, we should have

$$\int_{v=0}^{\infty} dv \frac{w(v)}{v^4} \left\{ \frac{\partial}{\partial v}\left[\left(\frac{E_\perp^2}{1+\beta_{\text{H}}^2} + E_\parallel^2 - E_{\text{eff}}^2\right)\frac{v^2}{\nu_{\text{m}}}\frac{\partial f_0}{\partial v}\right]\right\} \left\{ \frac{\partial}{\partial v}\left[\frac{v^2}{\nu_{\text{m}}}\frac{\partial f_0}{\partial v}\right]\right\} = 0 \tag{B.7}$$

Expanding the first derivative in the equation above we obtain

$$\begin{aligned}
&\frac{\partial}{\partial v}\left[\left(\frac{E_\perp^2}{1+\beta_{\text{H}}^2} + E_\parallel^2 - E_{\text{eff}}^2\right)\frac{v^2}{\nu_{\text{m}}}\frac{\partial f_0}{\partial v}\right] = \\
&\frac{\partial}{\partial v}\left[\frac{E_\perp^2}{1+\beta_{\text{H}}^2} + E_\parallel^2 - E_{\text{eff}}^2\right]\left(\frac{v^2}{\nu_{\text{m}}}\frac{\partial f_0}{\partial v}\right) + \left(\frac{E_\perp^2}{1+\beta_{\text{H}}^2} + E_\parallel^2 - E_{\text{eff}}^2\right)\frac{\partial}{\partial v}\left(\frac{v^2}{\nu_{\text{m}}}\frac{\partial f_0}{\partial v}\right) = \\
&\frac{\partial}{\partial v}\left[\frac{E_\perp^2}{1+\beta_{\text{H}}^2}\right]\left(\frac{v^2}{\nu_{\text{m}}}\frac{\partial f_0}{\partial v}\right) + \left(\frac{E_\perp^2}{1+\beta_{\text{H}}^2} + E_\parallel^2 - E_{\text{eff}}^2\right)\frac{\partial}{\partial v}\left(\frac{v^2}{\nu_{\text{m}}}\frac{\partial f_0}{\partial v}\right) = \\
&\frac{\partial}{\partial v}\left[\frac{E_\perp^2}{1+\beta_{\text{H}}^2}\right]\left(\frac{v^2}{\nu_{\text{m}}}\frac{\partial f_0}{\partial v}\right) + \frac{E_\perp^2}{1+\beta_{\text{H}}^2}\frac{\partial}{\partial v}\left(\frac{v^2}{\nu_{\text{m}}}\frac{\partial f_0}{\partial v}\right) + \left(E_\parallel^2 - E_{\text{eff}}^2\right)\frac{\partial}{\partial v}\left(\frac{v^2}{\nu_{\text{m}}}\frac{\partial f_0}{\partial v}\right) = \\
&\frac{\partial}{\partial v}\left[\left(\frac{E_\perp^2}{1+\beta_{\text{H}}^2}\right)\left(\frac{v^2}{\nu_{\text{m}}}\frac{\partial f_0}{\partial v}\right)\right] + \left(E_\parallel^2 - E_{\text{eff}}^2\right)\frac{\partial}{\partial v}\left(\frac{v^2}{\nu_{\text{m}}}\frac{\partial f_0}{\partial v}\right)
\end{aligned} \tag{B.8}$$

so that

$$\int_{v=0}^{\infty} dv \frac{w(v)}{v^4} \left\{ \frac{\partial}{\partial v}\left[\left(\frac{E_\perp^2}{1+\beta_{\text{H}}^2}\right)\left(\frac{v^2}{\nu_{\text{m}}}\frac{\partial f_0}{\partial v}\right)\right] + \left(E_\parallel^2 - E_{\text{eff}}^2\right)\frac{\partial}{\partial v}\left(\frac{v^2}{\nu_{\text{m}}}\frac{\partial f_0}{\partial v}\right)\right\} \cdot \left\{ \frac{\partial}{\partial v}\left[\frac{v^2}{\nu_{\text{m}}}\frac{\partial f_0}{\partial v}\right]\right\} = 0 \tag{B.9}$$

Distributing the integral into the two terms we arrive at

$$\int_{v=0}^{\infty} \left\{ \frac{1}{v^2}\frac{\partial}{\partial v}\left[\left(\frac{E_\perp^2}{1+\beta_{\text{H}}^2}\right)\left(\frac{v^2}{\nu_{\text{m}}}\frac{\partial f_0}{\partial v}\right)\right]\right\} \cdot \left\{ \frac{1}{v^2}\frac{\partial}{\partial v}\left[\frac{v^2}{\nu_{\text{m}}}\frac{\partial f_0}{\partial v}\right]\right\} w(v) dv = \left(E_{\text{eff}}^2 - E_\parallel^2\right)\int_{v=0}^{\infty}\left[\frac{1}{v^2}\frac{\partial}{\partial v}\left(\frac{v^2}{\nu_{\text{m}}}\frac{\partial f_0}{\partial v}\right)\right]^2 w(v) dv \tag{B.10}$$

Defining

$$I_1 = \int_{v=0}^{\infty} \left[\frac{1}{v^2} \frac{\partial}{\partial v} \left(\frac{v^2}{\nu_\mathrm{m}} \frac{\partial f_0}{\partial v} \right) \right]^2 w(v) dv \tag{B.11}$$

and

$$I_2 = \int_{v=0}^{\infty} \left\{ \frac{1}{v^2} \frac{\partial}{\partial v} \left[\left(\frac{1}{1+\beta_\mathrm{H}^2} \right) \left(\frac{v^2}{\nu_\mathrm{m}} \frac{\partial f_0}{\partial v} \right) \right] \right\} \cdot \left\{ \frac{1}{v^2} \frac{\partial}{\partial v} \left[\frac{v^2}{\nu_\mathrm{m}} \frac{\partial f_0}{\partial v} \right] \right\} w(v) dv \tag{B.12}$$

we arrive at

$$E_\perp^2 I_2 = \left(E_\mathrm{eff}^2 - E_\parallel^2 \right) I_1 \tag{B.13}$$

In conclusion

$$E_\mathrm{eff}^2 = E_\parallel^2 + E_\perp^2 \frac{I_2}{I_1} = E_\parallel^2 + \frac{E_\perp^2}{\frac{I_1}{I_2}} = E_\parallel^2 + \frac{E_\perp^2}{1+\beta_\mathrm{eff}^2} \tag{B.14}$$

Appendix C
Simplified transcendental method when $w(v) = w_3(v)$

Using $w_3(v)$ as defined in equation (3.16) and applying integration by parts to I_1 we have

$$I_1^{w_3} = \int_{v=0}^{\infty} v^2 \left[\frac{\partial}{\partial v}\left(\frac{v^2}{\nu_{\rm m}}\frac{\partial f_0}{\partial v}\right)\right] dv = v^2\left(\frac{v^2}{\nu_{\rm m}}\frac{\partial f_0}{\partial v}\right)\Bigg|_{v=0}^{\infty} - \int_{v=0}^{\infty}\left(\frac{v^2}{\nu_{\rm m}}\frac{\partial f_0}{\partial v}\right)(2v)dv \quad \text{(C.1)}$$

Thus,

$$I_1^{w_3} = \frac{v^4}{\nu_{\rm m}}\frac{\partial f_0}{\partial v}\Bigg|_{v=0}^{\infty} - 2\int_{v=0}^{\infty}\frac{v^3}{\nu_{\rm m}}\frac{\partial f_0}{\partial v}dv = C_1^{w_3}\Bigg|_{v=0}^{\infty} - 2I_{1,1}^{w_3} \quad \text{(C.2)}$$

Before demonstrating that $I_{1,1}^{w_3}$ is proportional to $\mu_{\|}$, i.e., electron mobility parallel to magnetic field (when $B \neq 0$), we show that $C_1^{w_3}(v=\infty) = 0$. Let's assume there is at least a single constant $k > 0$ for which one can find a constant v_0 so that the inequality $0 \leq v^\ell \leq k f_0(v) 4\pi v^2$ holds for $v > v_0$. In other words $v^\ell \in O[f_0(v)4\pi v^2]$. Then

$$n_{\rm e} = \int_{v=0}^{\infty} f_0(v)4\pi v^2 dv = \int_{v=0}^{v_0} f_0(v)4\pi v^2 dv + \int_{v=v_0}^{\infty} f_0(v)4\pi v^2 dv \quad \text{(C.3)}$$

and based on the inequality introduced above

$$\int_{v=0}^{v_0} f_0(v)4\pi v^2 dv + \frac{1}{k}\int_{v=v_0}^{\infty} v^\ell dv \leq n_{\rm e} \quad \text{(C.4)}$$

Note that $n_{\rm e} - \int_{v=0}^{v_0} f_0(v)4\pi v^2 dv$ is a bounded positive quantity and therefore, the integral above including v^ℓ should be convergent. Introducing the change of variable $t = v/v_0$ we have $\int_{t=1}^{\infty} t^\ell dt < \infty$, which occurs only if $\ell < -1$. Consequently, $f_0(v) \geq \frac{1}{4\pi k} v^{\ell-2}$, i.e., $f_0(v)$ falls off faster than v^{-3} as $v \to \infty$. This implies that as $v \to \infty$, $\frac{\partial f_0}{\partial v}$ falls off faster

than v^{-4} such that $C_1^{w_3}(v \to \infty)$ falls off faster than v^{-1} since $\nu_{\rm m} = N\sigma_{\rm m} v = N\sigma_{\rm m}\gamma\varepsilon^{\frac{1}{2}}$. Thus, $C_1^{w_3}(v = \infty) = 0$.

To be consistent with BOLSIG+'s definition of mobility [*Hagelaar and Pitchford*, 2005, manual], we now switch to ε to obtain

$$I_{1,1}^{w_3} = \int_{\varepsilon=0}^{\infty} \frac{\left(\gamma\varepsilon^{\frac{1}{2}}\right)^3}{\nu_{\rm m}} 2\gamma^{-1}\varepsilon^{\frac{1}{2}} \frac{\partial}{\partial\varepsilon}\left[\frac{n_{\rm e}}{2\pi\gamma^3}F_0(\varepsilon)\right]\left(\frac{\gamma}{2}\varepsilon^{-\frac{1}{2}}d\varepsilon\right) = \frac{1}{2\pi\gamma}\frac{n_e}{N}\int_{\varepsilon=0}^{\infty}\frac{\varepsilon}{\sigma_{\rm m}}\frac{\partial}{\partial\varepsilon}F_0(\varepsilon)\,d\varepsilon \tag{C.5}$$

In [*Hagelaar and Pitchford*, 2005, manual] we have mobility parallel to the magnetic field defined as

$$\mu_{\parallel} N = -\frac{\gamma}{3}\int_{\varepsilon=0}^{\infty}\frac{\varepsilon}{\sigma_{\rm m}}\frac{\partial}{\partial\varepsilon}F_0(\varepsilon)\,d\varepsilon \tag{C.6}$$

Thus,

$$I_{1,1}^{w_3} = -\frac{3}{2\pi}\gamma^{-2} n_{\rm e}\mu_{\parallel} \to I_1^{w_3} = \frac{3}{\pi}\gamma^{-2} n_{\rm e}\mu_{\parallel} \tag{C.7}$$

Similarly for $I_2^{w_3}$ we have

$$I_2^{w_3} = \int_{v=0}^{\infty} v^2 \frac{\partial}{\partial v}\left[\left(\frac{1}{1+\beta_{\rm H}^2}\right)\left(\frac{v^2}{\nu_{\rm m}}\frac{\partial f_0}{\partial v}\right)\right]dv = \tag{C.8}$$
$$\frac{1}{1+\beta_{\rm H}^2}\frac{v^4}{\nu_{\rm m}}\frac{\partial f_0}{\partial v}\bigg|_{v=0}^{\infty} - 2\int_{v=0}^{\infty}\frac{1}{1+\beta_{\rm H}^2}\frac{v^3}{\nu_{\rm m}}\frac{\partial f_0}{\partial v}dv = C_2^{w_3}\bigg|_{v=0}^{\infty} - 2I_{2,1}^{w_3}$$

The same arguments detailed above result in $C_2^{w_3}(v = \infty) = 0$ and

$$I_2^{w_3} = \frac{3}{\pi}\gamma^{-2} n_{\rm e}\mu_{\perp}^0 \tag{C.9}$$

where $\mu_{\perp}^0$ is in the same format of perpendicular mobility defined in [*Hagelaar and Pitchford*, 2005, manual], i.e.,

$$\mu_{\perp} N = -\frac{\gamma}{3}\int_{\varepsilon=0}^{\infty}\frac{1}{1+\beta_{\rm H}^2}\frac{\varepsilon}{\sigma_{\rm m}}\frac{\partial}{\partial\varepsilon}F_0(\varepsilon)\,d\varepsilon \tag{C.10}$$

We note that $\mu_{\perp}^0$ as opposed to $\mu_{\parallel}$ is not a direct output of BOLSIG+ when $B = 0$ since perpendicular mobility is defined only when $B \neq 0$. As such, we calculate $\mu_{\perp}^0$ manually using the EEDF output of BOLSIG+. In conclusion, for $w = w_3$ the simpler

transcendental expression

$$E_{\text{eff}}^2 = E_{\parallel}^2 + \frac{E_{\perp}^2}{\left(\frac{\mu_{\parallel}}{\mu_{\perp}^0}\right)} \tag{C.11}$$

where $\mu_{\parallel}N$ is a function of E_{eff}/N exclusively whereas $\mu_{\perp}^0 N$ is dependent on both E_{eff}/N and ω_{ce}/N. Note that $\mu_{\parallel}N$ is provided by BOLSIG+.

Appendix D
Simplified transcendental method when $w(v) = w_3(v)$ and $\beta_{\rm H}^2 \gg 1$

A special case of the current version of the transcendental method is obtained when $\beta_{\rm H} > 1$ such that $\beta_{\rm H}^2 \gg 1$. We start with

$$\mu_\perp^0 N = -\frac{\gamma}{3}\int_{\varepsilon=0}^{\infty} \frac{1}{1+\beta_{\rm H}^2}\frac{\varepsilon}{\sigma_{\rm m}}\frac{\partial}{\partial\varepsilon}F_0(\varepsilon)\,d\varepsilon \simeq -\frac{\gamma}{3}\int_{\varepsilon=0}^{\infty} \frac{1}{\beta_{\rm H}^2}\frac{\varepsilon}{\sigma_{\rm m}}\frac{\partial}{\partial\varepsilon}F_0(\varepsilon)\,d\varepsilon \tag{D.1}$$

Since $\beta_{\rm H} = \frac{\omega_{\rm ce}}{\nu_{\rm m}} = \frac{\omega_{\rm ce}/N}{\sigma_{\rm m} v} = \frac{\omega_{\rm ce}/N}{\sigma_{\rm m}\left(\gamma\varepsilon^{\frac{1}{2}}\right)}$ we have $\beta_{\rm H}^{-2} = \frac{\gamma^2\sigma_{\rm m}^2\varepsilon}{(\omega_{\rm ce}/N)^2}$ and

$$\mu_\perp^0 N \simeq -\frac{\gamma^3}{3}\int_{\varepsilon=0}^{\infty} \frac{\gamma^2\sigma_{\rm m}^2\varepsilon}{(\omega_{\rm ce}/N)^2}\frac{\varepsilon}{\sigma_{\rm m}}\frac{\partial F_0}{\partial\varepsilon}\,d\varepsilon = -\frac{\gamma^3}{3}\left(\frac{\omega_{\rm ce}}{N}\right)^{-2}\int_{\varepsilon=0}^{\infty}\varepsilon^2\sigma_{\rm m}\frac{\partial F_0}{\partial\varepsilon}\,d\varepsilon \tag{D.2}$$

Using $\sigma_{\rm m} v = \sigma_{\rm m}\gamma\varepsilon^{\frac{1}{2}}$ we have

$$\mu_\perp^0 N \simeq -\frac{\gamma^3}{3}\left(\frac{\omega_{\rm ce}}{N}\right)^{-2}\int_{\varepsilon=0}^{\infty}\frac{1}{\gamma}\left(\gamma\varepsilon^{\frac{1}{2}}\sigma_{\rm m}\right)\left(\varepsilon^{\frac{3}{2}}\frac{\partial F_0}{\partial\varepsilon}\right)d\varepsilon \tag{D.3}$$

Since $P_0(\varepsilon) = \varepsilon^{\frac{1}{2}}F_0(\varepsilon)$ where $\int_{\varepsilon=0}^{\infty}P_0(\varepsilon)d\varepsilon = 1$ (see Sections 1.2.1 and 1.2.3) and

$$\frac{\partial}{\partial\varepsilon}\left(\varepsilon^{\frac{3}{2}}F_0\right) = \frac{\partial\varepsilon^{\frac{3}{2}}}{\partial\varepsilon}F_0 + \varepsilon^{\frac{3}{2}}\frac{\partial F_0}{\partial\varepsilon} \rightarrow \frac{\partial}{\partial\varepsilon}(\varepsilon P_0) = \frac{3}{2}\varepsilon^{\frac{1}{2}}F_0 + \varepsilon^{\frac{3}{2}}\frac{\partial F_0}{\partial\varepsilon} = \frac{3}{2}P_0 + \varepsilon^{\frac{3}{2}}\frac{\partial F_0}{\partial\varepsilon} \tag{D.4}$$

we have

$$\mu_\perp^0 N \simeq -\frac{\gamma^2}{3}\left(\frac{\omega_{\rm ce}}{N}\right)^{-2}\int_{\varepsilon=0}^{\infty}\left(\gamma\varepsilon^{\frac{1}{2}}\sigma_{\rm m}\right)\left[\frac{\partial}{\partial\varepsilon}(\varepsilon P_0) - \frac{3}{2}P_0\right]d\varepsilon \tag{D.5}$$

Distributing the integral we obtain

$$\mu_{\perp}^{0} N \simeq -\frac{\gamma^2}{3}\left(\frac{\omega_{\mathrm{ce}}}{N}\right)^{-2}\left[\gamma\int_{\varepsilon=0}^{\infty}\varepsilon^{\frac{1}{2}}\sigma_{\mathrm{m}}\frac{\partial}{\partial\varepsilon}\left(\varepsilon P_0\right)\,d\varepsilon-\frac{3}{2}\frac{\nu_{\mathrm{m}}}{N}\right] \tag{D.6}$$

where for the second integral we used the definition of momentum transfer collision frequency

$$\nu_{\mathrm{m}} \equiv \int_{\varepsilon=0}^{\infty}\left(N\sigma_{\mathrm{m}}v\right)P_0(\varepsilon)d\varepsilon \tag{D.7}$$

Using integration by parts for the first integral in the brackets we obtain

$$\int_{\varepsilon=0}^{\infty}\sigma_{\mathrm{m}}\varepsilon^{\frac{1}{2}}\frac{\partial}{\partial\varepsilon}\left(\varepsilon P_0\right)\,d\varepsilon=\left(\sigma_{\mathrm{m}}\varepsilon^{\frac{1}{2}}\right)\varepsilon P_0\Big|_{\varepsilon=0}^{\infty}-\int_{\varepsilon=0}^{\infty}\varepsilon P_0\frac{\partial}{\partial\varepsilon}\left(\sigma_{\mathrm{m}}\varepsilon^{\frac{1}{2}}\right)\,d\varepsilon \tag{D.8}$$

where the limit term vanishes due to arguments already made in the beginning of this section and the integral term may be expressed as

$$\int_{\varepsilon=0}^{\infty}\varepsilon\frac{\partial}{\partial\varepsilon}\left(\sigma_{\mathrm{m}}\varepsilon^{\frac{1}{2}}\right)\,P_0 d\varepsilon\equiv\left\langle\varepsilon\frac{\partial}{\partial\varepsilon}\left(\sigma_{\mathrm{m}}\varepsilon^{\frac{1}{2}}\right)\right\rangle \tag{D.9}$$

The average $\left\langle\varepsilon\frac{\partial}{\partial\varepsilon}\left(\sigma_{\mathrm{m}}\varepsilon^{\frac{1}{2}}\right)\right\rangle$ is a measure of the variation of momentum transfer collision frequency as a function of electron energy. That is, $\sigma_{\mathrm{m}}(\varepsilon)\propto\varepsilon^{-\frac{1}{2}}$ for which the average is identically zero corresponds to a constant momentum transfer collision frequency since $\nu_{\mathrm{m}}(\varepsilon)=N\sigma_{\mathrm{m}}v\propto\varepsilon^{-\frac{1}{2}}\left(\gamma\varepsilon^{\frac{1}{2}}\right)=\text{const}$. Assuming the average $\left\langle\varepsilon\frac{\partial}{\partial\varepsilon}\left(\sigma_{\mathrm{m}}\varepsilon^{\frac{1}{2}}\right)\right\rangle$ is negligible:

$$\mu_{\perp}^{0}N\simeq-\frac{\gamma^2}{3}\left(\frac{\omega_{\mathrm{ce}}}{N}\right)^{-2}\left(-\frac{3}{2}\right)\frac{\nu_{\mathrm{m}}}{N}=\frac{\gamma^2}{2}\left(\frac{\omega_{\mathrm{ce}}}{N}\right)^{-2}\left(\frac{\nu_{\mathrm{m}}}{N}\right) \tag{D.10}$$

Subsequently,

$$\frac{\mu_{\parallel}}{\mu_{\perp}^{0}}=\frac{\mu_{\parallel}N}{\mu_{\perp}^{0}N}=\frac{\left(\frac{\gamma^2}{2}\right)\left(\frac{\nu_{\mathrm{m}}}{N}\right)^{-1}}{\frac{\gamma^2}{2}\left(\frac{\omega_{\mathrm{ce}}}{N}\right)^{-2}\left(\frac{\nu_{\mathrm{m}}}{N}\right)}=\frac{\left(\frac{\omega_{\mathrm{ce}}}{N}\right)^{2}}{\left(\frac{\nu_{\mathrm{m}}}{N}\right)^{2}}=\left(\frac{\omega_{\mathrm{ce}}}{\nu_{\mathrm{m}}}\right)^{2}\simeq 1+\left(\frac{\omega_{\mathrm{ce}}}{\nu_{\mathrm{m}}}\right)^{2} \tag{D.11}$$

where we used the fact that $\beta_{\mathrm{eff}}^{2}\gg 1$ and that by definition $\nu_{\mathrm{m}}/N=\frac{q_{\mathrm{e}}}{m_{\mathrm{e}}\left(\mu_{\parallel}N\right)}=\left(q_{\mathrm{e}}/m_{\mathrm{e}}\right)/\left(\mu_{\parallel}N\right)=\left(\gamma^2/2\right)/\left(\mu_{\parallel}N\right)$ where ν_{m}/N is the rate constant for momentum

transfer when $B = 0$, which varies only as a function of E_{eff}/N. In conclusion

$$E_{\text{eff}}^2 = E_{\parallel}^2 + \frac{E_{\perp}^2}{\left(\frac{\mu_{\parallel}}{\mu_{\perp}}\right)} = E_{\parallel}^2 + \frac{E_{\perp}^2}{1 + \left(\frac{\omega_{\text{ce}}}{\nu_{\text{m}}}\right)^2} = E_{\parallel}^2 + \frac{E_{\perp}^2}{1 + \beta_{\text{eff}}^2} \tag{D.12}$$

Appendix E
I_1 and I_2 integrals in terms of BOLSIG+ variables

From equation (1.23) we have

$$v = \gamma\varepsilon^{\frac{1}{2}} \quad \Rightarrow \quad \frac{dv}{d\varepsilon} = \frac{\gamma}{2}\varepsilon^{-\frac{1}{2}} \quad \Rightarrow \quad \frac{d\varepsilon}{dv} = \frac{2}{\gamma}\varepsilon^{\frac{1}{2}} \tag{E.1}$$

where, as defined earlier, $\gamma = (2q_e/m_e)^{\frac{1}{2}}$, and ε denotes electron energy in eV. Thus,

$$\frac{\partial}{\partial v}(\cdot) = \frac{\partial}{\partial \varepsilon}(\cdot)\frac{\partial \varepsilon}{\partial v} = \frac{2}{\gamma}\varepsilon^{\frac{1}{2}}\frac{\partial}{\partial \varepsilon}(\cdot) \tag{E.2}$$

The EEDF in BOLSIG+, i.e., $F_0(\varepsilon)$ is related to $f_0(v)$ via equation (1.21) as

$$f_0(v) = \frac{n_e}{2\pi\gamma^3}\, F_0(\varepsilon). \tag{E.3}$$

where n_e denotes electron density. Defining $W(\varepsilon)$ such that $W(\varepsilon)d\varepsilon \equiv w(v)dv$, we have

$$\frac{W(\varepsilon)}{w(v)} = \frac{dv}{d\varepsilon} = \frac{\gamma}{2}\varepsilon^{-\frac{1}{2}}. \tag{E.4}$$

Substituting equations (E.1)-(E.4) in equations (B.11) and (B.12) results in expressions for the integrals I_1 and I_2 in terms of ε and $F_0(\varepsilon)$ as

$$I_1 = \int_{\varepsilon=0}^{\infty} \left[\frac{1}{\gamma^2\varepsilon}\, 2\gamma^{-1}\varepsilon^{\frac{1}{2}}\, \frac{\partial}{\partial \varepsilon}\left\{\frac{\gamma^2\varepsilon}{\nu_m} 2\gamma^{-1}\varepsilon^{\frac{1}{2}}\frac{\partial}{\partial \varepsilon}\left(\frac{n_e}{2\pi\gamma^3}F_0(\varepsilon)\right)\right\}\right]^2 W(\varepsilon)\, d\varepsilon$$

$$\Rightarrow I_1 = \left(\frac{2}{\pi}\gamma^{-5}n_e\right)^2 \int_{\varepsilon=0}^{\infty} \left[\frac{\partial}{\partial \varepsilon}\left\{\frac{\varepsilon^{\frac{3}{2}}}{\nu_m}\frac{\partial F_0(\varepsilon)}{\partial \varepsilon}\right\}\right]^2 \varepsilon^{-1} W(\varepsilon)\, d\varepsilon \tag{E.5}$$

and

$$I_2 = \int_{\varepsilon=0}^{\infty} \left\{ \frac{1}{\gamma^2 \varepsilon} 2\gamma^{-1} \varepsilon^{\frac{1}{2}} \frac{\partial}{\partial \varepsilon} \left[\frac{1}{1+\beta_{\mathrm{H}}^2} \frac{\gamma^2 \varepsilon}{\nu_{\mathrm{m}}} 2\gamma^{-1} \varepsilon^{\frac{1}{2}} \frac{\partial}{\partial \varepsilon} \left(\frac{n_{\mathrm{e}}}{2\pi\gamma^3} F_0(\varepsilon) \right) \right] \right\} \cdot \left\{ \frac{1}{\gamma^2 \varepsilon} 2\gamma^{-1} \varepsilon^{\frac{1}{2}} \frac{\partial}{\partial \varepsilon} \left[\frac{\gamma^2 \varepsilon}{\nu_{\mathrm{m}}} 2\gamma^{-1} \varepsilon^{\frac{1}{2}} \frac{\partial}{\partial \varepsilon} \left(\frac{n_{\mathrm{e}}}{2\pi\gamma^3} F_0(\varepsilon) \right) \right] \right\} W(\varepsilon)\, d\varepsilon$$

$$\Rightarrow I_2 = \left(\frac{2}{\pi} \gamma^{-5} n_{\mathrm{e}} \right)^2 \int_{\varepsilon=0}^{\infty} \left\{ \frac{\partial}{\partial \varepsilon} \left[\frac{1}{1+\beta_{\mathrm{H}}^2} \frac{\varepsilon^{\frac{3}{2}}}{\nu_{\mathrm{m}}} \frac{\partial F_0(\varepsilon)}{\partial \varepsilon} \right] \right\} \left\{ \frac{\partial}{\partial \varepsilon} \left[\frac{\varepsilon^{\frac{3}{2}}}{\nu_{\mathrm{m}}} \frac{\partial F_0(\varepsilon)}{\partial \varepsilon} \right] \right\} \varepsilon^{-1} W(\varepsilon)\, d\varepsilon. \quad \text{(E.6)}$$

Note that since $\beta_{\mathrm{eff}} \propto \frac{I_1}{I_2}$, the absolute value of electron density or the constant γ is irrelevant in this analysis.

Bibliography

Aleksandrov, N., A. Bazelyan, E. Bazelyan, and I. Kochetov (1995), Modeling of long streamers in atmospheric-pressure air, *Plasma Phys. Repo.*, *21*(1), 57–75.

Barrington-Leigh, C. P., U. S. Inan, and M. Stanley (2001), Identification of sprites and elves with intensified video and broadband array photometry, *J. Geophys. Res.: Space Phys.*, *106*(A2), 1741–1750.

Bhalla, M. S., and J. D. Craggs (1960), Measurement of ionization and attachment coefficients in carbon dioxide in uniform fields, *Proc. Phys. Soc.*, *76*(3), 369–377.

Bittencourt, J. A. (2004), *Fundamentals of Plasma Physics*, Third ed., Springer, New York, NY.

Bjørge-Engeland, I., N. Østgaard, A. Mezentsev, C. A. Skeie, D. Sarria, J. Lapierre, A. Lindanger, T. Neubert, M. Marisaldi, N. Lehtinen, O. Chanrion, K. Ullaland, S. Yang, G. Genov, F. Christiansen, and V. Reglero (2022), Terrestrial gamma-ray flashes with accompanying elves detected by ASIM, *J. Geophys. Res.: Atmos.*, *127*(11), e2021JD036368.

Bortner, T. E., G. S. Hurst, and W. G. Stone (1957), Drift velocities of electrons in some commonly used counting gases, *Rev. Sci. Instr.*, *28*(2), 103–108.

Bourdon, A., V. P. Pasko, N. Y. Liu, S. Célestin, P. Ségur, and E. Marode (2007), Efficient models for photoionization produced by non-thermal gas discharges in air based on radiative transfer and the Helmholtz equations, *Plasma Sources Sci. Technol.*, *16*(3), 656–678.

Burden, R. L., and J. D. Faires (2005), *Numerical Analysis*, Eighth ed., Thomson Brooks/Cole, Belmont, CA.

Chachereau, A., M. Rabie, and C. M. Franck (2016), Electron swarm parameters of the hydrofluoroolefine HFO1234ze, *Plasma Sources Sci. Technol.*, *25*(4), 045005.

Chatterton, P. A., and J. D. Craggs (1961), Measurements of attachment coefficients in oxygen using an electron filter technique, *Int. J. Electron.*, *11*(6), 425–437.

Chatterton, P. A., and J. D. Craggs (1965), Attachment coefficient measurements in carbon dioxide, carbon monoxide, air and helium-oxygen mixtures, *Proc. Phys. Soc.*, *85*(2), 355–362.

Chen, F. F. (2016), *Introduction to Plasma Physics and Controlled Fusion*, Third ed., Springer.

Elford, M., and G. Haddad (1980), The drift velocity of electrons in carbon dioxide at temperatures between 193 and 573 K, *Aust. J. Phys.*, *33*(3), 517–530.

Elford, M. T. (1966), The drift velocity of electrons in carbon dioxide at 293°K, *Aust. J. Phys.*, *19*, 629.

Franz, R. C., R. J. Nemzek, and J. R. Winckler (1990), Television image of a large upward electrical discharge above a thunderstorm system, *Science*, *249*(4964), 48–51.

Frommhold, L. (1960), Eine untersuchung der elektronenkomponente von elektronenlawinen im homogenen feld II, *Z. Physik*, *160*(5), 554–567.

Fukunishi, H., Y. Takahashi, M. Kubota, K. Sakanoi, U. S. Inan, and W. A. Lyons (1996), Elves: Lightning-induced transient luminous events in the lower ionosphere, *Geophy. Res. Lett.*, *23*(16), 2157–2160.

Golant, V. E., A. P. Zhilinsky, and I. E. Sakharov (1980), *Fundamentals of Plasma Physics*, Wiley, Hoboken, NJ.

Hagelaar, G. J. M., and L. C. Pitchford (2005), Solving the Boltzmann equation to obtain electron transport coefficients and rate coefficients for fluid models, *Plasma Sources Sci. Technol.*, *14*(4), 722–733.

Hake, R. D., and A. V. Phelps (1967), Momentum-transfer and inelastic-collision cross sections for electrons in O_2, CO, and CO_2, *Phys. Rev.*, *158*, 70–84.

Hasegawa, H., H. Date, M. Shimozuma, K. Yoshida, and H. Tagashira (1996), The drift velocity and longitudinal diffusion coefficient of electrons in nitrogen and carbon dioxide from 20 to 1000 Td, *J. Phys. D: Appl. Phys.*, *29*(10), 2664–2667.

Hernandez-Avila, J., E. Basurto, and J. de Urquijo (2002), Electron transport and swarm parameters in CO_2 and its mixtures with SF_6, *J. Phys. D: Appl. Phys.*, *35*(18), 2264–2269.

Holstein, T. (1946), Energy distribution of electrons in high frequency gas discharges, *Phys. Rev.*, *70*, 367–384.

Huxley, L. G. H., and R. W. Crompton (1974), *The Diffusion and Drift of Electrons in Gases*, Wiley, New York, NY.

Inan, U. S., C. Barrington-Leigh, S. Hansen, V. S. Glukhov, T. F. Bell, and R. Rairden (1997), Rapid lateral expansion of optical luminosity in lightning-induced ionospheric flashes referred to as 'elves', *Geophys. Res. Lett.*, *24*(5), 583–586.

Itikawa, Y. (2002), Cross sections for electron collisions with carbon dioxide, *J. Phys. Chem. Ref. Data*, *31*(3), 749–767.

Janalizadeh, R., and V. P. Pasko (2020), A framework for efficient calculation of photoionization and photodetachment rates with application to the lower ionosphere, *J. Geophys. Res.: Space Phys.*, *125*(7), e2020JA027979.

Janalizadeh, R., and V. P. Pasko (2023), Preliminary modeling of magnetized sprite streamers on Jupiter following Juno's observations of possible transient luminous events, *J. Geophys. Res.: Space Phys.*, *128*(2), e2022JA031009.

Janalizadeh, R., Z. Pervez, and V. P. Pasko (2023), Efficient modeling of electron kinetics under influence of externally applied electric field in weakly ionized magnetized plasma, manuscript submitted for publication to *Plasma Sources Sci. Technol.*, manuscript ID: PSST-105715, submission date: 03/06/2023.

Jánský, J., and V. P. Pasko (2020), Modeling of streamer ignition and propagation in the system of two approaching hydrometeors, *J. Geophys. Res.: Atmos.*, *125*(6), e2019JD031337.

Kabirzadeh, R., N. G. Lehtinen, and U. S. Inan (2015), Latitudinal dependence static mesospheric E fields above thunderstorms, *Geophys. Res. Lett.*, *42*(10), 4208–4215.

Kucukarpaci, H. N., and J. Lucas (1979), Simulation of electron swarm parameters in carbon dioxide and nitrogen for high E/N, *J. Phys. D: Appl. Phys.*, *12*(12), 2123–2138.

Kuo, C.-L., A. B. Chen, Y. J. Lee, L. Y. Tsai, R. K. Chou, R. R. Hsu, H. T. Su, L. C. Lee, S. A. Cummer, H. U. Frey, S. B. Mende, Y. Takahashi, and H. Fukunishi (2007), Modeling elves observed by FORMOSAT-2 satellite, *J. Geophys. Res.: Space Phys.*, *112*(A11).

Lakshminarasimha, C. S., J. Lucas, and N. Kontoleon (1974), Diffusion and ionization studies for electron swarms in carbon monoxide and carbon dioxide, *J. Phys. D: Appl. Phys.*, *7*(18), 2545–2553.

Lehtinen, N. G., M. Walt, U. S. Inan, T. F. Bell, and V. P. Pasko (1996), γ-ray emission produced by a relativistic beam of runaway electrons accelerated by quasi-electrostatic thundercloud fields, *Geophys. Res. Lett.*, *23*(19), 2645–2648.

Liu, N., J. R. Dwyer, and S. A. Cummer (2017), Elves accompanying terrestrial gamma ray flashes, *J. Geophys. Res.: Space Phys.*, *122*(10), 10,563–10,576.

Loureiro, J., and J. Amorim (2016), *Kinetics and Spectroscopy of Low Temperature Plasmas*, Springer.

Lowke, J. J., and J. H. Parker (1969), Theory of electron diffusion parallel to electric fields. II. Application to real gases, *Phys. Rev.*, *181*, 302–311.

Lowke, J. J., A. V. Phelps, and B. W. Irwin (1973), Predicted electron transport coefficients and operating characteristics of CO_2–N_2–He laser mixtures, *J. Appl. Phys.*, *44*(10), 4664–4671.

Lyu, F., S. A. Cummer, and L. McTague (2015), Insights into high peak current in-cloud lightning events during thunderstorms, *Geophys. Res. Lett.*, *42*(16), 6836–6843.

Marshall, R. A. (2009), Very low frequency radio signatures of transient luminous events above thunderstorms, Ph.D. Thesis, Stanford University.

Marshall, R. A. (2012), An improved model of the lightning electromagnetic field interaction with the D-region ionosphere, *J. Geophys. Res.: Space Phys.*, *117*(A3).

Marshall, R. A., U. S. Inan, and V. S. Glukhov (2010), Elves and associated electron density changes due to cloud-to-ground and in-cloud lightning discharges, *J. Geophys. Res.: Space Phys.*, *115*(A4).

Marshall, R. A., C. L. da Silva, and V. P. Pasko (2015), Elve doublets and compact intracloud discharges, *Geophys. Res. Lett.*, *42*(14), 6112–6119.

Morgan, W., and B. Penetrante (1990), ELENDIF: A time-dependent Boltzmann solver for partially ionized plasmas, *Comput. Phys. Commun.*, *58*(1), 127–152.

Morrow, R., and J. J. Lowke (1997), Streamer propagation in air, *J. Phys. D*, *30*(4), 614.

Moss, G. D., V. P. Pasko, N. Liu, and G. Veronis (2006), Monte Carlo model for analysis of thermal runaway electrons in streamer tips in transient luminous events and streamer zones of lightning leaders, *J. Geophys. Res.: Space Phys.*, *111*(A2).

Pack, J. L., R. E. Voshall, and A. V. Phelps (1962), Drift velocities of slow electrons in krypton, xenon, deuterium, carbon monoxide, carbon dioxide, water vapor, nitrous oxide, and ammonia, *Phys. Rev.*, *127*, 2084–2089.

Pasko, V. P. (2003), Electric jets, *Nature*, *423*(6943), 927–929.

Pasko, V. P. (2006), Theoretical modeling of sprites and jets, in *Sprites, Elves and Intense Lightning Discharges*, edited by M. Füllekrug, E. A. Mareev, and M. J. Rycroft, pp. 253–311, Springer Netherlands, Dordrecht.

Pasko, V. P., U. S. Inan, and T. F. Bell (1998), Ionospheric effects due to electrostatic thundercloud fields, *J. Atmos. Sol. Terr. Phys.*, *60*(7), 863–870.

Pasko, V. P., Y. Yair, and C.-L. Kuo (2012), Lightning related transient luminous events at high altitude in the Earth's atmosphere: Phenomenology, mechanisms and effects, *Space Sci. Rev.*, *168*(1-4), 475–516.

Pietanza, L. D., O. Guaitella, V. Aquilanti, I. Armenise, A. Bogaerts, M. Capitelli, G. Colonna, V. Guerra, R. Engeln, E. Kustova, A. Lombardi, F. Palazzetti, and T. Silva (2021), Advances in non-equilibrium CO_2 plasma kinetics: a theoretical and experimental review, *Eur. Phys. J. D*, *75*(237).

Pérez-Invernón, F. J., A. Luque, and F. J. Gordillo-Vázquez (2018), Modeling the chemical impact and the optical emissions produced by lightning-induced electromagnetic fields in the upper atmosphere: The case of halos and elves triggered by different lightning discharges, *J. Geophys. Res.: Atmos.*, *123*(14), 7615–7641.

Raizer, Y. P. (1991), *Gas Discharge Physics*, Springer-Verlag, New York, NY.

Roznerski, W., and K. Leja (1984), Electron drift velocity in hydrogen, nitrogen, oxygen, carbon monoxide, carbon dioxide and air at moderate E/N, *J. Phys. D: Appl. Phys.*, *17*(2), 279–285.

Saelee, H. T., J. Lucas, and J. W. Limbeek (1977), Time-of-flight measurement of electron drift velocity and longitudinal diffusion coefficient in nitrogen, carbon monoxide, carbon dioxide and hydrogen, *IEE J. Solid-State Electron Devices*, *1*, 111–116.

Salem, M. A., N. Liu, and H. K. Rassoul (2016), Modification of the lower ionospheric conductivity by thunderstorm electrostatic fields, *Geophys. Res. Lett.*, *43*(1), 5–12.

Schlumbohm, H. (1965), Stoßionisierungskoeffizient α, mittlere elektronenenergien und die beweglichkeit von elektronen in gasen, *Z. Physik*, *184*(5), 492–505.

Seeger, M., J. Avaheden, S. Pancheshnyi, and T. Votteler (2017), Streamer parameters and breakdown in CO_2, *J. Phys. D: Appl. Phys.*, *50*(1), 015207.

Smith, D. A., X. M. Shao, D. N. Holden, C. T. Rhodes, M. Brook, P. R. Krehbiel, M. Stanley, W. Rison, and R. J. Thomas (1999), A distinct class of isolated intracloud lightning discharges and their associated radio emissions, *J. Geophys. Res.: Atmos.*, *104*(D4), 4189–4212.

Soler, S., F. J. Pérez-Invernón, F. J. Gordillo-Vázquez, A. Luque, D. Li, A. Malagón-Romero, T. Neubert, O. Chanrion, V. Reglero, J. Navarro-Gonzalez, G. Lu, H. Zhang, A. Huang, and N. Østgaard (2020), Blue optical observations of narrow bipolar events by ASIM suggest corona streamer activity in thunderstorms, *J. of Geophy. Res.: Atmos.*, *125*(16), e2020JD032708.

Starikovskiy, A. Y., N. L. Aleksandrov, and M. N. Shneider (2021), Streamer self-focusing in an external longitudinal magnetic field, *Phys. Rev. E*, *103*, 063201.

Tilles, J. N., P. R. Krehbiel, M. A. Stanley, W. Rison, N. Liu, F. Lyu, S. A. Cummer, J. R. Dwyer, S. Senay, H. Edens, X. Fan, R. G. Brown, and J. Wilson (2020), Radio interferometer observations of an energetic in-cloud pulse reveal large currents generated by relativistic discharges, *J. Geophys. Res.: Atmos.*, *125*(20), e2020JD032603.

Tonev, P., and P. Velinov (2016), Vertical coupling between troposphere and lower ionosphere by electric currents and fields at equatorial latitudes, *J. Atmos. Sol. Terr. Phys.*, *141*, 39–47.

Vass, M., I. Korolov, D. Loffhagen, N. Pinhao, and Z. Donko (2017), Electron transport parameters in CO_2: scanning drift tube measurements and kinetic computations, *Plasma Sources Sci. Technol.*, *26*(6), 065007.

Veronis, G., V. P. Pasko, and U. S. Inan (1999), Characteristics of mesospheric optical emissions produced by lightning discharges, *J. Geophys. Res.: Space Phys.*, *104*(A6), 12,645–12,656.

Vojnović, M. M., M. M. Ristić, V. V. Stanković, and G. B. Poparić (2019), Electron-induced vibrational excitation of CO_2 in dc electric and magnetic fields, *Phys. Rev. E*, *99*, 063211.

Wagner, E. B., F. J. Davis, and G. S. Hurst (1967), Time-of-flight investigations of electron transport in some atomic and molecular gases, *J. Chem. Phys.*, *47*(9), 3138–3147.